©Copyright 2013
Thomas Joseph Long

www.manaraa.com

Tissue-Engineered Prostate Cancer Xenografts: A Biomaterials-Based Approach to Study Tumorigenesis and Dormancy Escape

Thomas Joseph Long

A dissertation
submitted in partial fulfillment of the
requirements for the degree of

Doctor of Philosophy

University of Washington

2013

Reading Committee:

Buddy D. Ratner, Chair

Stephen R. Plymate

Marta Scatena

Program Authorized to Offer Degree: Bioengineering

www.manaraa.com

University of Washington

Abstract

Tissue-Engineered Prostate Cancer Xenografts: A Biomaterials-Based Approach to Study Tumorigenesis and Dormancy Escape

Thomas Joseph Long

Chair of the Supervisory Committee:
Professor Buddy D. Ratner
Departments of Bioengineering and Chemical Engineering

Despite massive investments in research and development, it is estimated that 95% of oncology compounds that enter clinical trials ultimately fail to receive FDA approval [1]. This disconnect between pre-clinical testing and clinical success points to a need to develop improved pre-clinical model systems for cancer studies that more accurately reflect human disease states. Toward this goal, biomaterial scaffolds have shown promise as the basis for *in vitro* and *in vivo* 3D cancer models. Tumors engineered using biomaterials have shown evidence of being more physiologically relevant than some traditional preclinical model systems, and synthetic biomaterials provide the added potential for enhanced microenvironmental control. In this dissertation, we examine sphere-templated poly(2-hydroxyethyl methacrylate) (pHEMA) scaffolds as the basis for engineering *in vivo* xenografts from human prostate cancer cell lines.

Methods were developed to seed, culture, and measure the proliferation of prostate cancer cells *in vitro* within these porous hydrogels. A novel capillary force-based seeding method is described that improved cell number and distribution within the scaffolds compared to well-established protocols such as static and centrifugation seeding. Dynamic cell culture improved oxygen diffusion *in vitro*, and a PicoGreen-based DNA assay was used to evaluate cell proliferation.

www.manaraa.com

pHEMA scaffolds seeded and pre-cultured with tumorigenic M12 prostate cancer epithelial cells prior to implantation generated tumors in athymic nude mice, demonstrating the ability of the scaffolds to be used as a synthetic vehicle for xenograft generation. The resulting tumors showed no significant differences in tumor growth kinetics or vascularity compared to standard xenografts derived from Matrigel, which is consistent with observations that highly tumorigenic cells are not affected *in vivo* by 3D culture within biomaterial scaffolds.

Because Matrigel-based xenografts expose cells to exogenous growth factors and ECM proteins, it would be of interest to the cancer research field to develop a controllable, synthetic system as a replacement. We attempted to do this using pHEMA scaffolds seeded with LNCaP C4-2 metastatic prostate cancer cells. LNCaP C4-2 cells ordinarily require Matrigel or stromal cell support to form tumors *in vivo*, but when implanted within pHEMA, the constructs were poorly tumorigenic. Scaffold surface modification with collagen I did not improve tumorigenicity, but the synthetic nature of the scaffold lends itself to further surface modifications and controlled growth factor release in future studies that may allow tumor development within a controllable microenvironment.

Finally, M12mac25 cells, an epithelial prostate cancer cell line that is ordinarily rendered non-tumorigenic through the expression of the tumor suppressor insulin-like growth factor binding protein 7 (IGFBP7), displayed a tumorigenic response when implanted within porous pHEMA scaffolds. These findings show the potential for this biomaterials-based model system to be used in the study of *in vivo* prostate cancer dormancy and dormancy escape. The M12mac25 tumors showed no significant difference in vascularity compared to their dormant Matrigel counterparts, but did demonstrate a significantly higher macrophage infiltration within the scaffolds mediated by the foreign body response to the materials. Cytokine arrays, DNA oligonucleotide arrays, *in vitro* macrophage-conditioned media studies, and *in vivo* studies using clondronate liposomes to eliminate macrophages showed evidence that macrophages could be the key cellular player mediating this dormancy escape.

www.manaraa.com

Acknowledgements

This work would not have been possible without a tremendous amount of support and guidance. In this collaborative project, I was very lucky to have fantastic mentors in both engineering and cancer biology. I would first like to thank my advisor, Dr. Buddy Ratner, for giving me a chance to work in his lab and then offering me the freedom to grow as a scientist and pursue these studies while always being there to offer his expert opinion. I would also like to thank Dr. Steve Plymate for his vision in biomaterials applications in cancer biology and who as my co-advisor was a constant source of support, knowledge, and encouragement. I would like to thank my other committee members, Dr. Pete Nelson, Dr. Marta Scatena, and Dr. Amy Shen, for their guidance and expertise to help get me through the PhD process. I would also like to acknowledge Dr. Miqin Zhang, who as the head of the University of Washington's Physical Science and Nanotechnology Training Program in Cancer Research, provided me with some of my graduate funding for these studies.

There are too many to list individually, but I would like to thank all Ratner and Plymate lab members who not only may have assisted me directly or indirectly, but also made the graduate school experience as enjoyable and painless as possible. In particular, I would like to thank Dr. Cynthia Sprenger, who displayed never-ending patience while being my go-to person for technical advice and support on the cancer biology side of my project. Colleen Irvin helped me with all my *in vivo* work and kept the Ratner lab running smoothly all these years. I would also like to thank Dr. Eric Sussman for helpful technical discussions and for lending his expertise in histology and the foreign body response. Finally, I could not have done this without the constant support and encouragement of my family back in Maryland and the lifelong friends that I have made here in Seattle.

www.manaraa.com

Table of Contents

www.manaraa.com

www.manaraa.com

www.manaraa.com

www.manaraa.com

Glossary

2D	two-dimensional
3D	three-dimensional
AB	alamarBlue®
bFGF	basic fibroblast growth factor
BSA	bovine serum albumin
BMDM	bone marrow-derived macrophage
CAF	carcinoma-associated fibroblast
CL	clondronate liposome
CTC	circulating tumor cell
DAB	3,3-diaminobenzidine
DI	de-ionized
DiI	lipophilic fluorescent dye
DMEM	Dulbecco's modified eagle's medium
DTC	disseminated tumor cell
DVI	digital volumetric imaging
ECM	extracellular matrix
EDC	1-ethyl-3-[3-dimethylaminopropyl]carbodiimide hydrochloride
EDTA	ethylenediaminetetraacetic acid
EGF	epidermal growth factor
EMT	epithelial-mesenchymal transition
EpCAM	epithelial cell adhesion molecule
EtOH	ethanol
F4/80	activated macrophage marker
FBR	foreign body response
FBS	fetal bovine serum
FDR	false discovery rate
FIJI	image analysis software
GSEA	gene set enrichment analysis
H+E	hematoxylin and eosin
HA	hyaluronic acid
HRP	horseradish peroxidase
IACUC	institutional animal care and use committee
IFN-γ	interferon gamma
IGFBP7	insulin-like growth factor binding protein 7
IGFBP-rp1	insulin-like growth factor binding protein-related protein 1
IHC	immunohistochemistry
IL-4	interleukin 4
IP	intraperitoneal
IRGACURE	2,2-dimethyoxy-2-phenylacetophenone
JAK	janus kinase
LAL	limulus amebocyte lysate
LNCaP	human lymph node prostate cancer cell line
LPS	lipopolysaccharide
M12	human prostate epithelial cancer cell line

www.manaraa.com

MAA	methacrylic acid
mac25	gene encoding for IGFBP7
MAFIA	macrophage fas-induced apoptosis
MAPK	mitogen-activated protein kinase
M12mac25	M12 cell line transfected with mac25 plasmid
MCM	macrophage conditioned media
M-CSF	macrophage colony stimulating factor
MECA	mouse endothelial cell antigen
mPER	mammalian protein extraction reagent
MTT	3-(4,5-dimethylthiazol-2-yl)-2,5-diphenytltetrazolium bromide
NES	normalized enrichment score
NHS	*N*-hydroxysuccinimide
OCT	optimal cutting temperature
oligo	oligonucleotide
P69	non-tumorigenic human prostate epithelial cancer cell line
pA	poly(acrylamide)
PBS	phosphate-buffered saline
PBSL	PBS liposome
PEG	poly(ethylene glycol) (aka poly(ethylene oxide))
PG	PicoGreen ®
pHEMA	poly(2-hydroxyethyl methacrylate)
PI3K	phosphatidylinositol-3-kinase
PLA	poly(lactic acid)
PLG	poly(lactide-co-glycolide)
PDGF	platelet-derived growth factor
PMMA	poly(methyl methacrylate)
PSA	prostate specific antigen
pNIPAM	poly(N-isopropyl acrylamide)
SA	streptavidin
SEM	scanning electron microscopy
SF	serum free
STAT	signal transducer and activator of transcription
SV40T	SV40 large T antigen cell immortalization vector
TAM	tumor-associated macrophage
TBS	tris-buffered saline
TCPS	tissue culture polystyrene
TE	tris-EDTA buffer
TEDGMA	tetraethyleneglycol dimethacrylate
TGF-β	transforming growth factor-β
TRAMP	transgenic adenocarcinoma of the mouse prostate
V-CAM1	vascular cell adhesion molecule 1
VEGF	vascular endothelial growth factor
XPS	x-ray photoelectron spectroscopy

www.manaraa.com

List of Figures

www.manaraa.com

List of Tables

www.manaraa.com

Chapter 1. Introduction

1.1 Motivation and Significance

Prostate cancer is the most common cancer diagnosis and the second leading cause of cancer death for men. In 2013 it was estimated that there would be over 230,000 new cases and 29,000 deaths in the United States alone [2]. The odds of developing prostate cancer at some point over the course of a man's life are about one in six [3]. Age is one of the primary risk factors for prostate cancer, and with increasing life expectancy and an aging population prostate cancer will no doubt remain a significant health issue as research continues and novel treatment options are developed.

1.2 Bioengineering in Cancer Research

As our knowledge of cancer biology grows, there is increasing demand for more sophisticated technologies in research and therapies that can harness and maximize existing knowledge while laying the foundation for future advancements. Bioengineers are playing many critical interdisciplinary roles in cancer research with a focus on technology development. Thrust areas include novel targeted drug therapies, single cell and high-throughput analysis tools, microfluidic technologies, bioinformatics, more sophisticated imaging modalities, improved diagnostic systems, and many others. The bioengineering project described here focuses on applying the principles of biomaterials science and tissue engineering to prostate cancer research to generate a novel pre-clinical 3D *in vivo* tumor model system.

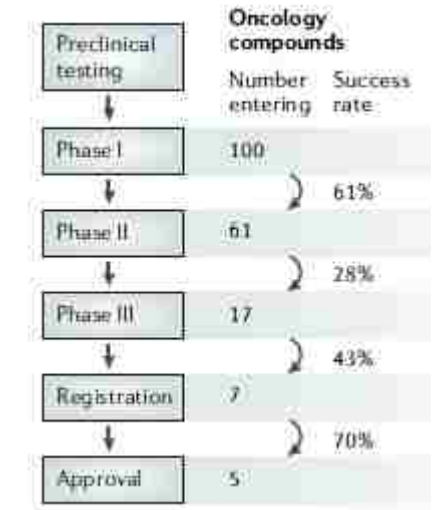

1.3 Pre-clinical Cancer Models

Despite significant investments in research and development in the cancer field, about 95% of oncology drugs in clinical trials fail to receive FDA approval (see Figure 1.1) [1]. Part of the reason for this disconnect is the lack of adequate pre-clinical models that capture the complexity of the disease and accurately represent disease progression. Many researchers

www.manaraa.com

continue to rely exclusively on two-dimensional (2D) cell culture systems despite the abundance of data establishing that cells cultured in a three-dimensional (3D) environment tend to behave in a manner more physiologically relevant to live tissues. 3D cell culture has been shown to impact cell morphology, gene/protein expression, signal transduction, proliferation, migration, polarization, and drug tolerance [4][5][6][7][8]. A variety of technologies have been developed for *in vitro* 3D cell culture, though there are few widely accepted standards because application dictates platform choice. Typical 3D culture techniques include suspending cells in a matrix such as collagen I or Matrigel or culturing cells within biomaterial scaffolds that can be fabricated into custom architectures from a variety of materials [9].

In the cancer field, many studies involving 3D cell culture for drug screening utilize tumor spheroids as a model system, particularly for high-throughput applications. Spheroids are 20 to 1000 μm-diameter clusters of cells that self-aggregate when cultured in spinner flasks or rotary wall vessels. Spheroid culture generates distinct cell populations along the radius of the sphere that differ in response to diffusion limitations and can serve as a model that bridges the gap between more basic cell systems and complex *in vivo* systems [10][11].

There are a variety of *in vivo* mouse model systems that are used to study cancer biology and screen therapeutics for efficacy, toxicology, and pharmacokinetics. Most common is the traditional xenograft, where human cancer cells are injected subcutaneously with or without a supportive extracellular matrix (ECM) into an immunocompromised mouse and grow tumors that can be observed and measured easily under the skin. The advantage of this method is its simplicity, but that simplicity can also be a disadvantage in terms of relevancy to human disease [12]. The subcutaneous xenograft model views cancer as a mostly homogenous mixture of cells, but it has been well established that cancer is a complex, dynamic, heterogenous tissue system. Orthotopic xenografts, where cancer cells are injected directly to the organ of interest, provide the potential for a more relevant local microenvironment than subcutaneous xenografts. For example, Stephenson, *et al*. demonstrated that some prostate cancer cells showed metastatic potential after orthotopic but not subcutaneous injection [13]. Human tumor transplants, where biopsies of human tumors are implanted into mice, maintain much of their original cellular content and architecture (including a human vascular network, for example) and can thus be

www.manaraa.com

advantageous in some studies involving the tumor microenvironment [14]. However, it is important to note that immunocompromised systems may lack elements of the microenvironment such as T cells that can play critical roles in the regulation of tumorigenesis.

The use of genetically modified mice can get around some of the limitations of the xenograft model system. Genetically modified mice can be broken down into two categories, mice that overexpress oncogenes in specific tissues and mice that have genetic deletions. In prostate cancer, transgenic adenocarcinoma of the mouse prostate (TRAMP) mice and PTEN-null mice are common examples of the former and latter categories, respectively [15]. Genetically modified mice can spontaneously form tumors with the similar progression to human prostate cancer and retain an immune-competent and organ-relevant microenvironment. However, the disadvantages to these systems include high cost and a general lack of flexibility compared to xenografts, where it is easier to perform specific cellular manipulations.

1.4 Matrigel

As described in section 1.3, standard *in vivo* xenograft models primarily consist of subcutaneously injected cells or cells mixed with ECM prior to injection and result in largely homogenous growths derived from one cell line. Matrigel has been used as the gold standard matrix for xenografts in many labs for years. Matrigel, a basement membrane formulation derived from the Engelbreth-Holm-Swarm mouse sarcoma, can expose cancer cells to exogenous soluble signaling molecules and ECM interactions that may not be representative of their native environment and cannot be specifically identified or managed due to batch variability [16]. In addition, Matrigel contains a number of growth factors and cytokines that may or may not be appropriate for the microenvironment of all malignancies. The major ECM components of Matrigel include laminin-1 ($\alpha1\beta1\gamma1$), collagen IV, enactin (nidogen-1), and perlecan (heparin sulfate proteoglycan). Caution regarding interpretation of results when cells have been exposed to Matrigel has been expressed for over 20 years due to the identification of several growth factors that were purified along with the basement membrane matrix components. These growth factors include transforming growth factor beta (TGF-β), platelet-derived growth factor (PDGF), basic fibroblast growth factor (bFGF), and epidermal growth factor (EGF). In fact, proteomic analysis demonstrated over 1800 unique proteins across multiple batches of Matrigel [17]. These

www.manaraa.com

results suggest that exposing cells to Matrigel in any model system introduces elements that cannot be controlled, which is undesirable given the already complex nature of the tumor microenvironment.

1.5 The Tumor Microenvironment

The study of a disease as complex as prostate cancer requires preclinical model systems that accurately capture the tumor microenvironment as a dynamic, heterogeneous tissue system. For many years, there has been an increasing recognition that the tumor microenvironment plays a critical role in events from tumorigenic initiation through metastasis, which are defined by signaling between cancer cells, immune cells, fibroblasts, endothelial vessels, and ECM proteins [18][19]. It has been shown that in many carcinomas, much of the tumor mass is made up of stromal components [20]. Carcinoma-associated fibroblasts (CAFs) are typically myofibroblastic in lineage, expressing alpha smooth muscle actin. This differentiation can be stimulated by secretion of factors such as TGF-β and PDGF from cancer cells. In turn, CAFs can secrete proteins such as matrix metalloproteinases that alter the local ECM and allow tumor progression [21]. Olumi, *et al*. showed that CAFs injected into mice with non-tumorigenic prostate epithelial cells spurred their proliferation and altered their histology while normal fibroblasts did not [22]. Tumor-associated macrophages (TAMs) are another critical component of the tumor stroma. Infiltrating TAMs are harnessed by the tumor microenvironment to differentiate to a largely pro-tumorigenic phenotype where they are responsible for the stimulation of angiogenesis, the re-organization of ECM proteins, and the suppression of the adaptive immune response (see section 5.1.4 for more information about TAMs) [23]. One of the classical hallmarks of cancer is that soluble signaling factors such as vascular endothelial growth factor (VEGF), bFGF, and IL-8 that are mediated by hypoxia, tumor cells, and stromal cells can flip the microenvironmental angiogenic switch and induce blood vessel growth into the tumor, allowing it to continue to expand. In order for this angiogenesis to take place, local ECM structure must be re-organized in order for blood vessels to infiltrate into the tumor tissue [24]. This re-organization is mediated by CAFs, TAMs, and other cell types. The new blood vessels tend to be immature, however, and interstitial fluid build-up and incomplete waste exchange can lead to higher tissue pressures within the tumor along with permanent areas of hypoxia.

www.manaraa.com

Because of the critical roles of the tumor microenvironment in cancer progression, it remains a viable target for many anti-cancer therapies [18], with some anti-angiogenic therapies having already made it to the clinic. However, an incomplete understanding of the microenvironment and the ability of cancer to adapt to this therapeutic strategy has limited its overall effectiveness. Many of the current preclinical models used to study basic cancer biology and screen potential future drug candidates are insufficient because they do not provide adequate control over these tumor-microenvironmental interactions.

1.6 Biomaterials-Based Cancer Model Systems

To address the issue of microenvironmental control in preclinical cancer model systems, an emerging area of research involves the tissue engineering of 3D tumor models for both *in vitro* and *in vivo* analysis [25][26][27][28]. These models are generated using a standard tissue engineering paradigm, which starts with fabricating a natural or synthetic biomaterial scaffold, seeding that scaffold with cells of interest, and culturing the seeded scaffold to grow a 3D tissue. It has been well established that cancer cells cultured in three dimensions better reflect *in vivo* behavior than their two dimensional counterparts [29][30]. Synthetic biomaterial scaffolds provide an opportunity for advanced studies involving precise manipulation of the tumor microenvironment in a controlled way through surface chemistry, sustained soluble factor release, tunable degradation rates, and variable mechanical properties [31]. Thus, a tissue engineered tumor construct can re-create more physiologically relevant representations of cell proliferation, signaling, and cell-matrix interactions than many model systems currently in widespread use [25].

Biomaterials that have been used as platforms to generate cancer models include poly(lactide-co-glycolide) (PLG) [32], poly(lactic acid) (PLA) [33][34], poly(ethylene glycol) (PEG) [35], alginate [36][37], chitosan [38][39][40], silk [41], and hyaluronic acid (HA) [42][43]. In general, studies comparing 3D models derived from biomaterials to 2D cultures from cell lines across a range of cancer types have demonstrated *in vitro* proliferation rates closer to those measured *in vivo* [32][39], differential gene expression most notably in the form of upregulated angiogenic factors [32][38][39][44], and enhanced drug resistance [32][34][39][45]. In addition, when seeded biomaterials are implanted *in vivo*, xenografts have displayed accelerated tumor growth

www.manaraa.com

with higher vascularization [32][39][42]. Biomaterial scaffolds have also been used as the basis for metastasis models and the study of tumor/engineered microenvironment interactions. Moreau, *et al*. used silk scaffolds seeded with bone marrow stromal cells and doped in bone morphogenic protein-2 to attract metastatic human breast cancer cells in mice [46]. Pathi, *et al*. accomplished the same end using PLG scaffolds containing hydroxyapatite nanoparticles [47]. Ko, *et al*. demonstrated preferential migration of metastatic cancer cells to areas of inflammation induced by the injection of PLA microspheres, which could be modulated by controlled chemotactic factor release [48]. Lee, *et al*. showed recruitment of leukemic cells to implanted porous poly(acrylamide) scaffolds seeded with bone marrow stromal cells [49].

1.7 Summary

The purpose of the studies presented in this dissertation is to generate *in vivo* prostate cancer xenografts derived from synthetic biomaterial scaffolds. Chapter two focuses on *in vitro* methods development from scaffold fabrication through 3D cell culture within the scaffolds. Chapters three and four focus on the *in vivo* implantation of scaffolds seeded with human prostate cancer cell lines and the analysis of the resulting xenografts. Chapters five and six focus on more detailed cellular and molecular investigations of scaffold-derived tumors from a cell line that under standard xenograft conditions represents a prostate cancer dormancy model.

www.manaraa.com

Chapter 2. *In Vitro* Methods for 3D Cell Culture and Analysis within Porous Scaffolds

2.1 Background

2.1.1 Motivation

The primary reason that the use of 3D cell culture technologies has been limited is because the third dimension can present numerous technical challenges, including but not limited to substrate/surface selection, cell seeding, oxygen/nutrient diffusion, cell viability/proliferation assays, and imaging. In this chapter, methods to seed, culture, and measure proliferation of prostate cancer cells in three dimensions within porous biomaterials will be described. In subsequent chapters, these techniques will be used to tissue engineer *in vivo* prostate cancer xenografts.

2.1.2 Sphere-Templated Biomaterials

There are many choices when it comes to a 3D substrate for cell culture, and there is no defined standard that is generally accepted like the tissue culture polystyrene (TCPS) in widespread use for 2D analysis. Since substrate materials can be natural or synthetic, they can vary greatly in chemistry, and can be fabricated into numerous architectures or topographies with varying mechanics and cell attachment sites. Every element of the substrate that can be manipulated has the potential to affect cellular response. The studies presented here utilize non-degradable cross-linked poly(2-hydroxyethyl methacrylate) (pHEMA) hydrogels fabricated by sphere-templating for 3D cell culture. Sphere-templated biomaterials have been used for cardiac tissue engineering [50], bone regeneration [51], percutaneous devices [52], and fundamental studies of the foreign body response [53]. Sphere-templated materials are comprised of a network of interconnected spherical pores of uniform size displaying an inverted colloidal crystal geometry (see Figure 2.2). The biological rationale for the choice of pHEMA and the sphere-templated porous architecture for an *in vivo* cancer model can be found in section 3.1.2, but for the purposes of this chapter we will focus on the challenges and optimization associated with the application of these scaffolds for *in vitro* 3D cell culture.

www.manaraa.com

2.1.3 Cell Seeding Methodologies

One of the primary obstacles in generating tissue-engineered 3D cancer models or other tissue engineered constructs used for regenerative medicine is developing efficient and reliable methods to seed cells within scaffolds. A variety of seeding protocols have been described in the literature, and in general they can be classified as either static or dynamic methods. Static methods involve simply pipetting a cell suspension on top of the 3D scaffold and allowing gravity and/or natural cell migration to facilitate scaffold seeding [54]. Dynamic seeding methods typically involve some convection or other action designed to ensure better cell distribution within the scaffold. Common dynamic methods described in the literature include spinner flasks [55], perfusion bioreactors [56], injection [57], centrifugation [58], and vacuum filtration [59]. However, in many papers details regarding this critical step in the tissue engineering process remain vague or unmentioned.

Seeding optimization is strongly dependent on scaffold architecture. The architecture created by sphere-templating fabrication can present challenges for cell seeding because small pore sizes and pore interconnect (throat) diameters can restrict the ability of cells to infiltrate the scaffolds. However, the sphere-templating fabrication protocol allows for controllable modulation of these parameters, and thus the empirical optimization of cell seeding. Here, a quick, simple, and inexpensive dynamic method using capillary force is described to seed M12 and LNCaP C4-2 human prostate cancer cell lines into sphere-templated pHEMA hydrogels. The biological rationale for the choice of these cell lines is presented in section 3.1.3 and 4.1.2, respectively.

2.1.4 Culturing Cells in Three Dimensions

Another challenge for *in vitro* tissue engineering is the optimization of cell culture conditions. Techniques for 3D cell culture can be categorized as static, dynamic, or perfusion. Static methods are reminiscent of 2D cell culture where scaffolds are placed in a multi-well plate or petri dish containing media. Static culture is most common due to its simplicity, and is most effective for thinner constructs or short culture times due to the potential for oxygen/nutrient diffusional limitations. When placed in a static environment, cells in the center of thicker scaffolds may not survive and areas of necrosis may form within the seeded scaffolds. Dynamic culture adds a convective element that aids in oxygen/nutrient transport. Dynamic culture

www.manaraa.com

apparatuses can include rocking platforms, orbital shakers, spinner flasks, and many batch bioreactors. Perfusion culture usually involves a bioreactor system that pumps fresh media continuously around or through the seeded scaffold. In the studies presented here, dynamic 3D cell culture is performed using an orbital shaker, where cell-seeded 1 mm-thick scaffold discs are placed in multi-well plates on top of custom platforms designed to allow media circulation over and under the scaffold.

2.1.5 Measuring Cell Proliferation in Three Dimensions

Assays and experiments that are relatively simple to perform and analyze in two dimensions can become much more cumbersome and often unreliable after adding a third dimension due to diffusional concerns and imaging difficulties [60]. For example, proliferation assays such as alamarBlue® (AB), MTT, or WST-1® that rely on cell metabolism to generate a quantifiable product require the applied reagent to diffuse to all cells in the scaffold and the resulting product to diffuse back into solution and out of the scaffold for accurate quantification. Depending on the porosity, tortuosity and cell density within a 3D construct, there can be questions regarding whether the measurements are accurate because the reaction may be diffusion-limited. Terminal analyses involving lysed cells can be attractive alternatives as the basis for proliferation assays in scaffolds because all cells from the scaffold surface to the interior are lysed and contribute to the final measurements. These endpoint analyses include measurement of DNA content. The following studies will utilize PicoGreen® (PG), a highly sensitive fluorescent double stranded DNA binder, for the measurement of prostate cancer cell proliferation within porous pHEMA scaffolds.

2.2 Hypothesis

It is hypothesized that:

(1) Capillary force can be used as a dynamic cell seeding technique that is effective for evenly distributing prostate cancer cells within sphere-templated pHEMA hydrogels

(2) Dynamic 3D cell culture using an orbital shaker will improve prostate cancer cell viability and proliferation within porous pHEMA hydrogels

(3) PicoGreen DNA analysis can be used as the basis for a prostate cancer cell proliferation assay within non-degradable porous pHEMA hydrogels

www.manaraa.com

2.3 Materials and Methods

2.3.1 Scaffold Fabrication

Sphere-templated pHEMA scaffolds were prepared as previously described [53]. An overview of the fabrication protocol is shown in Figure 2.1. Briefly, spherical poly(methyl methacrylate) (PMMA) beads (Kupa, Inc.) were sieved using an ATM sonic sifter to a uniform size range of 74-86 µm. The beads were inserted into 1 mm thick glass rectangular molds and sonicated for 20 min to ensure particle packing. The molds were then sintered overnight at 140 °C for 22 or 24 hours in a convection oven (Thermo Scientific) to fuse the beads at points of contact. pHEMA was prepared by first infiltrating the sintered molds with a mixture comprised of monomeric HEMA (ophthalmic grade, Polysciences, Inc.) (60% vol/vol), cross-linker tetraethylene glycol dimethacrylate (TEGDMA, Polysciences, Inc) (1.8% mol/mol HEMA), initiator 2,2-dimethyoxy-2-phenylacetophenone (IRGACURE 651, Ciba) (1% mol/mol HEMA), ethylene glycol (JT Baker) (17% vol/vol), water (18% vol/vol), and cell attachment substrate collagen I (BD Biosciences) (15% wt/vol). Polymerization was photoinitiated under a UV lamp (Hanovia) for 10 minutes. The polymer-bead cakes were then continuously washed with dichloromethane for 72 hours in a soxhlet extractor, solubilizing the PMMA beads and leaving a cross-linked polymer network with uniform spherical pores interconnected at the regions where the beads were sintered together. The polymer scaffolds were sterilized for 48 hours in 70% ethanol prior to rehydration in sterile phosphate buffered saline and cell culture.

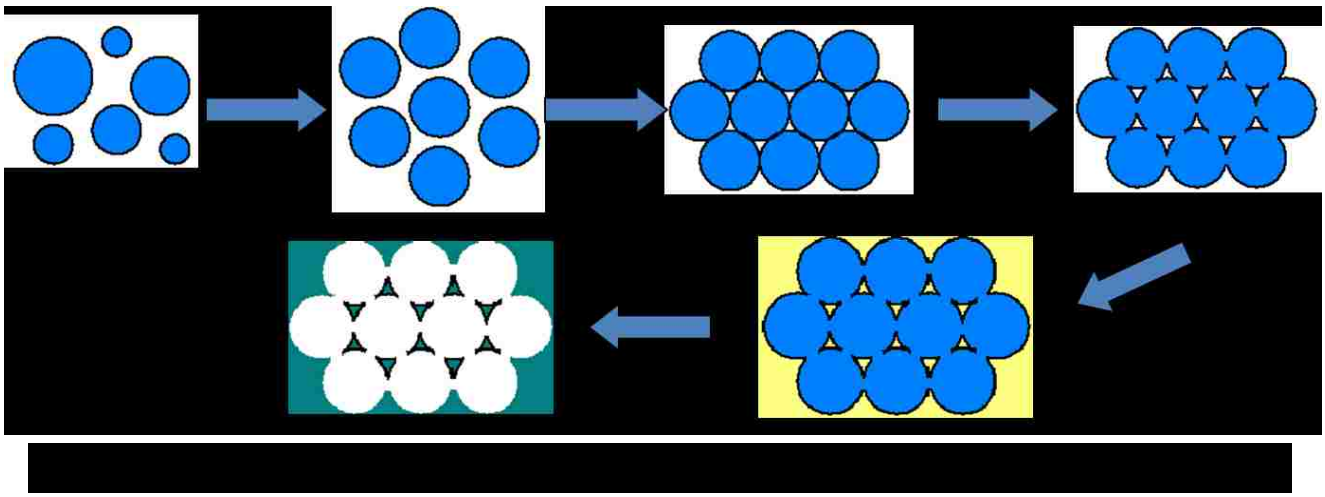

www.manaraa.com

2.3.2 Cell Culture

After rehydration, pHEMA scaffolds were punched into 6 mm discs using sterile biopsy punches (Acuderm) using and pre-incubated in media for 1 hour at 37 °C prior to cell seeding. Two human prostate cancer cell lines, LNCaP C4-2 (from R.A. Sikes, University of Delaware) and M12 [60] were used for this study. LNCaP C4-2 cells were cultured in RPMI 1640 containing 10% fetal bovine serum (FBS). M12 cells were cultured in RMPI supplemented with 5% fetal bovine serum (FBS), 10 µg/mL insulin, 5.5 µg/mL transferrin, 6.7 ng/mL sodium selenite, 250 ng/mL amphotericin B, 50 µg/mL gentamycin, 10 ng/mL epidermal growth factor (EGF), and 78 ng/mL dexamethasone (all media and supplements from Cellgro). All 3D cell cultures within scaffolds were performed in 24-well plates containing 1 mL of culture media and a custom sterile stainless steel mesh platform that raised the scaffold ~ 1.5 mm and allowed media to circulate under the scaffold. Those plates were placed on an orbital shaker set to 300 rpm within a tissue culture incubator. Culture media was replaced every two days.

2.2.2 Cell seeding

Cells were seeded into the scaffolds using three methods. For static and centrifugation seeding, scaffold discs were fit into the wells of a 96-well plate that matched their 6 mm diameter to direct cell infiltration into, and not around, the scaffolds. A 200 µL suspension of $1x10^6$ cells was pipetted on top of the scaffold. For centrifugation seeding, the cell suspensions were centrifuged into the scaffolds at 200 x g for 15 min. For capillary force seeding, scaffolds were placed on top of a stack of five to six Kimwipes (Kimberly-Clark) and 50 µL of a $1x10^7$ cells/mL suspension was twice layered on top of each scaffold, allowing cells to be drawn into the pores. For all methods, seeded cells were allowed to attach to the scaffolds overnight before being transferred to a 24-well dynamic culture in an orbital shaker.

2.3.4 Histological Analysis

Cells were cultured *in vitro* for up to seven days within the scaffold. Cell proliferation was tracked qualitatively using histological methods. Scaffolds were fixed overnight at 4 °C in a solution of 90% methanol and 10% acetic acid. After fixation, the scaffolds were dehydrated in ethanol and cleared with xylene prior to paraffin embedding. The embedded scaffolds were sectioned into 5 µm thick sections with a Leica microtome and placed on positively charged

www.manaraa.com

slides (Fisher) that prevented pHEMA section detachment during staining. Fixed paraffin sections were heated at 53 °C for 30 minutes prior to xylene deparaffinization and rehydration through a graded ethanol series. Slides were stained using a standard hematoxylin and eosin (H+E) protocol and imaged on a Nikon E800 microscope equipped with Metamorph software (version 6.0, Molecular Devices).

2.3.5 Quantitative Proliferation Analysis

Seeding efficacy and proliferation of M12 and LNCaP C4-2 cells within the scaffolds were quantitatively measured using a PicoGreen® DNA assay (Invitrogen). To establish working sample dilutions and a cell number reference, fluorescence standard curves were produced by freeze–thawing triplicate aliquots of M12 and LNCaP C4-2 cells from 2D culture in 1 mL nuclease-free water at -80 °C (Ambion). Samples ranged from $6.25x10^4$ cells to $2x10^6$ cells. To determine the minimum dilution necessary to eliminate PicoGreen fluorescence quenching, standard curve samples were serially diluted from 1:1 to 1:50 in the TE buffer. 100 µL of diluted DNA sample was added to 100 µL of 1x PicoGreen in blackwalled 96-well plates and 480 nm excitation/525nm emission fluorescence was measured using a Safire2 microplate reader (Tecan). 1:20 and 1:50 sample dilutions were sufficient to eliminate quenching concerns for M12 and LNCaP C4-2 cells, respectively.

To determine seeding efficacy and proliferation in three dimensions, scaffolds were seeded with M12 and LNCaP C4-2 cells for 0-, 1-, 3-, 5-, and 7-day proliferation endpoints. Five day 0 (D0) samples for each cell line were frozen immediately after seeding, whereas other samples were cultured in triplicate as described until their respective endpoints. Scaffolds were frozen at -80 °C in 1 mL of nuclease- free water. After thawing, 0.1% Triton-X-100 detergent was added and samples were vortexed for 60 s, sonicated for 10 min, and vortexed again before 1:20 (M12) or 1:50 (LNCaP C4-2) sample dilution in the TE buffer for analysis. Cell samples from 2D culture for a same-day standard curve comparison were treated the same and analyzed along with all scaffold samples. 100 µL of a diluted DNA sample was added to 100 µL of 1x PicoGreen and fluorescence was measured. Linear standard curves of 480/525nm fluorescence versus the cell number were prepared and the 3D scaffold cell content was determined. To confirm effective decellularization of the scaffolds, freeze–thawed scaffolds were fixed, paraffin processed, and

www.manaraa.com

stained with H&E as described.

2.3.6 Scanning Electron Microscopy (SEM)

SEM was performed at the University of Washington Nanotech User Facility. Scaffolds were frozen, lyophilized, and gold sputter-coated prior to observation on an FEI Sirion scanning electron microscope.

2.3.7 Digital Volumetric Imaging (DVI)

DVI was performed using an apparatus manufactured by The Microscience Group, Inc. After fixation, scaffolds were stained with the fluorescent dyes eosin Y and acridine orange *en bloc* ("whole-mount"), dehydrated in a graded ethanol series to xylene, and embedded in opacified epoxy resin. This opacification blocked out-of-plane fluorescence for clearer imaging of the current section. Blocks were serially sectioned with an automated diamond knife microtome. After each section was cut, a fluorescence microscope and digital camera were used to capture a multi-wavelength image of the block face, and the block was advanced. Sections were acquired at either 0.9 or 0.45 μm thickness (corresponding to 10x or 20x magnification, respectively), and a typical DVI acquisition consisted of 300 to 1000 sections. The resulting aligned stack of images was compiled into a three-dimensional data set. Custom software allowed data rendering and navigation in all orientations, as well as segmentation of regions of interest [62].

2.4 Results

2.4.1 In Vitro *Cell Seeding*

Figure 2.2 shows representative DVI and SEM images of sphere-templated pHEMA scaffolds displaying a network of interconnected spherical pores around 80 μm in diameter. Cell seeding into this construct was performed using static, centrifugation, and capillary force-based techniques. Figure 2.3 shows H+E-stained histological cross sections and DVI of cell-seeded scaffolds. As evaluated qualitatively by histology, the capillary force method was more successful at loading cells within the scaffolds than static seeding or centrifugation, which resulted in fewer cells in the construct and cells largely being confined to surface pore layers. In contrast, the capillary force-seeding technique yielded a higher cell content and a relatively even cell distribution within the scaffolds immediately after seeding (see Fig. 2.3 A, D, F, G). Cell

www.manaraa.com

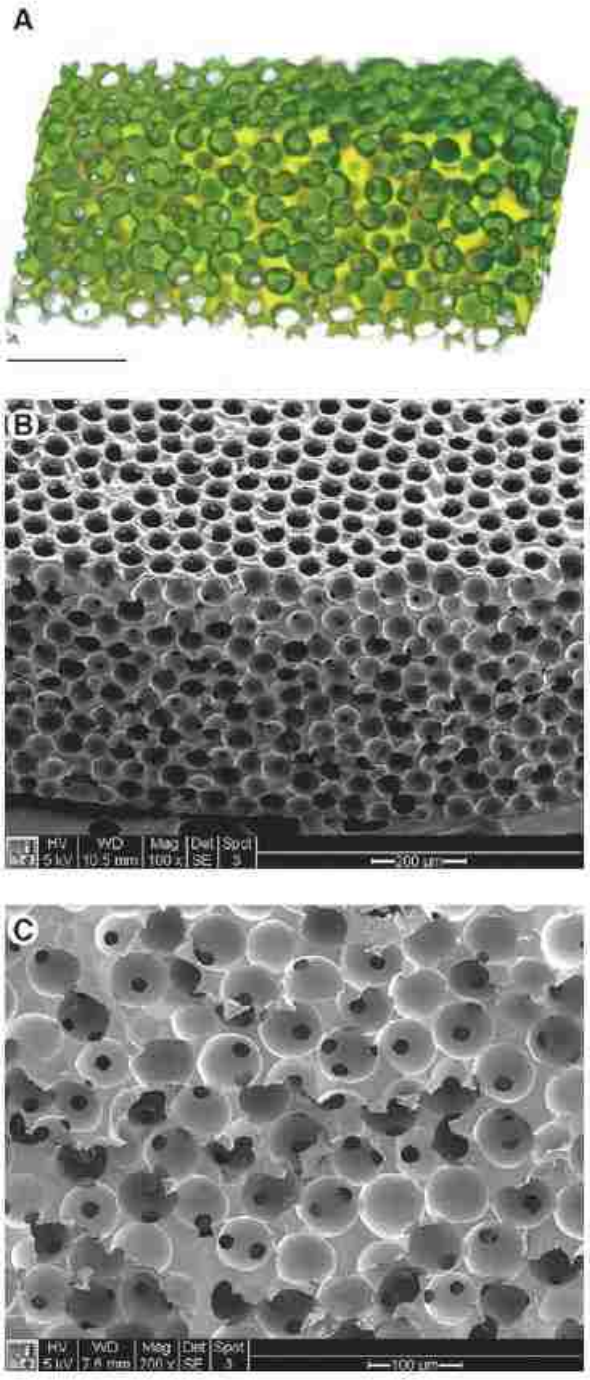

infiltration for the capillary force method was empirically optimized for each cell line by modulating sintering time during scaffold fabrication, which altered the pore interconnect (throat) diameter. Cell navigation through these pore interconnects during seeding is likely a constraint on seeding efficacy, where the cell size relative to the pore throat diameter is a critical parameter. The sphere-templated scaffold has high pore interconnectivity, and many pores have multiple pore throats. As cell suspensions move through the scaffold, smaller pore throats will be occluded by trapped cells, but larger pore throats exist for cells to pass successfully through. As evaluated by SEM, 22 h sintering on 76-84 µm PMMA particles yielded an average pore throat diameter of 19.3 +/- 1.7 µm and 24 h sintering yielded an average pore throat diameter of 20.9 +/- 2.5 µm. Twenty-two hours sintering was most effective for seeding M12 cells, which have a rounded cell diameter of 11.8 +/- 2.0 µm, whereas 24 h sintering worked best for the larger LNCaPC4-2 cells, which have a rounded cell diameter of 17.1 +/- 2.6 µm. Although the difference in the pore throat size between 22 and 24 h sintering times was not statistically significant, it was large enough to affect seeding. For the smaller M12 cells, the increase of 1.6 µm/2.4 µm (average/upper bound) for the 24 h sintered scaffolds was enough to allow many more M12

www.manaraa.com

cells to pass entirely through the scaffolds. Conversely, for the LNCaP C4-2 cells, the smaller pores associated with the 22 h sintered scaffolds resulted in more cells getting stuck as they navigated through the porous network.

2.4.2 In Vitro *Cell Culture*

Histological images of M12 and LNCaP C4-2 cells seeded within the pHEMA scaffolds showed consistent patterns of growth between the cell lines. After 24 h, cells had attached to the collagen-embedded pore walls of the scaffold, and by 7 days, cells had proliferated to fill many of the pores and the interconnects between the pores (see Fig. 2.3 C, H, I). By 7 days in culture, a necrotic zone was noted in the center of the scaffold (see Fig. 2.3 B, E), presumably due to limitations in nutrient/oxygen diffusion and waste exchange. The distance penetrated into the scaffold by cells at 7 days under static culture was 145.2 – 29.3 μm, which corresponds approximately to the limit of oxygen diffusion in tissues. The size of the necrotic zone decreased when scaffolds were placed in dynamic culture using an orbital shaker, with convection increasing the distance penetrated by cells to 237.3 – 33.0 μm. In addition, stainless steel mesh inserts that allowed media to circulate under the scaffolds improved cell viability on the bottom scaffold surface.

Because comparisons between biomaterial scaffold-derived grafts and traditional xenografts in vivo require seeded cell quantification, a PicoGreen DNA assay was developed to track cell seeding efficacy and proliferation within the scaffolds (see Figure 2.4). During capillary force seeding, it is possible that some cells will pass all the way through the porous network and, thus, will not be retained after being applied to the scaffold. Indeed, we found variability in the number of cells present after seeding on D0, with seeding efficacies ranging from 27.3%–66.5% for M12 cells and 37.0%–72.8% for LNCaP C4-2 cells. Both cell lines also experienced an average loss of cells by D1, which can be potentially explained by cells on the top surface or bottom pore layers of the scaffold falling off or out of the scaffold when it was transferred to dynamic culture. Both cell lines showed significant increases in cell number on D3, D5, and D7 compared to D1. M12 cell number reached $1x10^6$ by D3 and this value remained statistically equivalent over D5 and D7. This consistency may be attributed to cells reaching their proliferation capacity within the pores that are not diffusion limited. LNCaP C4-2 cells showed a

www.manaraa.com

more gradual increase in cell number over time, with no significant difference between D3 and D5, but a significant increase from D5 to D7.

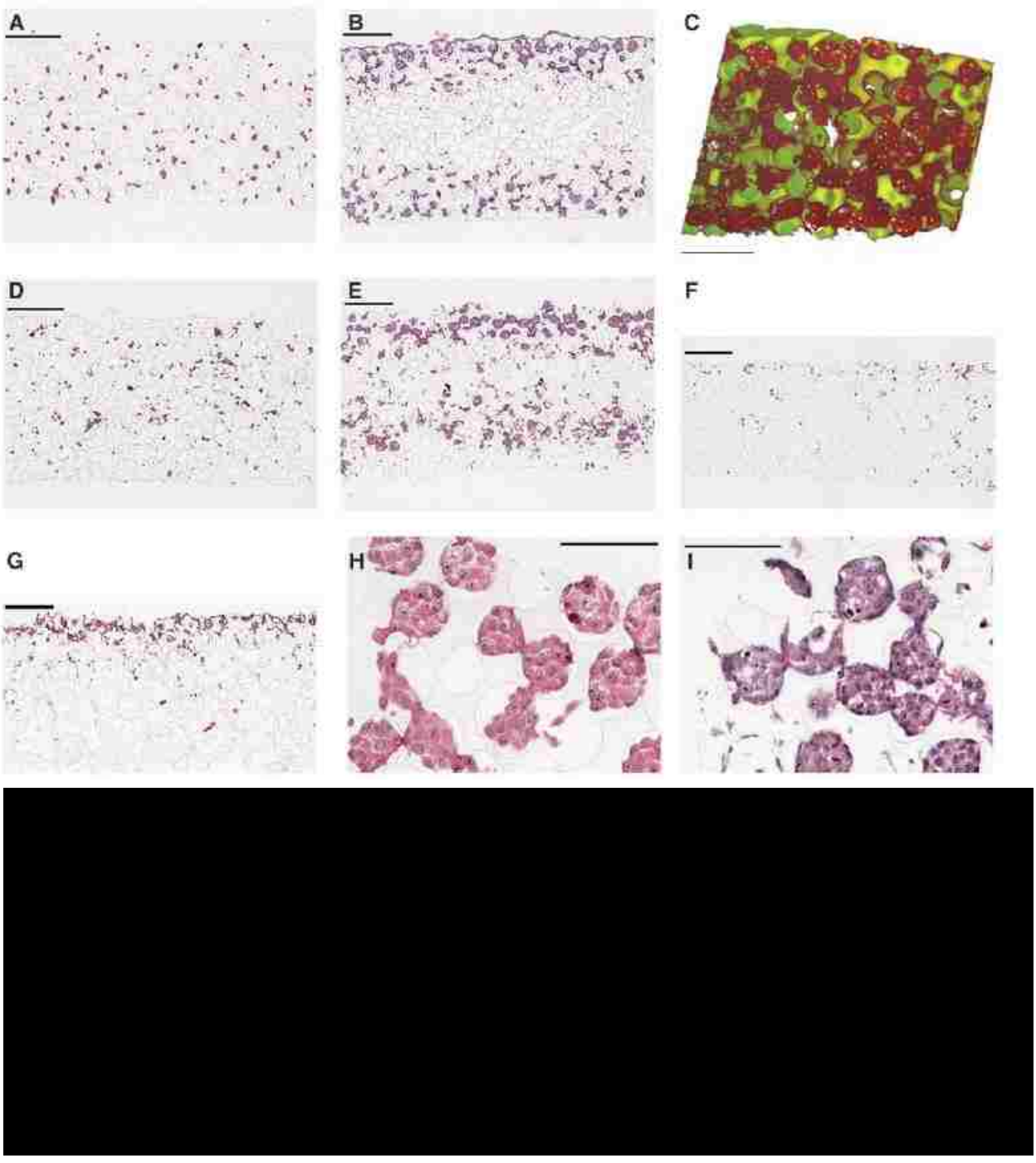

www.manaraa.com

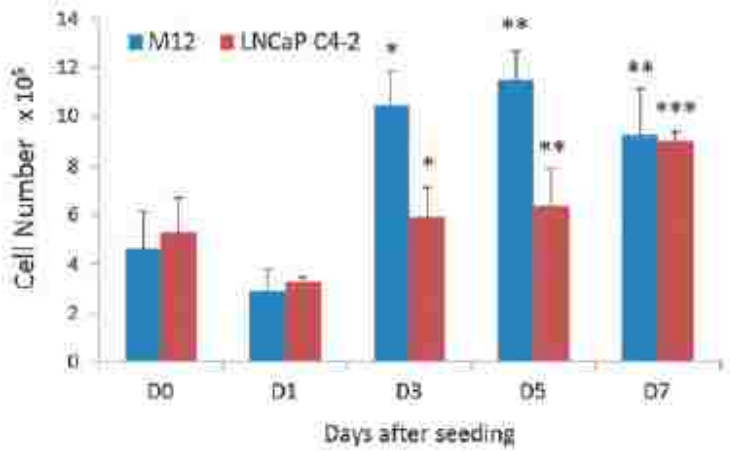

2.5 Discussion

In these studies, we have developed *in vitro* cell seeding and culture methodologies that can be used in the generation and analysis of engineered tumor models based on sphere-templated pHEMA scaffolds. Capillary force-based cell seeding of these scaffolds can be empirically optimized by modulating the following parameters: scaffold pore size, sintering time (interconnect throat size), cell suspension concentration, and the number of times an aliquot of cells is applied to the scaffold. M12 and LNCaP C4-2 prostate cancer cells were most effectively seeded into scaffolds with a pore size around 80 µm using 22 and 24 hour sintering times, respectively. A longer sintering time accommodated the larger LNCaP C4-2 cells by allowing them to pass through larger pore interconnects. It should be noted that the same sintering times with different pore sizes (i.e. different template sphere sizes) yielded sub-optimal results, so these parameters need to both be adjusted for each cell line. For this reason, optimization for co-culture studies where there are large differences in size between cell types could be challenging. In addition, for larger cells it may be difficult to seed small pore size materials using capillary force since most cells will be confined to the surface pore layers. This pore size limitation is particularly important because it has been demonstrated that a 38 µm pore size is optimal for biointegration upon material implantation, with highest vascularity and lowest fibrous capsule thickness [53]. To potentially avoid seeding limitations for small pores, a thermoresponsive poly(N-isopropylacrylamide) (pNIPAM) scaffold can be seeded at room temperature and then cultured at 37 ºC, as demonstrated by Galperin, *et al*. [63-64]. The expanded pores at 25 ºC will shrink at 37 ºC and trap cells in smaller pores. At the other extreme, pores that are too large may

www.manaraa.com

lead to significant cell loss using the capillary force technique since cells will too easily pass through the pore network and leave the scaffold. In this case, sintering time may be reduced to decrease the pore interconnect size or other seeding methodologies may be more appropriate.

Varying cell suspension concentrations and the number of times a suspension is applied to the scaffold can also impact seeding efficiency. In this case, the application of $1x10^6$ total cells from twice layering 50 µL of a $1x10^7$ cells/mL suspension was optimal. Applying too dilute a suspension many times usually resulted in significant cell loss, while too concentrated a suspension yielded cells clustered in one or two surface pore layers. Material selection also makes a difference; if cells adhere strongly to the material, they are less likely to travel quickly through it and seeding efficiency may be improved. These studies utilized pHEMA with embedded collagen I. Without the collagen, the low cell adhesion associated with the hydrophilic pHEMA may have reduced the seeding efficacy. Finally, it should be noted that cancer cells may be more amenable to this type of seeding than other non-transformed cell types due to their enhanced elasticity [65], which may have provided them the capacity to deform while navigating the porous scaffold network. That said, capillary force seeding subjects cells to a minimal amount of force compared with methods such as vacuum filtration, which can shear and deform cells.

Once seeded, maintaining viable cells within a sphere-templated scaffold *in vitro* for longer than a few days also presented challenges. It was determined that necrotic zone thickness could be reduced using the convection provided by a simple orbital shaker. This enhanced cell penetration into the scaffold using dynamic culture agrees with previously demonstrated results with inverted colloidal crystal scaffolds [66]. In addition, scaffolds in both static and dynamic culture lost viable cells over seven days along the edge of the scaffold lying on the bottom of the tissue culture plate. To compensate for this, a stainless steel mesh platform was used to raise the scaffold and allow media to flow under the scaffold, which significantly improved cell viability and decreased necrotic zone size.

Concerns regarding the measurement of cell proliferation in three dimensions have been expressed [60]. In a non-degradable tortuous construct, extracting viable cells is a difficult if not

www.manaraa.com

impossible task. Non-endpoint metabolic analyses such as alamarBlue® are limited by diffusional concerns, and it was observed that proliferation trends measured by alamarBlue did not correlate reliably with histology (data not shown). In addition, cell number comparisons between standard curves obtained using cells from 2D monolayer culture would just be approximations since cell metabolism can change between 2D and 3D culture. Endpoint DNA analysis allows for the elimination of these diffusional and metabolic concerns. In these studies, a PicoGreen DNA assay was developed to accurately quantify cells, which allowed for the estimation of seeding efficiency and cellular proliferation of two prostate cancer cell lines within sphere-templated pHEMA scaffolds. The observed variability in seeding efficacy was expected given the nature of the capillary force cell seeding technique, but the resulting cell proliferation generated seeded scaffolds reliably containing around $1x10^6$ cancer cells after seven days culture. These constructs will serve as the basis for the biomaterials-derived tissue engineered prostate cancer xenografts presented in chapter three.

www.manaraa.com

Chapter 3. Porous Scaffold-Based M12 Prostate Cancer Xenografts

3.1 Background

3.1.1 Motivation

Biomaterial scaffolds have shown promise as the basis for *in vitro* and *in vivo* 3D cancer models. Tumors engineered from biomaterials have shown evidence of being more physiologically relevant than some traditional preclinical model systems, and synthetic biomaterials provide the added potential for enhanced microenvironmental control (see section 1.6). In this chapter, sphere-templated pHEMA scaffolds are used as the basis for engineering *in vivo* xenografts from M12 human prostate cancer cell lines. The following studies detail the implantation and analysis of these engineered cancer constructs.

3.1.2 Sphere-Templated Biomaterials and the Foreign Body Response

The foreign body response (FBR) is a well-studied immune reaction to implanted biomaterials [67]. In the classical FBR, neutrophils are the first cellular responders to the implant, followed by activated macrophages that attempt to surround and phagocytose the material by fusing together into foreign body giant cells. Since the material cannot be degraded (frustrated phagocytosis), fibroblasts are recruited to lay down a dense collagenous avascular foreign body capsule to segregate the material from the surrounding tissue. A driving force in biomaterials research has been to develop materials that show better healing properties that can integrate with surrounding tissue and become vascularized [68]. Sphere-templated materials, the fabrication of which was described in section 2.3.1, display a FBR where the material itself is vascularized and the foreign body capsule thickness is decreased compared to non-porous slabs of the same material. The FBR to sphere-templated materials is pore size-dependent [50], and a pore size around 38 μm in diameter has been shown to optimize healing by maximizing vascular density and minimizing foreign body capsule thickness [53]. These properties exist independently of material chemistry. pHEMA was selected for these studies due to its well-characterized biocompatibility.

The rationale for sphere-templated scaffolds in the generation of *in vivo* prostate cancer xenografts is that this vascularization will allow an adequate blood supply for tumors to grow. In addition, macrophages and fibroblasts are also recruited to scaffold pores as part of the FBR to the material, which can generate a more complex microenvironment than is attainable through

www.manaraa.com

most *in vitro* or more basic *in vivo* tumor model systems. The scaffold model is potentially advantageous over Matrigel-based xenografts because it lacks exogenous growth factors and ECM proteins that can form an uncontrolled microenvironment. pHEMA is readily modifiable in terms of surface chemistry. For example, co-polymerization with methacrylic acid (MAA) introduces carboxylic acids to the polymer surface, which can be used to attach proteins through 1-ethyl-3-[3-dimethylaminopropyl]carbodiimide hydrochloride / *N*-hydroxysuccinimide (EDC/NHS) chemistry (see Figure 4.1). The synthetic nature of pHEMA also renders it reproducible in terms of fabrication and tunable in terms of its degradation and mechanical properties.

3.1.4 M12 and P69 Cells

M12 cells were developed as a mouse model system for the tumorigenesis of prostate epithelial cells. Bae, *et al*. isolated human prostate epithelial cells and immortalized them using the SV40 large T antigen (SV40T) to form the P69 cell line. When injected subcutaneously into nude mice, P69 cells were poorly tumorigenic, with only two of eighteen mice forming tumors. These tumor cells were isolated, expanded *in vitro*, and re-injected several times to form a highly tumorigenic prostate epithelial line known as M12 [61] (see Appendix 1 for cell line generation diagram). M12 cells do not require Matrigel to form subcutaneous tumors, so these cells were chosen (1) to confirm that sphere-templated pHEMA scaffolds can be used as vehicles for xenograft formation and (2) to determine if there are any potential differences in cell growth rates and vascularity when cells are pre-cultured and implanted within porous scaffolds. P69 cells serve as a negative control for M12 tumor growth.

3.2 Hypothesis

It is hypothesized that sphere-templated pHEMA scaffolds can be used as the basis for *in vivo* prostate cancer xenografts from M12 cells that display unique properties and serve as a potential alternatives to gold standard Matrigel-based xenografts.

www.manaraa.com

3.3 Materials and Methods

3.3.1 3D Cell Culture

M12pc (plasmid control, hereafter referred to as M12) and P69 cells were cultured in RMPI complete media (see section 2.3.2). Sphere-templated pHEMA scaffolds were fabricated and re-hydrated as described in section 2.3.1, and for these cell lines the scaffolds were sintered for 22 hours to optimize pore interconnect size for cell loading. Scaffolds were punched into 6 mm discs and soaked in media for 1 hour at 37 °C prior to cell seeding, which was performed using capillary force as described in section 2.3.2. The same process was used for seeding scaffolds with concentrated Matrigel, with the cell suspension mixed 1:1 by volume with Matrigel at 4 °C while holding the total cell number applied to each scaffold constant at $1x10^6$ cells. Seeded scaffolds were cultured in 24 well plates as previously described in section 2.3.2, where cells were allowed to attach to the scaffold overnight in static culture before being transferred to a dynamic orbital shaker. Cells were cultured in scaffolds for five days prior to *in vivo* implantation with media changed every two days.

3.3.2 Pilot In Vivo *Study*

Animal experiments were approved by the University of Washington Animal Care and Use Committee (IACUC) and followed federal guidelines for laboratory animal use. Scaffold cytotoxicity was evaluated by placing scaffolds in Dulbecco's Modified Eagle Medium (DMEM) for 24 hours, exposing NIH-3T3 fibroblasts to the conditioned media for 48 hours, and visually confirming lack of cytotoxic response by light microscopy. Scaffolds were evaluated for endotoxicity using a standard limulis amebocyte lysate (LAL) gel clot protocol (Lonza). All scaffold batches tested for less than 0.06 EU/mL endotoxin prior to implantation. The pilot M12 study design used is shown in Table 3.1. Seven week old athymic nude mice (Harlan) were anesthetized using 2% isofluorane and one scaffold per mouse was implanted subcutaneously in the dorsal right flank. For mice with cells but without scaffolds,

	pHEMA	pHEMA + Matrigel	Matrigel
No cell control	6	6	5
M12 cells	6	6	6
P69 cells	5	5	5

Table 3.1 *In vivo* M12 and P69 pilot study design showing numbers of athymic nude mice per experimental group. Each group was comprised of a cell line either pre-cultured within pHEMA scaffolds, mixed with Matrigel, or mixed with Matrigel and pre-cultured within pHEMA. pHEMA scaffolds were subcutaneously implanted and cell/Matrigel mixtures were subcutaneously injected.

www.manaraa.com

200 µL of a 1:1 mixture of Matrigel and $1x10^6$ cells were subcutaneously injected. Tumor volume was measured using the equation $V = (LxW^2)/2$, where length and width were determined with calipers. Scaffolds/tumors from two mice in each group were removed after three weeks for preliminary analysis. The rest of the mice were allowed to reach a tumor volume-based study endpoint of twelve weeks. Half of each explant was embedded in optimal cutting temperature (OCT) and stored at -20 °C for cryosectioning while the other half was fixed in 10% neutral buffered formalin overnight at 4 ºC.

3.3.3 Histological Analysis

Fixed explants were dehydrated in ethanol and cleared with xylene prior to paraffin embedding. The embedded scaffolds were sectioned with a Leica microtome, and sections were heated at 53 °C for 30 minutes prior to xylene deparaffinization and rehydration through a graded ethanol series. Slides were stained with a standard Masson's trichrome protocol to analyze basic tissue morphology and imaged on a Nikon E800 microscope equipped with Metamorph software (version 6.0, Molecular Devices). Low magnification trichrome images were stitched together into mosaics using Adobe Photoshop software. For immunohistochemical analysis, sections were washed in tris buffered saline (TBS) and endogenous peroxidases were blocked in a 3% hydrogen peroxide solution in TBS. Antigen retrieval was performed using heated 0.01 M pH 6 citrate buffer. After cooling, sections were blocked overnight at 4 ºC in TBS containing 0.5% tween-20, 4% normal serum (Vector) from the animal in which the secondary antibody was raised and 0.25% immunohistochemical grade bovine serum albumin (BSA) (Vector). Primary antibodies were incubated for one hour at room temperature with a concentration-matched isotype negative control section. Secondary antibodies were incubated at room temperature for 30 minutes. A Vectastain ABC kit (Vector) was used along with a 3,3'-diaminobenzidine (DAB) kit (Vector) to generate a brown positive stain. All sections were counterstained with hematoxylin before dehydration and slide mounting in Permount (Electron Microscopy Sciences). Using this procedure, paraffin sections were stained for the SV40 large T antigen (SV40T) [1:100 rabbit IgG (Santa Cruz), 1:200 goat anti-rabbit secondary (Vector)], F4/80 [1:100 rat IgG (AbD Serotec), 1:200 rabbit anti-rat (Vector)], and mouse pan-endothelial cell antigen (MECA-32) [1:20 rat IgG (BD), 1:200 rabbit anti-rat (Vector)]. OCT-embedded explants were sectioned with a Leica cryotome and dried overnight prior to fixation in cold acetone for 10

www.manaraa.com

min. Cryosections were immunostained using the same procedure as described without peroxidase blocking and with a fluorescent secondary antibody (1:100 donkey anti-rat alexafluor 594 (Invitrogen)) and Vectashield hard set mounting medium with DAPI (Vector).

3.3.4 Immunohistochemical Vasculature Analysis

The vasculature of M12 cell-derived xenografts was visualized by fluorescent immunostaining for MECA-32 on cryosections as described. Three sections per explant were stained. A 2x objective lens was used to take low magnification images of two distinct non-necrotic tumor areas away from the edge of the xenograft. Those images were divided digitally into 7x7 grids using Metamorph software. Five individual areas were selected randomly, and those areas were imaged at high magnification using bright field and fluorescence microscopy. For analysis, the percent area stained by MECA was quantified by applying a triangle threshold coupled with automatic de-speckling using FIJI software. This analysis was employed in place of counting lumens per area because extrapolation of the small number of lumens counted per image to the large explant area proved inaccurate.

3.4 Results

3.4.1 Implant Studies

The studies detailed in chapter two show the capacity of sphere-templated pHEMA scaffolds to support human prostate cancer cell attachment and proliferation during *in vitro* culture. For all *in vivo* studies, cell-seeded scaffolds were cultured for five days prior to implantation. Five days was chosen to avoid substantial necrotic core formation and to approximately match the $1x10^6$ M12 cell number in standard Matrigel xenografts (see section 2.4.2). Figure 3.1 shows growth curves for implanted seeded pHEMA scaffolds and their Matrigel counterparts. Figure 3.1A shows that the growth kinetics for the M12-seeded pHEMA implants with and without Matrigel are statistically equivalent to the standard Matrigel-based xenograft injections. The tumorigenic M12 cells proliferated outside the scaffold material by five to six weeks. Figure 3.2 shows a cross section of an explanted M12 seeded pHEMA-derived tumor at twelve weeks, where a tumor has grown around the scaffold. As expected, the poorly tumorigenic P69 negative control cell line did not form tumors up to twelve weeks after implantation in any experimental group (see Figure 3.1B).

www.manaraa.com

3.4.2 M12 Xenograft Analysis

Twelve week pHEMA explants of M12-derived xenografts show the scaffold in a necrotic core with viable tumor tissue well outside of the scaffold (see Figure 3.2). Cell debris and matrix proteins are retained within the scaffold at this late time point. However, three week explants provide a better indication of early events in tumor formation where M12 cells are actively involved with cells participating in the foreign body response to the material. After three weeks there is an infiltration of F4/80+ activated macrophages into the scaffold in the areas complementary to where SV40T+ M12 cells are located (see Figure 3.3). We have previously observed macrophage infiltration into unseeded implants as part of the natural response to these porous materials *in vivo* [50]. In the present study, by three weeks post-implantation, the M12 cells have begun to proliferate outside the scaffold and invade the foreign body capsule around the material. So, not only are the cells seeded within the scaffold exposed to the macrophages that infiltrate within it, but the cells that proliferate out of the scaffold are also exposed to the macrophages present in the capsule. Thus, one of the key microenvironmental differences between the scaffold-derived tumors and those from Matrigel is the potential for more significant macrophage signaling. Because sphere-templated scaffolds have also been shown to induce substantial vascularity [53], we tested whether this effect translated to xenografts derived from these materials. Figure 3.4 shows that the scaffold-derived M12 xenografts seeded with and without Matrigel showed a statistically equivalent vascularity to the standard M12 plus Matrigel xenografts based on percent MECA+ stained area.

www.manaraa.com

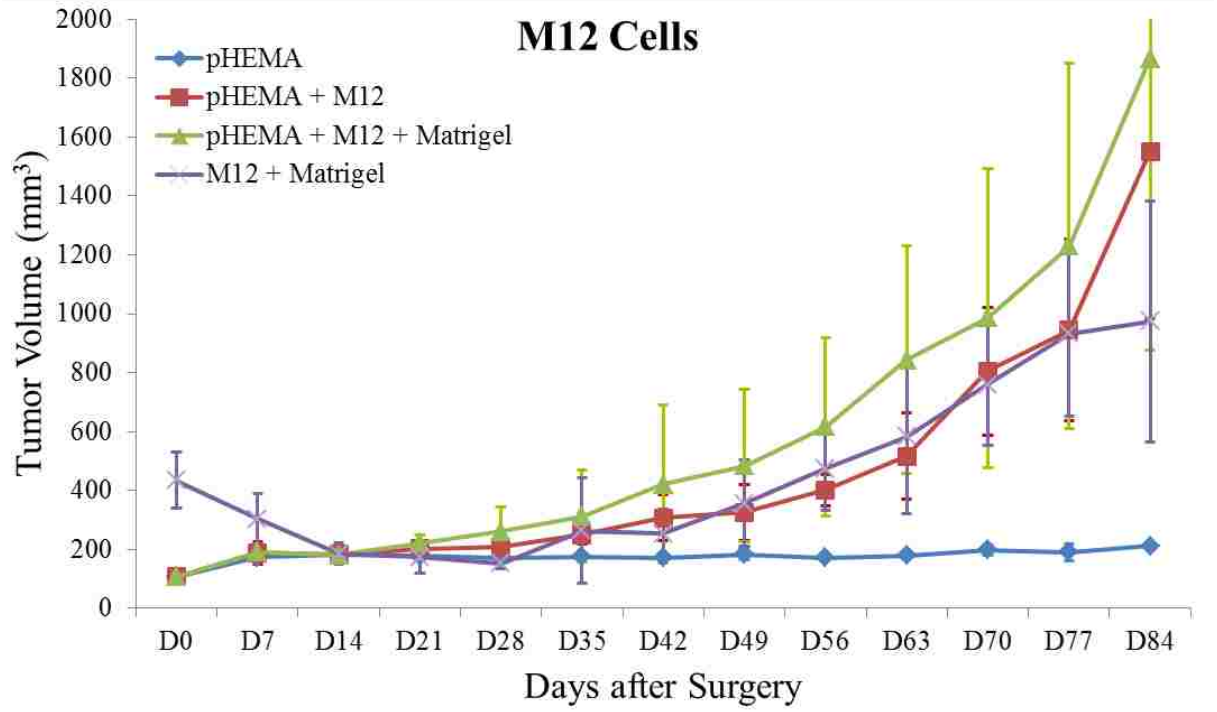

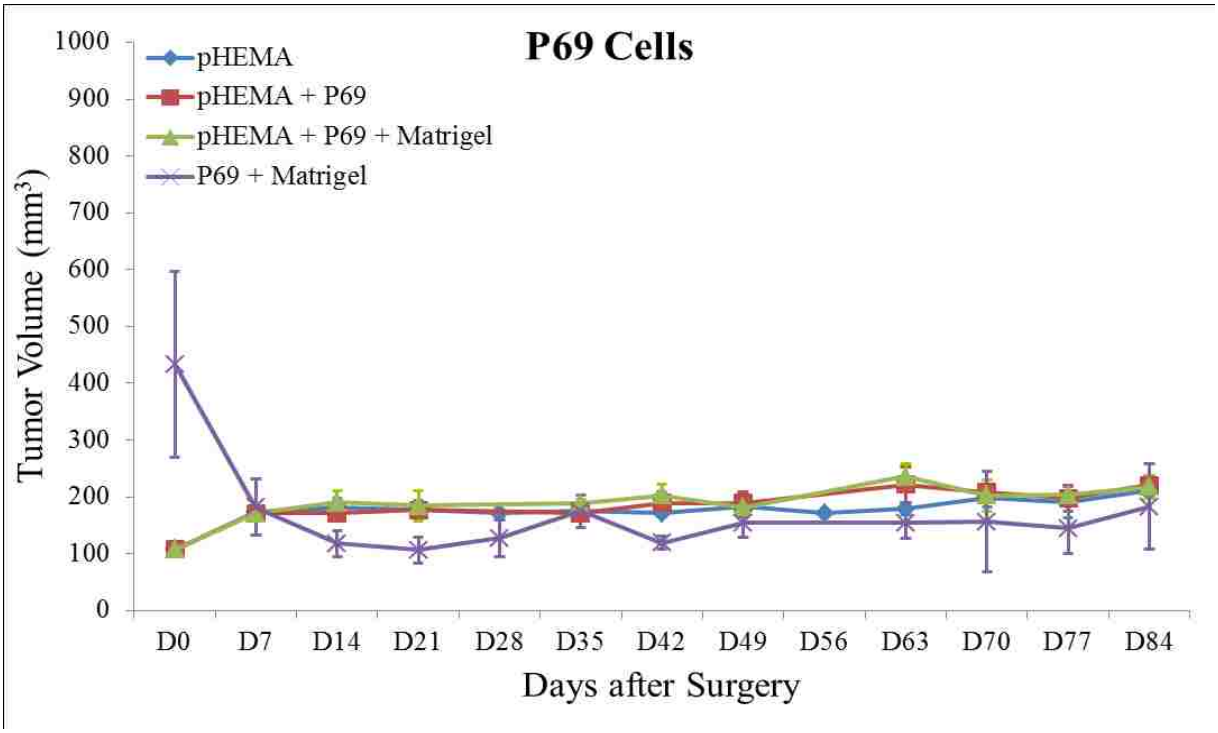

www.manaraa.com

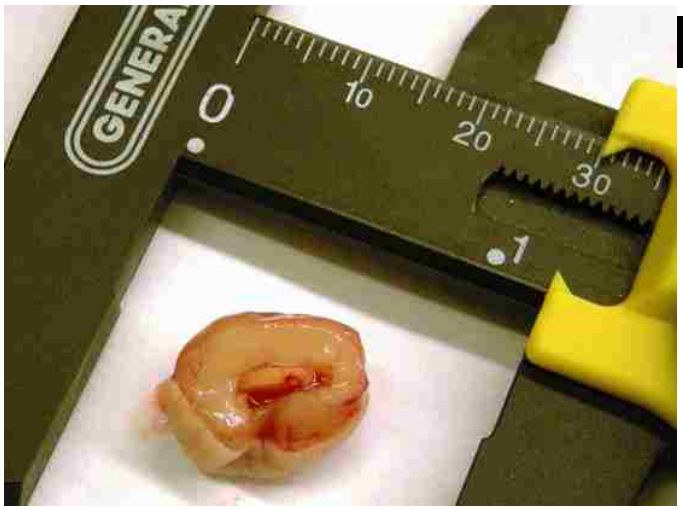

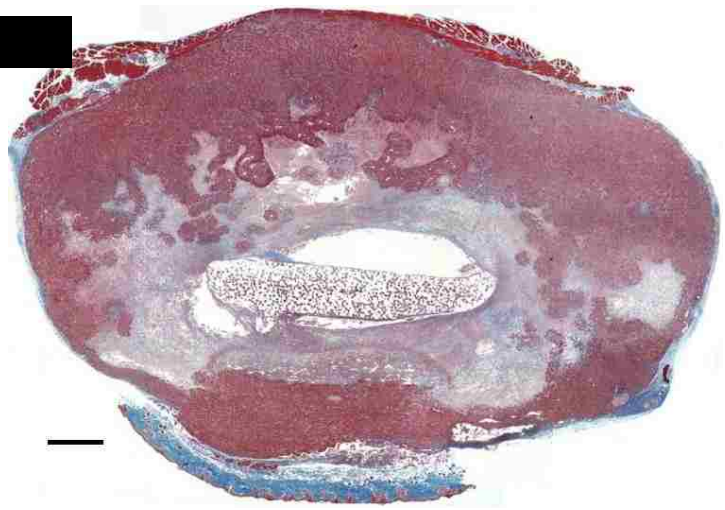

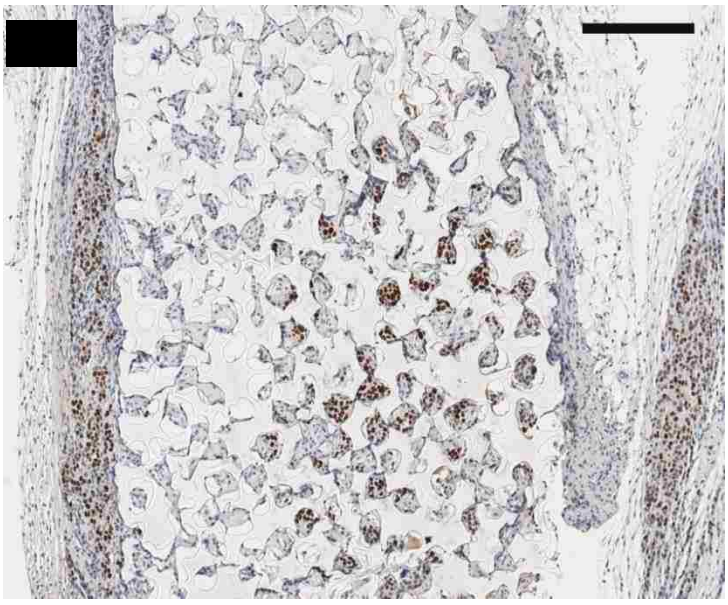

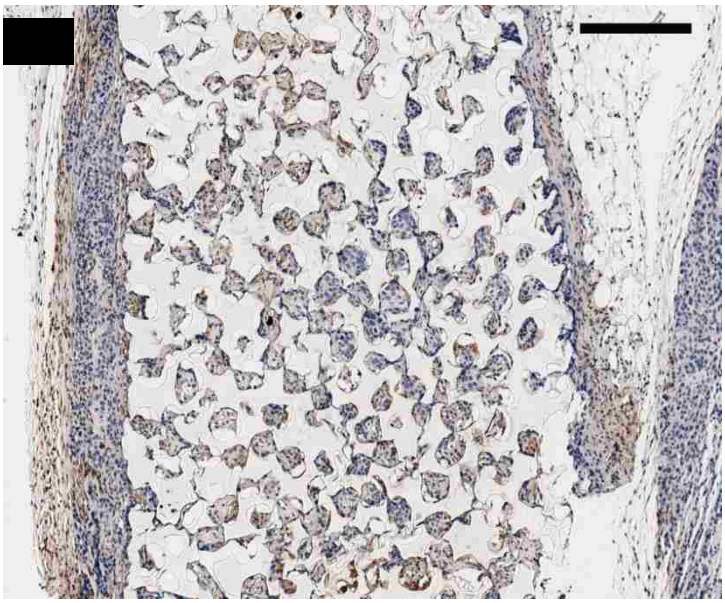

www.manaraa.com

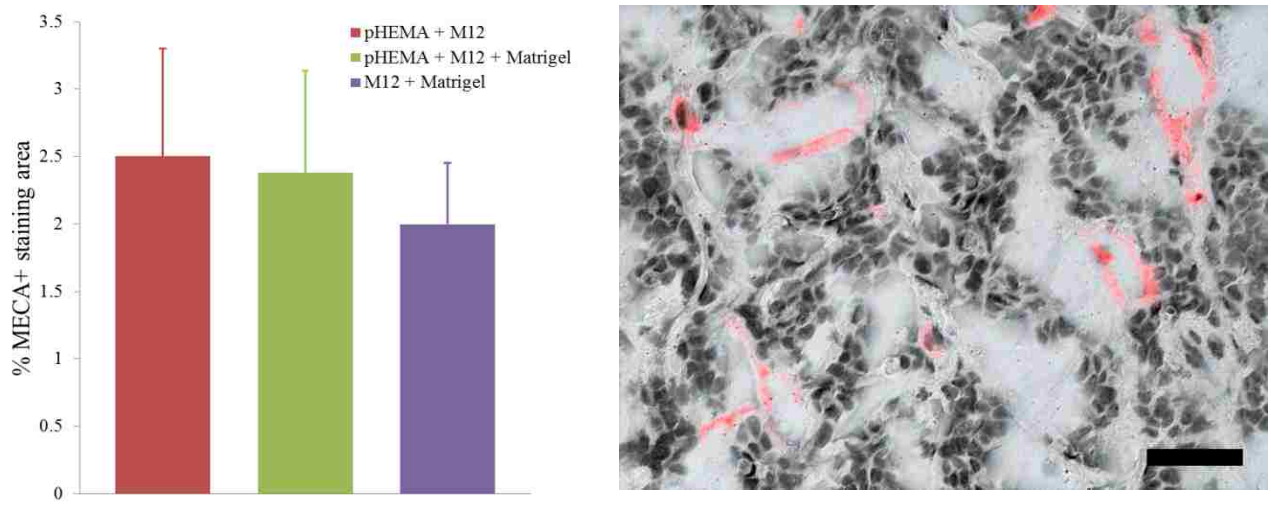

[redacted]

3.5 Discussion

In the studies presented in this chapter, we have engineered xenografts in athymic nude mice based on sphere-templated pHEMA scaffolds seeded with M12 human prostate cancer epithelial cells. M12 cells injected with Matrigel and seeded into pHEMA scaffolds both with and without Matrigel grew tumors at statistically equivalent rates over twelve weeks and showed no significant differences in vascularity. This demonstrates the capacity for porous pHEMA scaffolds to be used as a vehicle for xenograft generation, which satisfies part of the original hypothesis. However, because M12 cells are already highly tumorigenic in the subcutaneous space, it is not surprising that the cell line was unaffected by 3D *in vitro* pre-culture within the scaffolds or the macrophage-rich microenvironment produced *in vivo* by scaffold implantation. Kievit, *et al*. also observed that highly malignant C6 glioma cells did not respond significantly to 3D culture within chitosan-alginate scaffolds compared to other cell lines [38], so it is possible that the advantages of biomaterials-based *in vivo* tumor models could be limited in cell lines that display high inherent tumorigenicity in the environment in which they are implanted.

www.manaraa.com

Chapter 4. Porous Scaffold-Based LNCaP C4-2 Prostate Cancer Xenografts

4.1 Background

4.1.1 Motivation

As discussed in sections 1.6 and 3.1.2, synthetic biomaterials-based cancer model systems present a number of potential advantages to the cancer research field. *In vitro*, these materials can offer precision control over the cellular microenvironment, and *in vivo* they have the capacity to generate a complex, yet reproducible, microenvironment without the use of a naturally-derived support matrix like Matrigel (see section 1.4). It would be of interest to the cancer research community to be able to generate tumors *in vivo* in the absence of such a matrix. For example, studies of tumor cell-secreted ECM proteins would be difficult in the presence of excel concentrations of exogenous laminin 1 and collagen IV. The studies in chapter three used porous pHEMA scaffolds as a vehicle to generate xenografts from highly tumorigenic M12 cells. In this chapter, the same scaffolds will be used in an effort to generate tumors from LNCaP C4-2 cells that ordinarily require Matrigel to grow *in vivo*.

4.1.2 LNCaP C4-2 Cells

LNCaP C4-2 cells were developed as a mouse model system for human prostate cancer disease progression, possessing androgen independence and a tendency to metastasize to bone. To generate this cell line, Thalmann, *et al*. first isolated metastatic human prostate cancer cells (LNCaP parent cell line) from a patient's lymph node and then co-injected them with human bone stromal fibroblasts subcutaneously in nude mice. These mice were castrated and the resulting tumors grew in the absence of androgen (LNCaP C4 sub-line). When LNCaP C4 cells were again co-injected subcutaneously with human bone stromal fibroblasts, the cells from the resulting tumors were found to metastasize preferentially to bone (LNCaP C4-2 cell line) [69-70] (see appendix 2 for cell line generation diagram). LNCaP C4-2 cells are largely non-tumorigenic when injected subcutaneously, however they become tumorigenic when mixed and injected with an exogenous matrix such as Matrigel or bone marrow stromal cells. These cells secrete human prostate-specific antigen (PSA), which can be used as a marker to visualize them histologically.

www.manaraa.com

4.2 Hypothesis

It is hypothesized that sphere-templated pHEMA scaffolds can be used to generate xenografts *in vivo* from seeded LNCaP C4-2 cells, and that this may require scaffold surface modification through protein conjugation.

4.3 Materials and Methods

4.3.1 3D Cell Culture

LNCaP C4-2 cells were cultured in RPMI 1640 containing 10% FBS, L-glutamine, 1% sodium pyruvate, and 1% antibiotic/antimycotic. Sphere-templated pHEMA scaffolds were fabricated and re-hydrated as described in section 2.3.1, and for the LNCaP studies all scaffolds were sintered for 24 hours to optimize pore interconnect size for cell loading. For the pilot *in vivo* study, scaffolds were punched into 6 mm discs and soaked in media for 1 hour at 37 °C prior to cell seeding, which was performed using capillary force as described in section 2.3.3, where $1x10^6$ cells were loaded into the scaffold. The same process was used for seeding scaffolds with concentrated Matrigel, with the cell suspension mixed 1:1 by volume with Matrigel at 4 °C while holding the total cell number applied to each scaffold constant at $1x10^6$ cells. Seeded scaffolds were cultured in 24 well plates as previously described in section 2.3.2, where cells were allowed to attach to the scaffold overnight in static culture before being transferred to a dynamic orbital shaker. Cells were cultured in scaffolds for five days prior to *in vivo* implantation with media changed every two days.

4.3.2 Pilot In Vivo *Study*

Animal experiments were approved by the University of Washington Animal Care and Use Committee (IACUC) and followed federal guidelines for laboratory animal use. Scaffolds tested negative for cytotoxicity and endotoxin using the protocols described in section 3.3.2. The pilot study design used is shown in Table 4.1. Seven week old athymic nude mice (Harlan) were anesthetized using 2% isofluorane and one scaffold per mouse was implanted

	pHEMA	pHEMA + Matrigel	Matrigel
No cell control	6	6	5
LNCaP C4-2 cells	6	6	6

Table 4.1 *In vivo* LNCaP C4-2 pilot study design showing numbers of athymic nude mice per experimental group. Each experimental group was comprised of LNCaP C4-2 cells either pre-cultured within pHEMA scaffolds, mixed with Matrigel, or mixed with Matrigel and pre-cultured within pHEMA. pHEMA scaffolds were subcutaneously implanted and cell/Matrigel mixtures were subcutaneously injected.

www.manaraa.com

subcutaneously in the dorsal right flank. For mice with cells but without scaffolds, 200 µL of a 1:1 mixture of Matrigel and $2x10^6$ LNCaP C4-2 cells were subcutaneously injected. Tumor volume was measured using the equation $V = (LxW^2)/2$, where length and width were determined with calipers. Scaffolds/tumors from two mice in each group were removed after three weeks for preliminary analysis. The rest of the mice were allowed to reach a tumor volume-based study endpoint of seven weeks. Explants were fixed in 10% neutral buffered formalin overnight at 4 ºC.

4.3.3 Histological Analysis

Fixed explants were dehydrated in ethanol and cleared with xylene prior to paraffin embedding. The embedded scaffolds were sectioned with a Leica microtome, and sections were heated at 53 °C for 30 minutes prior to xylene deparaffinization and rehydration through a graded ethanol series. Slides were stained with a standard Masson's trichrome protocol to analyze basic tissue morphology and imaged on a Nikon E800 microscope equipped with Metamorph software (version 6.0, Molecular Devices). Low magnification trichrome images were stitched together into mosaics using Adobe Photoshop software. For immunohistochemical analysis, sections were washed in TBS and endogenous peroxidases were blocked in a 3% hydrogen peroxide solution in TBS. Antigen retrieval was performed using heated 0.01 M pH 6 citrate buffer. After cooling, sections were blocked overnight at 4 ºC in TBS containing 0.5% tween-20, 4% normal serum (Vector) from the animal in which the secondary antibody was raised and 0.25% IHC grade BSA (Vector). Primary antibodies were incubated for 30 minutes at room temperature unless otherwise indicated, with a concentration-matched isotype negative control section. Secondary antibodies were incubated at room temperature for 30 minutes. A Vectastain ABC kit (Vector) was used along with a DAB kit (Vector) to generate a brown positive stain. All sections were counterstained with hematoxylin before dehydration and slide mounting in Permount (Electron Microscopy Sciences). Using this procedure, paraffin sections were stained for the human prostate specific antigen [1:300 rabbit IgG (Dako), 1:200 goat anti-rabbit secondary].

4.3.4 Twelve-Week In Vivo *Study*

A second animal study was run to test whether longer implantation time would result in scaffold-mediated LNCaP C4-2 tumor growth. Six additional athymic nude mice were implanted with

www.manaraa.com

pHEMA seeded LNCaP C4-2 cells as described in section 4.3.1. After twelve weeks, LNCaP C4-2 explants were fixed for histological analysis.

4.3.5 pHEMA-co-MAA Scaffold Surface Modifications

Scaffolds were fabricated using the protocol from section 2.3.1 with one modification where pHEMA was co-polymerized with 5% MAA (mol/mol HEMA). pHEMA-co-MAA scaffolds were surface-modified by protein conjugation using N-(2-dimethylaminopropyl)-N'-ethylcarbodiimide hydrochloride (EDC, Sigma)/N-hydroxysuccinimide (NHS, Covachem) chemistry (see Figure 4.1). Scaffolds were first equilibrated in ethanol, then reacted in a solution of 0.1 M EDC/0.2 M NHS in ethanol for 1 hour at room temperature. For adsorbed collagen controls the EDC/NHS incubation step was skipped. Scaffolds were rinsed with ethanol and incubated with a 100 µg/mL solution of collagen I in ethanol for 30 minutes at room temperature. Protein solutions were removed and replaced with fresh proteins at the same concentration for an overnight incubation at room temperature. Scaffolds for cell seeding were sterilized in 70% ethanol and re-hydrated in PBS. Scaffolds for surface analysis were washed 5x in DI H2O and dried in a vacuum oven.

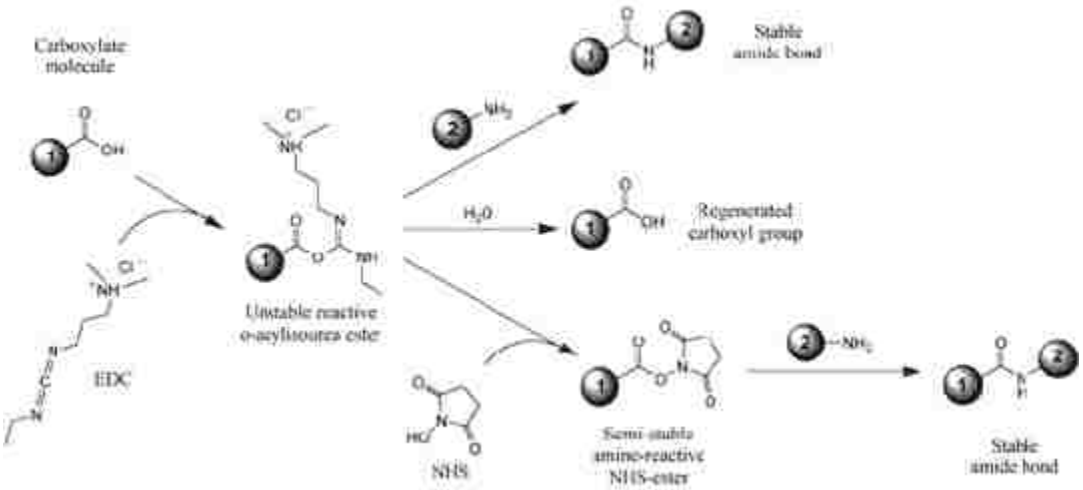

Figure 4.1 EDC/NHS Reaction Scheme (Thermo Scientific)

4.3.6 Scaffold Surface Analysis

X-ray photoelectron spectroscopy (XPS) was performed on pHEMA-co-MAA samples by the National ESCA and Surface Analysis Center for Biomedical Problems (NESAC/BIO) center at

www.manaraa.com

the University of Washington. All XPS spectra were taken on a Surface Science Instruments S-probe spectrometer. Triplicate samples of vacuum-dried pHEMA-co-MAA, pHEMA-co-MAA + EDC/NHS, pHEMA-co-MAA + adsorbed collagen I, and pHEMA-co-MAA + EDC/NHS + collagen I were analyzed by XPS. Percent atomic carbon, oxygen, and nitrogen on the sample surfaces were calculated and percent nitrogen was used to confirm protein surface conjugation.

4.3.7 Modified 3D Cell Culture

For the follow-up *in vivo* study with surface-conjugated pHEMA scaffolds (see section 4.3.8), several modifications were made to the *in vitro* LNCaP C4-2 cell culture process to load $2x10^6$ cells into each scaffold. Scaffolds were punched into 8 mm discs and loaded with capillary force using two applications of 50 µL of a $2x10^7$ cell suspension. The seeded scaffolds were cultured for seven days *in vitro* prior to implantation. PicoGreen DNA analysis was performed as in section 2.1.5 to confirm cell number with the added modification of dicing the scaffold into small pieces using scalpel blades after freeze-thawing.

4.3.8 In Vivo *Study with Modified 3D Cell Culture and Scaffold Surface Modification*

Six athymic nude mice were used for a third LNCaP C4-2 animal study. Two scaffolds per mouse were subcutaneously implanted, on one flank an 8 mm pHEMA-co-MAA scaffold with surface-conjugated collagen I seeded with $2x10^6$ LNCaP C4-2 cells, and on the other flank an 8 mm pHEMA scaffold with embedded collagen I seeded with $2x10^6$ LNCaP C4-2 cells to serve as a control. Tumor growth was measured over twelve weeks.

4.4 Results

4.4.1 Pilot and Twelve Week Implant Studies

Figure 4.2 shows growth curves for implanted LNCaP C4-2 seeded pHEMA scaffolds and their Matrigel counterparts from both the pilot and twelve week *in vivo* studies. Compared to the standard Matrigel xenografts, which grew large tumors quickly over twelve weeks, pHEMA with embedded collagen I was unable to be used as the basis for LNCaP C4-2 xenografts. Up to twelve weeks after implantation, LNCaP C4-2 cells showed no significant proliferation outside the pHEMA scaffold even when seeded into the scaffolds with Matrigel. Histological examination of explants using immunohistochemistry for PSA showed that by the seven and

www.manaraa.com

twelve week endpoints for the two *in vivo* studies, only half of the explants stained positive for PSA, confirming that LNCaP C4-2 cells were present in the scaffold (see Figure 4.3A). In the other half of the explants there was no PSA+ signal (see Figure 4.3B), indicating that the LNCaP C4-2 cells were no longer present. The standard Matrigel injections stained strongly for PSA as a positive control for the LNCaP C4-2 cell line (see Figure 4.3C).

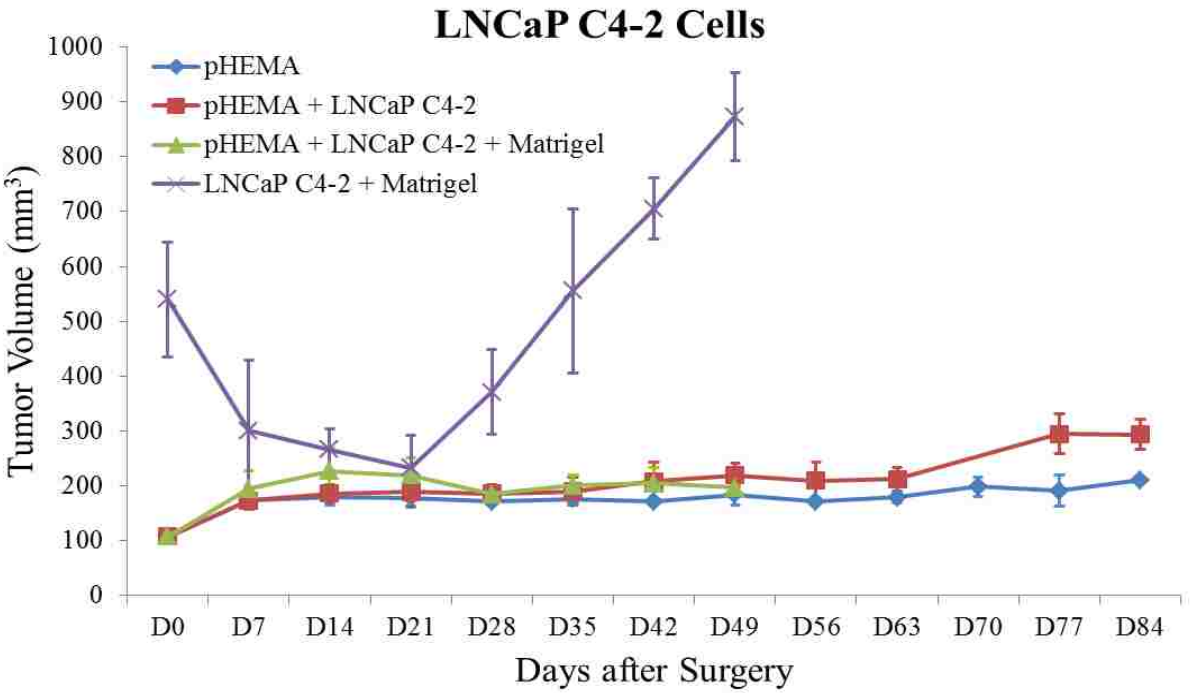

[redacted]

4.4.2 Scaffold Surface Analysis

Figure 4.4 shows XPS survey spectra of pHEMA-co-MAA scaffolds with adsorbed collagen I and reacted with EDC/NHS and collagen I. Figure 4.5 shows the relative atomic percent of nitrogen in pHEMA-co-MAA, pHEMA-co-MAA + EDC/NHS, pHEMA-co-MAA + adsorbed collagen, and pHEMA-co-MAA + EDC/NHS + collagen I. It is clear from the raw spectra and the atomic percent analysis that nitrogen content on the scaffold surface spikes dramatically from zero in the original polymer to over 11% after the EDC/NHS + collagen I reaction. This value is

www.manaraa.com

consistent with a protein monolayer on a surface and confirms the surface reaction of collagen I to the pHEMA-co-MAA scaffolds.

4.4.3 In Vivo *Study with Modified 3D Cell Culture and Scaffold Surface Modification*

Tumors developed over twelve weeks in one out of six mice implanted with the larger 8 mm scaffolds containing $2x10^6$ cells regardless of whether the scaffolds had embedded collagen like the pilot study or the surface-conjugated collagen I. IHC showed that 50% of scaffolds stained positive for PSA at twelve weeks for both the embedded and surface-conjugated sample groups.

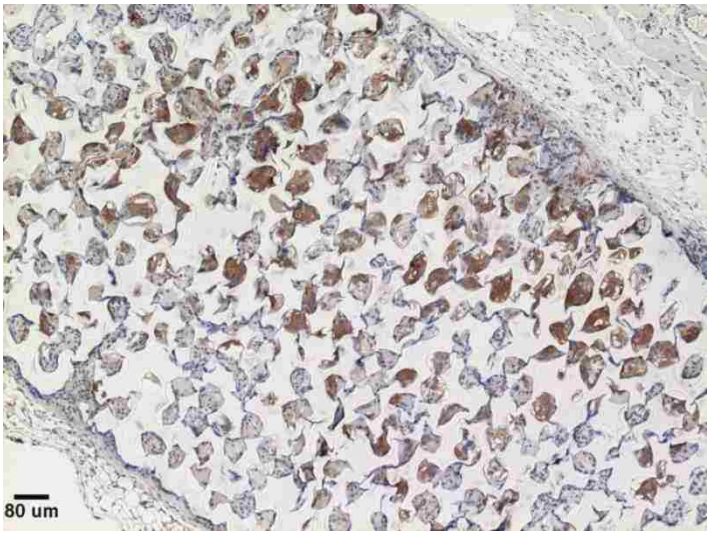

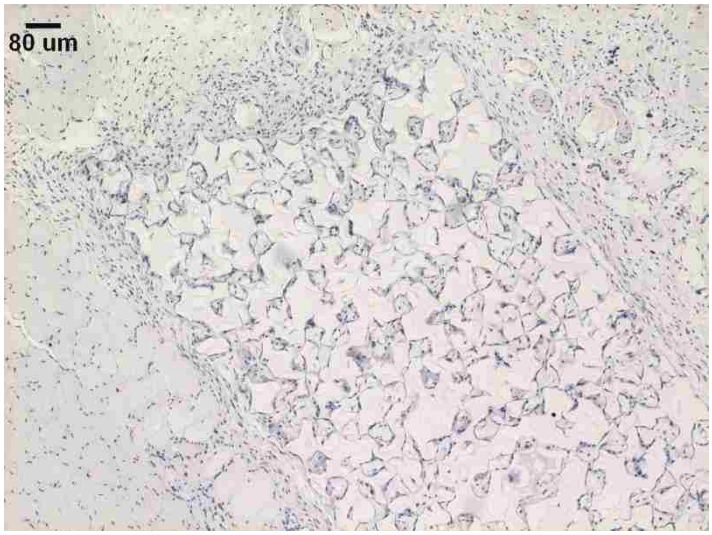

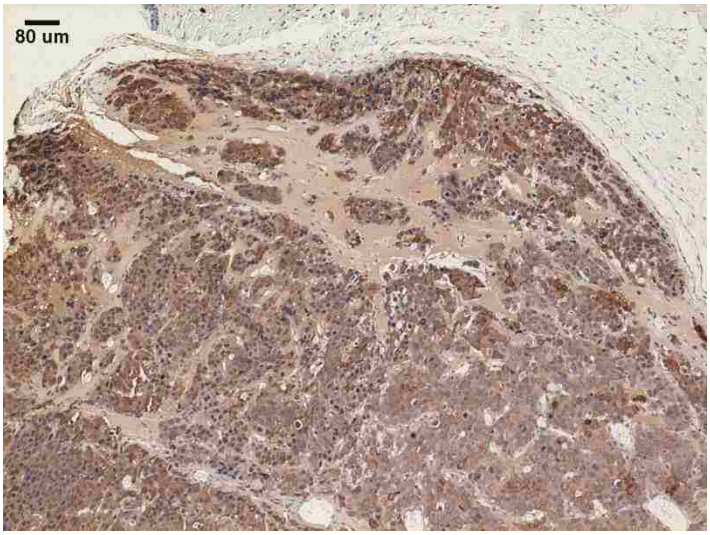

www.manaraa.com

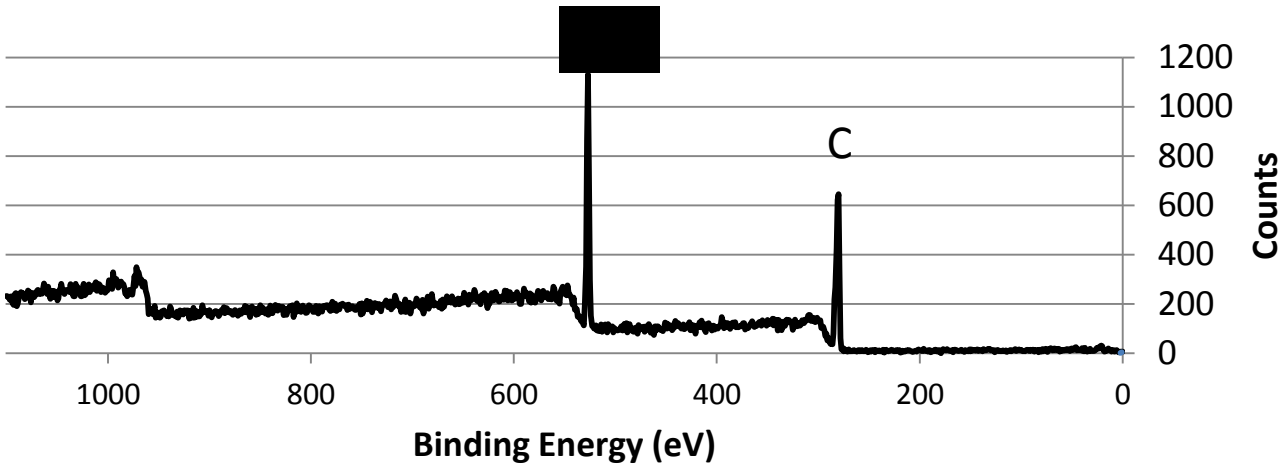

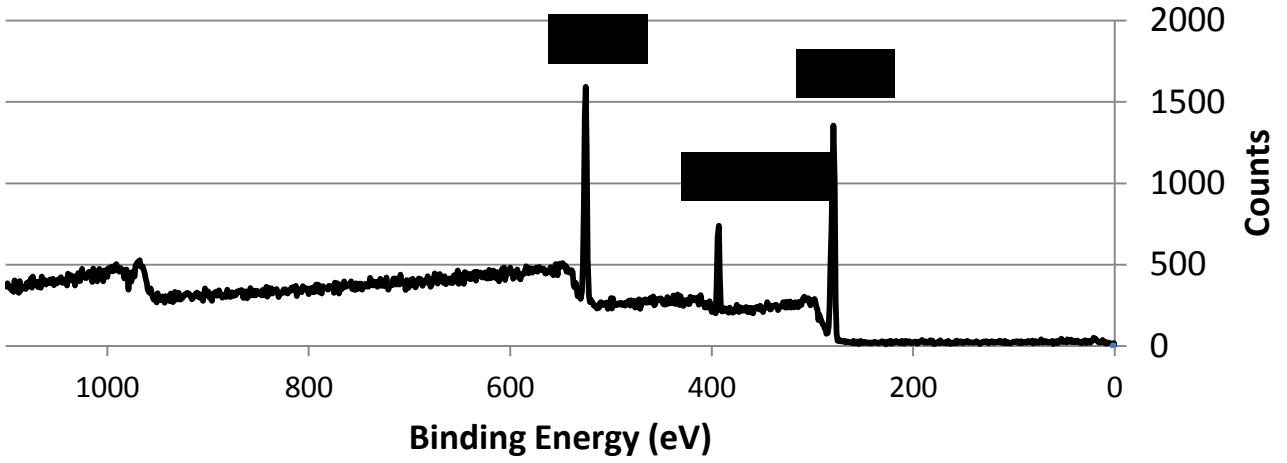

[redacted]

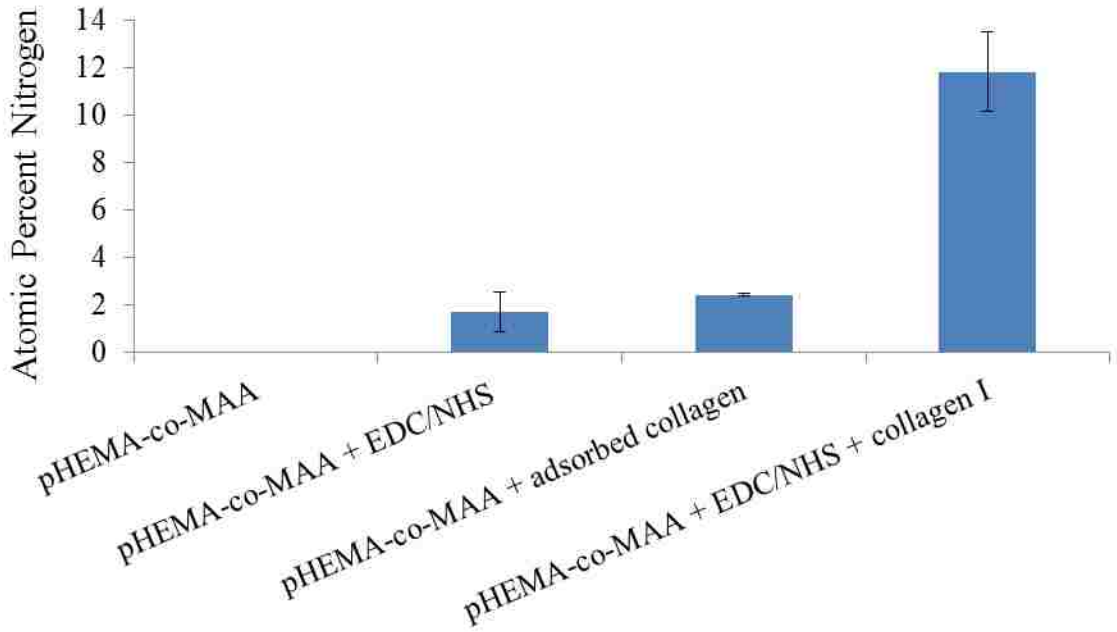

[redacted]

www.manaraa.com

4.5 Discussion

LNCaP C4-2 cells grew large tumors by seven weeks after subcutaneous injection with Matrigel but failed to form tumors after implantation over twelve weeks within 6 mm scaffolds seeded with $1x10^6$ cells. Histology demonstrated only 50% of explants contained the PSA-secreting LNCaP C4-2 cells by seven weeks. Because of the cell number mismatch with the Matrigel xenografts, which contain $2x10^6$ cells, an alternative 3D cell culture protocol was developed where larger scaffolds were seeded with a higher number of cells to arrive at a Matrigel-matching $2x10^6$ cells per scaffold. This modified method was used in a follow-up *in vivo* study that involved one group of pHEMA scaffolds with embedded collagen and another group of pHEMA-co-MAA scaffolds presenting surface-conjugated collagen I. It was hypothesized that scaffold surface modifications may allow tumors to grow from the synthetic materials. Only one out of six scaffolds in each group yielded a tumor, which indicates that having the higher cell number is enough for this construct to be considered poorly tumorigenic, and the collagen I surface modification did not add any value to this effect. We thus have not been able to validate the hypothesis that synthetic scaffolds can be used to generate tumors *in vivo* from LNCaP C4-2 cells. Fortunately, synthetic polymers like pHEMA are adaptable to studies designed to modify the microenvironment in a controlled way. It is possible that the collagen I attachment substrate cannot replace the pro-tumorigenic signaling provided by Matrigel constituents. Alternative surface modifications, such as laminin I or collagen IV, both major components of the basement membrane-rich Matrigel, may be able to serve as a replacement. It is also possible that surface modification alone is not sufficient, and the scaffolds may need to be designed to controllably release growth factors that contribute to tumor growth. Additionally, sphere-templated materials vascularize in a pore-size dependent manner, with a pore size around 38 μm showing the highest levels of vessel density [53]. Since this study used a pore size of around 80 μm optimized for cell seeding, it is possible that a significant increase in xenograft vascularity still could be achieved using the optimal pore size, which could enhance malignancy or potentially benefit cell lines such as LNCaP C4-2 to grow without the need for Matrigel.

www.manaraa.com

Chapter 5. A Biomaterials-Based *In Vivo* Model to Study Prostate Cancer Cell Dormancy Escape

5.1 Background

5.1.1 Motivation

This chapter focuses on the use of sphere-templated pHEMA scaffolds to study prostate cancer cell dormancy escape. Results will show that M12mac25 cells, a line that remains dormant *in vivo* when injected with Matrigel, regains tumorigenicity when implanted within porous pHEMA scaffolds. This is an interesting observation because the mechanisms behind prostate cancer dormancy escape are not well understood. Here, we explore the potential cellular and molecular mechanisms for the re-activation of M12mac25 cells and the impact of the *in vivo* macrophage-rich microenvironment generated by the scaffolds on the M12mac25 cells.

5.1.2 Cancer Dormancy and Escape from Dormancy

Clinically, cancer dormancy refers to disease recurrence after a long disease-free period following primary tumor resection. Cancer dormancy is commonly associated with breast and prostate cancers but has been observed in lymphoma, melanoma, thyroid, and renal cancers [71]. Current theory suggests that circulating tumor cells (CTCs), which are able to leave the primary tumor early in its development, can disseminate to secondary sites (most commonly the bone marrow in prostate and breast cancers) and remain dormant there for many years. In prostate cancer it has been shown that a majority of patients have disseminated tumor cells (DTCs) in their bone marrow at the time of primary treatment, but less than 30% of those patients developed recurrent disease 5-15+ years post initial treatment [72]. A majority of these cells have been demonstrated as viable but non-proliferative [73]. However, it is unlikely that all DTCs are in growth arrest because in breast cancer it has been shown that CTCs, which have very short half lives, can exist in disease-free patients 7-22 years after primary tumor removal, which may imply that some secondary site is generating CTCs [74].

The mechanisms of what drives DTCs to escape dormancy and form tumors at secondary sites are not well-understood. However, once these processes have been elucidated, it may be possible to use that information to clinically maintain dormancy and prevent recurrence such that cancer becomes a manageable condition [75]. In the literature, dormancy is divided into two categories.

www.manaraa.com

First, the DTCs themselves can be dormant in their secondary location; this condition is known as cellular dormancy, where the cells themselves are quiescent and can show G0/G1 cell cycle arrest in response to microenvironmental signals or stresses [76]. Second, disseminated micrometastases can also be dormant, and evidence suggests that this dormancy can be caused by lack of sufficient angiogenesis, a balance between proliferation and apoptosis, or immunosurveillance, though these theories are not without controversy [71].

Several groups have demonstrated models of cancer cellular dormancy, though to the best of our knowledge no mouse models of prostate cancer dormancy currently exist. Weaver, *et al*. showed that breast cancer cells can enter a non-proliferative state following the blocking of β1 integrins [77]. Aguirre-Ghiso, *et al*. showed a model of head and neck carcinoma where loss of the metastasis-associated urokinase receptor uPAR, which activates integrin α5β1 and the ERK pathway, resulted in the induction of quiescence *in vivo* despite the presence of fibronectin, which binds integrin α5β1. Loss of uPAR activated p38, a stress signaling pathway, which when disrupted returned cells to a proliferative state *in vivo* [76]. Finally, in the MMTV-PyMT transgenic mouse model for breast cancer, mice that were β1 integrin-null had tumor cells that were rendered non-proliferative and dormant [78].

5.1.3 M12mac25 Cells

The studies presented here will examine M12mac25 cells as a model system for prostate cancer dormancy [79]. M12mac25 cells are M12 cells that have been transfected with the mac25 gene, which codes for insulin-like growth factor binding protein 7 (IGFBP7), also known as insulin-like growth factor binding protein related protein 1 (IGFBP-rp1). IGFBP7 has been demonstrated as a potential tumor suppressor in breast [80][81], liver [82], bladder [83], skin [84], and prostate cancers [85][86][87]. The mac25 gene confers a senescence-associated gene expression profile and renders the M12mac25 line non-tumorigenic upon implantation with or without Matrigel. M12mac25 cells have been shown to be in G0/G1 arrest [87]. Prostate cancer dormancy and the mechanisms of dormancy escape are not well understood and present significant clinical challenges [76][88][89]. It has been shown that a majority of prostate cancer patients have disseminated tumor cells present in their bone marrow at the time of primary treatment, but less than 30% of those patients developed recurrent disease 5-15+ years post-initial treatment [72].

www.manaraa.com

Despite its clinical relevance, no mouse models of prostate cancer dormancy currently exist. Here, M12mac25 cells seeded within porous pHEMA scaffolds will be presented as a potential model system to study release from dormancy.

5.1.4 Tumor-Associated Macrophages

Many cancers, including prostate cancer, contain a substantial number of leukocytes that infiltrate as part of the immune response to the growing tumor. Of those leukocytes, tumor-associated macrophages (TAM) are the most common cell type found. TAM infiltration has been linked to poor clinical prognosis in a number of cancers [90], but there is conflicting data with respect to prostate cancer [91][92]. Circulating monocytes are recruited to tumors by chemotactic factors such as CCL2/MCP-1 and CCL5/RANTES [93]. TAM localization within tumors varies, but TAMs tend to accumulate in areas of hypoxia, where they can activate pro-angiogenic pathways through the production of proteins such as VEGF. They can also play roles in stimulating tumor cell proliferation, remodeling ECM proteins, and suppressing the adaptive immune system [94][23][95]. Because of their many pro-tumorigenic functions, some researchers have focused on TAMs as a potential therapeutic target [96][97][98].

Macrophage phenotype shows considerable plasticity in the face of microenvironmental stimulation [99]. The spectrum of activated macrophage phenotypes ranges from M1 'classically-activated' or 'pro-inflammatory' polarization to M2 'alternatively activated' polarization. The M1 state can be induced by stimulation with lipopolysaccharide (LPS) or interferon-gamma (IFN-γ) and can be characterized by the production of IL-1β, IL-6, IL-12, and the production of nitric oxide and reactive oxygen intermediates. The M2 state can be induced by stimulation with IL-4 and can be characterized by production of IL-10, IL-13, TGF-β, and mannose receptors. Many activated macrophages exist in somewhere in between these polarization extremes. TAMs typically demonstrate an M2-like phenotype with pro-tumor functions, whereas M1 macrophages have been shown to have considerable anti-tumor cell capabilities. The signaling environment within the tumor produced by tumor cells themselves and supplemented by entering TAMs tends to induce this M2 polarization [100].

www.manaraa.com

Macrophages are one of the main cellular actors in the foreign body response (see section 3.1.2). M1 macrophage polarization has been associated with inflammation, foreign body giant cell formation, and a poor healing response to implanted materials, whereas M2 macrophage polarization has been associated with a pro-fibrotic tissue remodeling response [101]. Following the subcutaneous implantation of sphere-templated pHEMA, macrophages that infiltrate the scaffold up to 4 weeks demonstrate both M1 and M2 polarization markers whereas the macrophages in the fibrous capsule outside the material tend to be more M2-polarized [50][102].

5.1.5 Clondronate Liposomes

In section 3.4.2 it was demonstrated that pHEMA-based tumor models recruit significant numbers of macrophages *in vivo*. Because of this, macrophages could play a key role in M12mac25 cell dormancy escape. One way to prove that macrophages are involved in the process is to eliminate them from the *in vivo* system. Because of the complexity of the foreign body response, it is likely not possible to do this by simply blocking a small finite number of factors that induce macrophage recruitment. For instance, Kyriakides, *et al*. demonstrated that blocking CCL2 (MCP-1) reduced foreign body giant cell formation as part of the FBR but did not limit macrophage recruitment to porous scaffolds [103]. In order to eliminate macrophages, clondronate liposomes can be employed. When encapsulated in phosphatidylcholine/cholesterol liposomes, clondronate, a small molecule bisphosphonate, can be delivered specifically to macrophages by liposome phagocytosis. As the liposome begins to degrade inside the macrophage, the clondronate is released and induces macrophage apoptosis. Using this methodology, it is possible to substantially reduce macrophage content *in vivo* in various target organs/areas depending on the liposome delivery strategy. In the subcutaneous space, macrophage infiltration to tumor xenografts has been dramatically reduced (up to 90%) using intraperitoneal (IP) injections [104][105]. In this chapter, clondronate liposomes will be used to remove macrophages from athymic nude mice prior to implantation with pHEMA scaffolds pre-seeded with M12mac25 cells.

The foreign body response to implanted scaffolds after macrophage elimination has been previously examined. Valentin, *et al*. used clondronate liposomes to eliminate macrophages in the study of the degradation of implanted natural intestinal matrix in a rat body wall model and

www.manaraa.com

found that neutrophils, cells involved early in the foreign body response, remained at the implant site longer than normal. However, the study did not last longer than two weeks. In addition, there was a significant observed macrophage knockdown with the liposomes, but elimination was more successful with non-cross-linked degradable implants than cross-linked non-degradable implants [106]. Mooney, et al. examined the effect of clondronate liposomes on intraperitoneal (IP) implants and found that over two weeks the macrophages around the implant were removed and foreign body capsule formation was eliminated [107].

5.1.6 CXCL5 Signaling in Prostate Cancer

Evidence in the literature suggests that the cytokine CXCL5 may play a role in prostate cancer progression [108][109]. CXCL5 has been shown to be correlated with malignancy and androgen independence, and is expressed by both prostate epithelial cells and immune cells. CXCL5 induces the proliferation and migration of PC3, DU145, and LNCaP prostate cancer cell lines *in vitro* while inducing the expression of epithelial-to-mesenchymal transition (EMT) transcription factors and phenotype. The data that will be presented in this chapter indicates that CXCL5 may play a role in M12mac25 cell dormancy escape.

5.1.7 Cell Response to Substrate Mechanics

The mechanical properties of cell substrates have been shown to affect numerous cellular properties including cell adhesion, spreading, proliferation, migration, morphology, intracellular signaling, and differentiation [110][111]. A common measure of substrate stiffness is the elastic modulus, which is defined as the linear slope of a stress-strain curve. In soft biological tissues, the elastic modulus ranges from 100 Pa to 100 kPa [112], a range that is simulated most commonly in a laboratory setting using cross-linked poly(acrylamide) (pA) gels [113][114]. However, many cell mechanics studies in the literature present data from moduli outside the relevant biological range. Studies correlating elastic modulus to cell proliferation and migration show conflicting results where increased proliferation or migration can be associated with either stiffer or softer matrices, so the effect seems to be cell type/material-dependent [115][116][117][118][119]. For cancer cells, some studies have linked stiffer mechanics to tumor cell invasion potential [120]. Microenvironmental mechanical properties could be potentially

www.manaraa.com

relevant for clinical dormancy escape since dormant lesions tend to be present in bone tissue, which is stiffer than other tissues in the body.

5.2 Hypothesis

It is hypothesized that pHEMA scaffolds can be used as the basis for an *in vivo* prostate cancer cell dormancy escape model. Further, it is hypothesized that the macrophage infiltration within porous biomaterials induced by the foreign body response is responsible for M12mac25 cell dormancy escape and tumor formation after implantation in the scaffold-based xenograft.

5.3 Materials and Methods

5.3.1 3D Cell Culture

M12mac25 cells were cultured in RMPI complete media (see section 2.3.2). Sphere-templated pHEMA scaffolds were fabricated and re-hydrated as described in section 2.3.1, and for these cell lines the scaffolds were sintered for 22 hours to optimize pore interconnect size for cell loading. Scaffolds were punched into 6 mm discs and soaked in media for 1 hour at 37 °C prior to cell seeding, which was performed using capillary force as described in section 2.3.3. The same process was used for seeding scaffolds with concentrated Matrigel, with the cell suspension mixed 1:1 by volume with Matrigel at 4 °C while holding the total cell number applied to each scaffold constant at $1x10^6$ cells. Seeded scaffolds were cultured in 24 well plates as previously described in section 2.3.2, where cells were allowed to attach to the scaffold overnight in static culture before being transferred to a dynamic orbital shaker. Cells were cultured in scaffolds for five days prior to *in vivo* implantation with media changed every two days.

5.3.2 Pilot In Vivo *Study*

Animal experiments were approved by the University of Washington Animal Care and Use Committee (IACUC) and followed federal guidelines for laboratory animal use. Scaffolds tested negative for cytotoxicity and endotoxin

	pHEMA	pHEMA + Matrigel	Matrigel
No cell control	6	6	5
M12mac25 cells	6	5	5

Table 5.1 *In vivo* M12mac25 pilot study design showing numbers of athymic nude mice per experimental group. Each experimental group was comprised of a M12mac25 either pre-cultured within pHEMA scaffolds, mixed with Matrigel, or mixed with Matrigel and pre-cultured within pHEMA. pHEMA scaffolds were subcutaneously implanted and cell/Matrigel mixtures were subcutaneously injected.

www.manaraa.com

using the protocols described in section 3.3.2. The pilot study design used is shown in Table 5.1. Seven week old athymic nude mice (Harlan) were anesthetized using 2% isofluorane and one scaffold per mouse was implanted subcutaneously in the dorsal right flank. For mice with cells but without scaffolds, 200 µL of a 1:1 mixture of Matrigel and $1x10^6$ M12mac25 cells were subcutaneously injected. Tumor volume was measured using the equation $V = (LxW^2)/2$, where length and width were determined with calipers. Scaffolds from two mice in each group were removed after three weeks for preliminary analysis. The rest of the mice were sacrificed after twelve weeks. Explants were fixed in zinc fixative overnight at 4 ºC.

5.3.3 Histological Analysis

Fixed explants were dehydrated in ethanol and cleared with xylene prior to paraffin embedding. The embedded scaffolds were sectioned with a Leica microtome, and sections were heated at 53 °C for 30 minutes prior to xylene deparaffinization and rehydration through a graded ethanol series. Slides were stained with a standard Masson's trichrome protocol to analyze basic tissue morphology and imaged on a Nikon E800 microscope equipped with Metamorph software (version 6.0, Molecular Devices). For immunohistochemical analysis, sections were washed in tris buffered saline (TBS) and endogenous peroxidases were blocked in a 3% hydrogen peroxide solution in TBS. Antigen retrieval was performed using heated 0.01 M pH 6 citrate buffer. After cooling, sections were blocked overnight at 4 ºC in TBS containing 0.5% tween-20, 4% normal serum (Vector) from the animal in which the secondary antibody was raised and 0.25% IHC grade BSA (Vector). Primary antibodies were incubated for one hour at room temperature, with a concentration-matched isotype negative control section. Secondary antibodies were incubated at room temperature for 30 minutes. A Vectastain ABC kit (Vector) was used along with a DAB kit (Vector) to generate a brown positive stain. All sections were counterstained with hematoxylin before dehydration and slide mounting in Permount (Electron Microscopy Sciences). Using this procedure, paraffin sections were stained for the SV40 large T antigen (SV40T) [1:100 rabbit IgG (Santa Cruz), 1:200 goat anti-rabbit secondary (Vector)], F4/80 [1:100 rat IgG (AbD Serotec), 1:200 rabbit anti-rat (Vector)], and mouse pan-endothelial cell antigen (MECA-32) [1:20 rat IgG (BD), 1:200 rabbit anti-rat (Vector)]. For fluorescent immunostaining, dried sectioned were fixed in cold acetone for 10 min and stained using the same procedure without

www.manaraa.com

peroxidase blocking and with a fluorescent secondary antibody (1:100 donkey anti-rat alexafluor 594 (Invitrogen)) and Vectashield hard set mounting medium with DAPI (Vector).

5.3.4 Immunohistochemical Macrophage Analysis

Macrophage content in M12mac25 explants was determined using DAB or fluorescent F4/80 immunohistochemistry on paraffin sections as described. For quantification, three slides per explant were stained. A low magnification 2x image was taken and a 7x7 grid was placed on the image. Five areas were selected randomly and each was imaged at high magnification. All F4/80+ cells were counted manually and the macrophage density was calculated.

5.3.5 Immunohistochemical Vasculature Analysis

For the quantification of M12mac25-derived xenograft vascularity, three zinc-fixed paraffin embedded sections per explant were stained with MECA-32 and visualized with DAB. One to two 2x low magnification images were taken encompassing the entire explant. These images were divided into grids in Metamorph and all areas were individually imaged at 20x. The number of lumens per area over the entire explant was counted manually. Alternative quantification with percent area stained was not performed as in section 3.3.4 because thresholding could not compensate for the non-specific staining of Matrigel using DAB.

5.3.6 Follow-Up In Vivo *Studies*

A second animal study was run to ensure reproducibility of the M12mac25 results from the pilot study. Six additional athymic nude mice were injected with M12mac25 cells + Matrigel or implanted with pHEMA seeded with M12mac25 cells as described. One mouse was sacrificed from the M12mac25 pHEMA group at D21 for histological analysis while the rest of the M12mac25 explants were removed and snap frozen after twelve weeks for RNA and protein extraction. In total between the pilot and follow-up studies, nine mice were analyzed at the twelve week endpoint for the pHEMA + M12mac25 and M12mac25 + Matrigel experimental groups.

www.manaraa.com

5.3.7 RNA/Protein Extraction

RNA and protein were extracted from snap frozen explants. For RNA isolation, tissues were homogenized in 1 mL Trizol reagent (Invitrogen) and RNA was collected following the manufacturer's protocol. RNA concentration was quantified using A260/280 measurements from a Nanodrop 2000 (Thermo Scientific). Total protein was isolated by homogenizing tissue in 1 mL mPER (mammalian protein extraction reagent) supplemented with protease inhibitor, phosphatase inhibitor, and EDTA (Thermo Scientific). Protein concentration was quantified using a standard BCA assay (Pierce).

5.3.8 qRT-PCR

RNA was converted to cDNA using the SuperScript First-Strand Synthesis System according to the manufacturer's protocol with random primers (Invitrogen). Relative real-time PCR was then performed using an ABI 7900HT sequence detection system using SYBR GREEN PCR master mix (Applied Biosystems) as follows: stage 1: 50°C for 2 minutes; 95°C for 10 minutes; stage 2 (40–45 cycles): 95°C for 15 seconds; 60°C for 1 minute; 72°C at 20 seconds; stage 3 (dissociation curve): 95°C for 15 seconds; 60°C for 15 seconds; 95°C for 15 seconds. Polymerase chain reaction data were analyzed using Primer Express Software v2.0 (Applied Biosystems). Target mRNA levels were normalized against glyceraldehyde 3-phosphate dehydrogenase (GAPDH) levels. The following primer pairs were used: (1) GAPDH, forward: GAAGGTGAAGGTCGGAGTC; reverse: GAAGATGGTGATGGGATTTC and (2) IGFBP-7 (NM_001553), forward: GCCATCACCCAGGTCAGCAAG; reverse: GGATTCCGATGACCTCACAGCT.

5.3.9 Cytokine Arrays

High-throughput protein analysis was performed using antibody membrane arrays purchased from Ray Biotech, Inc. The cytokine array mechanism is comparable to a sandwich ELISA run on an antibody-spotted membrane. Human cytokine array V and mouse cytokine array III were used for these studies. Appendix 3 shows cytokine maps for both the mouse and the human arrays. The cytokine array protocols were developed as recommended by the manufacturer.

www.manaraa.com

Membranes were blocked for 30 minutes at room temperature in 2 mL of the supplied 1X blocking buffer. Membranes were then incubated with protein samples for one hour at room temperature. Membranes were then washed three times with 2 mL of each 1X wash buffers I and II. 2 mL anti-cytokine primary antibodies were then incubated over the membranes overnight at 4 ºC, after which the membranes were washed 3X in each wash buffers I and II again. Horseradish peroxidase (HRP)-conjugated streptavidin (SA) was then incubated for two hours at room temperature followed by a washing step. 500 µL of supplied detection buffer was added to each membrane before exposure on Kodak x-ray film. Densitometric spot quantification was performed using the gel analysis tool in Image J software, where each spot was normalized to the average of positive control spots. Statistical analysis was performed using GraphPad Prism software.

5.3.10 M12mac25 Explant Lysate Cytokine Arrays

M12mac25 explant protein lysates were developed as described in section 5.3.7. Protein concentrations of M12mac25 explants lysed in mPER lysis buffer were determined using a BCA assay. 10 µg of protein diluted in 1 mL 1X blocking buffer were used as samples for both human cytokine array V and mouse cytokine array III. Because the human arrays have singlet spots per cytokine and the mouse arrays are spotted in duplicate, the human arrays were run in duplicate.

5.3.11 M12mac25 Explant Lysate DNA Oligonucleotide Arrays

DNA oligo arrays were performed and analyzed by Pete Nelson's lab at the Fred Hutchinson Cancer Research Center as previously described [121][122]. Reference RNA was pooled from several prostate cancer cell lines. Total RNA from experimental samples was amplified using the Ambion MessageAmp aRNA kit and hybridized to a 44K oligonucleotide microarray. Hybridization and data acquisition was performed as previously described. Spots with average intensity levels <300 were removed from the analysis. Genes were ranked based on up-regulation in pHEMA demonstrated by log2 fluorescence ratio measurements. Microarray results were subjected to Gene Set Enrichment Analysis as previously described [121].

www.manaraa.com

5.3.12 Tissue Digestion of Scaffold-Derived M12mac25 Tumors

Twelve M12mac25-seeded pHEMA scaffolds were implanted into six athymic nude mice (2 scaffolds per mouse). Tumor growth was monitored, and after twelve weeks the scaffold-derived M12mac25 tumors were explanted and placed in a tube with serum free RPMI media on ice. The tumors were diced into small pieces in PBS using sterile scalpel blades, and the tissue slurry was vortexed and pipetted through a 100 µm cell strainer (BD Falcon). The strained suspension was centrifuged and washed 2x with sterile PBS.

5.3.13 Staining and Flow Separation of Scaffold-Derived M12mac25 Tumors

Viable cell concentrations from the tumor suspension were estimated before staining using a hemocytometer with standard trypan blue exclusion. Cells were re-suspended in staining buffer (PBS with 2% FBS) at a concentration of $20x10^6$ cells/mL and stained with a PE-labeled antibody to EpCAM (epithelial cell adhesion molecule, BD) (50 µL per 2 mL sample) for 30 minutes on ice and the viability exclusion dye 7AAD (BD) (30 µL per 2 mL sample) for 10 minutes on ice. Stained cells were washed 3x in staining buffer with a final re-suspension in flow sorting buffer (PBS with 1% FBS and 10 nM HEPES). The cell suspension was filtered through a 40 µm cell strainer (BD) prior to flow separation.

Flow experiments were run on a FACSAris (BD) cell sorter with FACSDiva software at the UW Department of Immunology Cell Analysis Facility. Prior to sorting digested tissue, M12mac25 EpCAM expression validation was performed using flow cytometry of 2D-cultured *in vitro* M12mac25 cells prior. All gating and compensation settings for the tissue separation experiment were determined using unstained and stained M12mac25 cell line controls. The following gating progression was used to identify M12mac25 cells from the rest of the tumor suspension: FSC vs. SSC, 7AAD-negative, EpCAM-positive.

5.3.14 Re-Injection of Flow-Separated M12mac25 Cells in Matrigel

Flow-separated, tumor-derived M12mac25 cells were mixed 1:1 with Matrigel and 200 µL containing $1x10^6$ cells were subcutaneously injected in five mice. Mice were monitored for tumor formation and implant size was recorded over twelve weeks. Visible Matrigel plugs were

www.manaraa.com

explanted at twelve weeks, placed in zinc fixative overnight at 4 °C, processed for histology as in and immunostained for the SV40T antigen as in section 5.3.3.

5.3.15 Clondronate Liposome Pilot Study #1- Injection Strategy

Clondronate liposomes (CLs) and PBS-containing liposome (PBSL) controls were obtained through collaboration with the Clondronate Liposomes Foundation in the Netherlands. Liposome formulation has been previously described [123]. A series of three pilot studies were used to optimize and gauge the effectiveness of *in vivo* macrophage elimination within the scaffolds. The first pilot study was designed to validate an injection strategy to localize liposomes to subcutaneously-implanted scaffolds. Two athymic nude mice were implanted each with two porous pHEMA scaffolds containing no seeded cells. On day seven after implantation, PBS liposomes were injected and 24 hours later the scaffolds and spleen were explanted, embedded in OCT, and frozen for cryosectioning. PBSLs were labeled with the lipophilic dye DiI (Molecular Probes). 10 µL DiI was added to 1 mL PBSL suspension and incubated at room temperature in the dark. The liposomes were centrifuged at 20,000 x g for 10 minutes. The supernatant was replaced with sterile PBS and the liposomes were centrifuged and washed again in PBS to the original volume. For liposome injections, one mouse received an intraperitoneal (IP) injection of 200 µL DiI-labeled PBSLs (represents 1 mg/20 g mouse body weight dose) while the other mouse received an IP injection of 200 µL of standard, unlabeled PBSLs. Additionally, one scaffold per mouse was subcutaneously injected with 50 µL of DiI-labeled PBSLs. Cryosectioned spleen and subcutaneous tissue were observed under a fluorescent microscope in the Rhodamine channel.

5.3.16 Clondronate Liposome Pilot Study #2- Dosage Strategy

A second pilot study was designed to determine the frequency with which CLs must be dosed to have effectiveness. Four athymic nude mice were each implanted with two porous pHEMA scaffolds containing no seeded cells. On day seven after implantation, 100 µL of either CLs or PBSLs were subcutaneously injected around the left and right pHEMA scaffolds, respectively. Mice were sacrificed 24, 28, 72, and 96 hours after injection. Scaffold explants were fixed and processed for H+E histology as previously described.

www.manaraa.com

5.3.17 Clondronate Liposome Pilot Study #3- Long-Term FBR Knockdown

A third pilot study was designed to determine whether clondronate liposomes, when delivered using optimal injection and dosing frequency, could knock down macrophage infiltration and the foreign body response over longer time period. Six athymic nude mice were each implanted with two porous pHEMA scaffolds containing no seeded cells. Starting on the day of implantation, the area around each scaffold was subcutaneously injected with 100 µL of either CLs or PBSLs around the left and right pHEMA scaffolds, respectively. Liposomes were repeatedly injected every five days. Two mice were sacrificed at seven, fourteen, and twenty-one days after surgery. Scaffold explants were fixed and processed for Masson's trichrome and IHC as previously described.

5.3.18 M12mac25 Clondronate Liposome Study

Eleven athymic nude mice were each implanted with two porous pHEMA scaffolds containing M12mac25 cells cultured in 3D for five days as described in section 5.3.1. Starting on the day of surgery, the area around each scaffold was subcutaneously injected with 100 µL of either CLs, PBSLs, or sham sterile PBS. The injections took place every five days. The scaffolds were randomized for which received each kind of injection, but seven scaffolds were chosen for CLs, seven scaffolds for PBSLs, and eight scaffolds for sham injections. Two mice containing one CL scaffold, one PBSL scaffold, and two sham scaffolds were sacrificed after three weeks. The study endpoint was twelve weeks, but due to the formation of skin ulcerations in mice injected repeatedly with clondronate liposomes, the study was cut short. Six mice were sacrificed after six weeks (four scaffolds per experimental group) and the remaining three mice were sacrificed after eight weeks (two scaffolds per experimental group). All scaffold explants were fixed and processed for histology as previously described. Explant sections were stained with Masson's trichrome, and IHC was performed with SV40T, F4/80, and MECA-32.

5.3.19 In Vitro *Clondronate Liposome Analysis*

To confirm that clondronate liposomes are not cytotoxic to M12mac25 cells, an *in vitro* study was performed where M12mac25 cells and bone marrow-derived macrophages (see section 6.3.1) were cultured in 2D in 48-well plates (seeding densities of 10,000 and 20,000 cells, respectively). After overnight plate attachment, triplicate wells of each cell type were exposed to

www.manaraa.com

1% (v/v) CLs, PBSLs, and sterile PBS. After 72 hours, a 1:10 volume of alamarBlue was added to each well for proliferation analysis (see section 6.3.2).

5.4 Results

5.4.1 Pilot and Follow-Up Implant Studies

M12mac25 cells are non-tumorigenic when injected subcutaneously with or without Matrigel. However, in a pilot study (see section 5.3.2) it was observed that in all mice, M12mac25 cells formed tumors when seeded in the pHEMA scaffolds with and without Matrigel. Tumors became noticeable approximately eight weeks post-implantation. To confirm the reproducibility of these results and do further molecular analysis, a follow-up *in vivo* study was run (see section 5.3.6) and the same trends were produced. Figure 5.1 shows tumor growth data combined between these studies. In total, 9/9 pHEMA scaffolds seeded with M12mac25 cell formed tumors, 3/3 pHEMA scaffolds seeded with M12mac25 cells and Matrigel formed tumors, 7/9 M12mac25 cells + Matrigel injections remained dormant, while 2/9 M12mac25 cells + Matrigel grew tumors.

www.manaraa.com

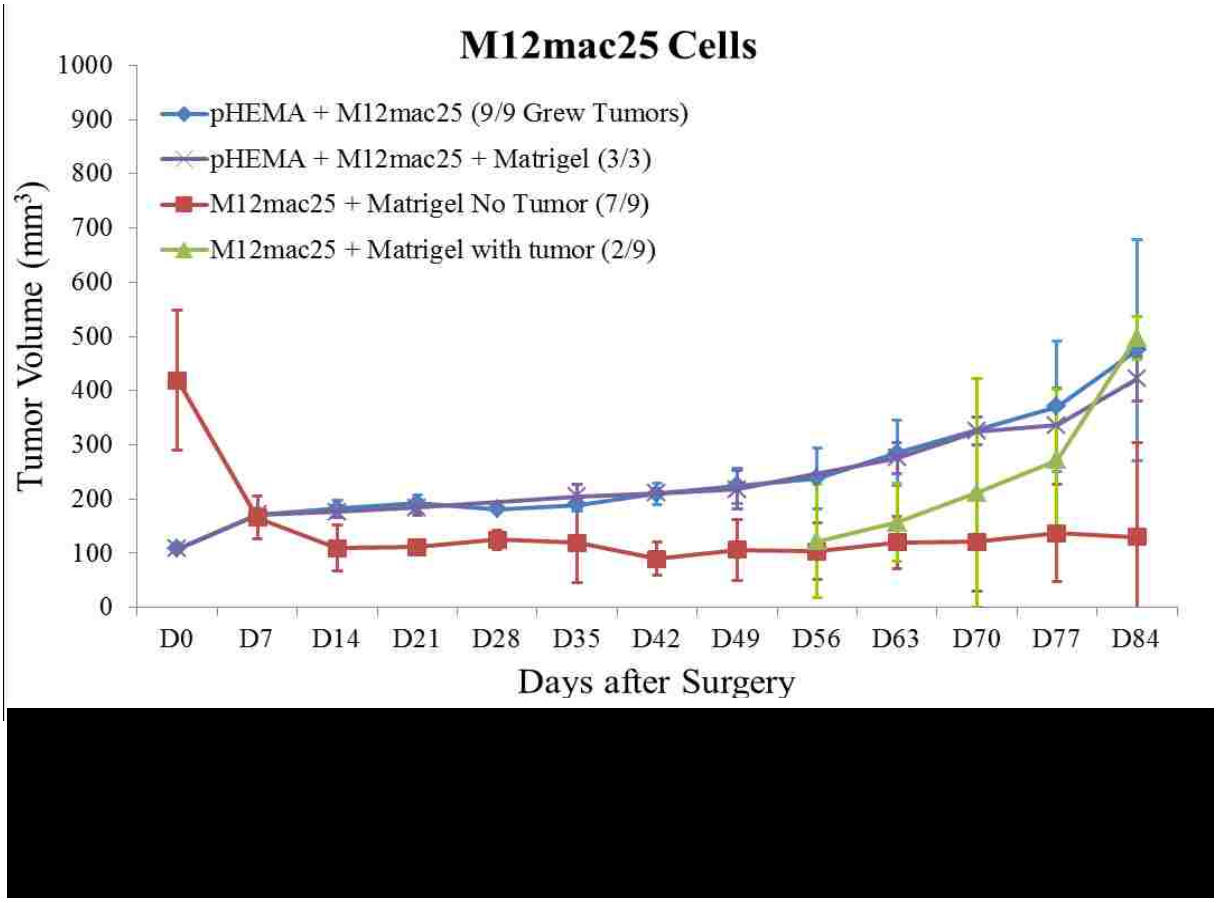

5.4.2 M12mac25 Xenograft Histological Analysis

Figure 5.2 shows a representative trichrome stain of a D84 M12mac25-seeded pHEMA explant that demonstrates a clear proliferation of cells outside the scaffold that were confirmed as SV40T+ M12mac25 cells using immunohistochemistry (see Figure 5.3A). IHC analysis of D21 M12mac25 + pHEMA explants shows that M12mac25 cells have not yet begun to significantly proliferate within the scaffold at this early time point (see Figure 5.3B). In contrast to the tumors formed within the pHEMA scaffolds, IHC of M12mac25 + Matrigel explant shows SV40T+ human cells to be largely confined to their small Matrigel plug (see Figure 5.3C).

MECA staining showed no statistically significant differences in vascularity between the scaffold and Matrigel-derived explants at D21 or D84 (see Figure 5.4). However, a significant increase in F4/80+ macrophage density was observed in the pHEMA-derived explants compared with those from Matrigel at three weeks ($p<0.005$), with average macrophage density still higher in pHEMA at D84 (see Figure 5.5A). Macrophage density within the scaffolds themselves was noticeably lower at D84 compared to D21, and macrophage density increased around the edges

www.manaraa.com

of the Matrigel explants at D84 compared to D21. However, it is notable that D84 macrophage localization differed between the sample groups. Macrophages in the Matrigel samples were present largely around clusters of M12mac25 cells, whereas macrophages in the pHEMA samples were present in close proximity to M12mac25 cells both within the scaffold and in the bulk tumor region (see Figure 5.5B-D).

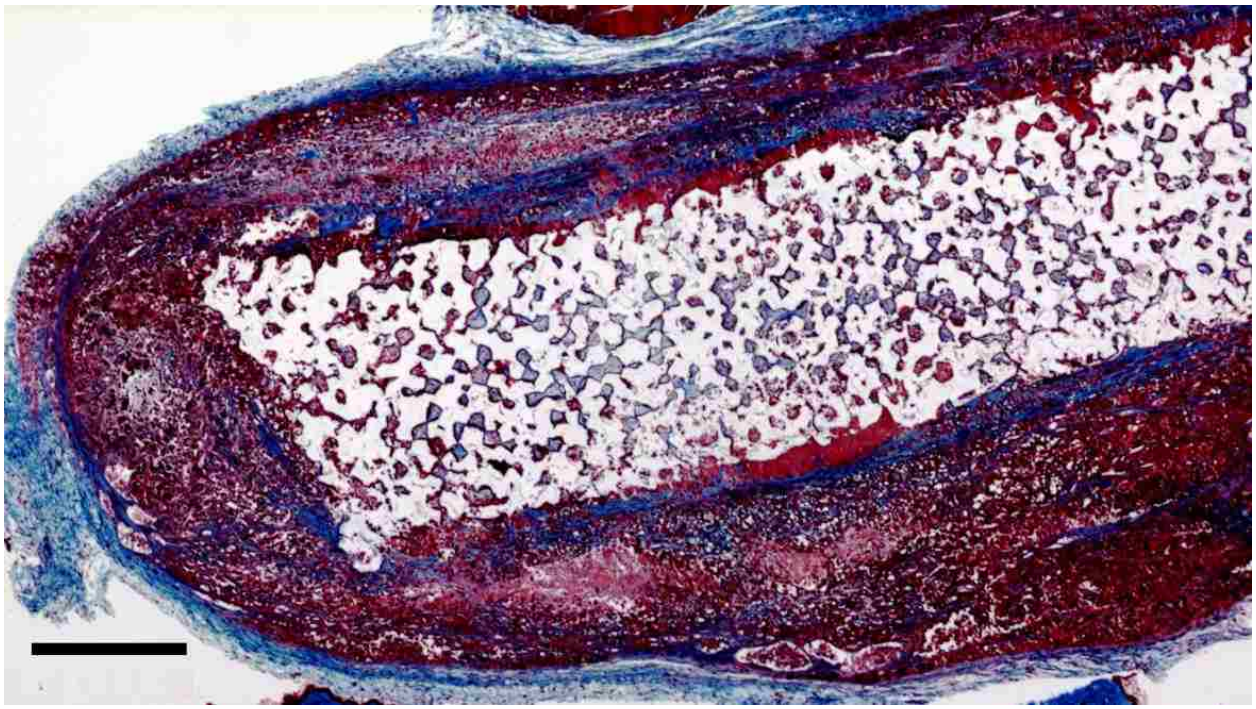

5.4.3 Explant mac25 qRT-PCR Analysis

One possible explanation for M12mac25 tumorigenesis is the loss of IGFBP7 expression. RT-PCR showed a decline in IGFBP7 transcript levels from *in vitro* culture in all twelve week explants, likely due to the heterogeneous cell population *in vivo*. However, IGFBP7 mRNA was significantly higher in the pHEMA group compared with both the growth ($p<0.01$) and no growth ($p<0.05$) Matrigel groups (see Figure 5.6). IGFBP7 levels were also significantly higher in the Matrigel explants that grew tumors compared with those that did not ($p<0.05$). These data demonstrate that mac25/IGFBP7 loss is likely not responsible for the observed M12mac25 phenotypic change.

www.manaraa.com

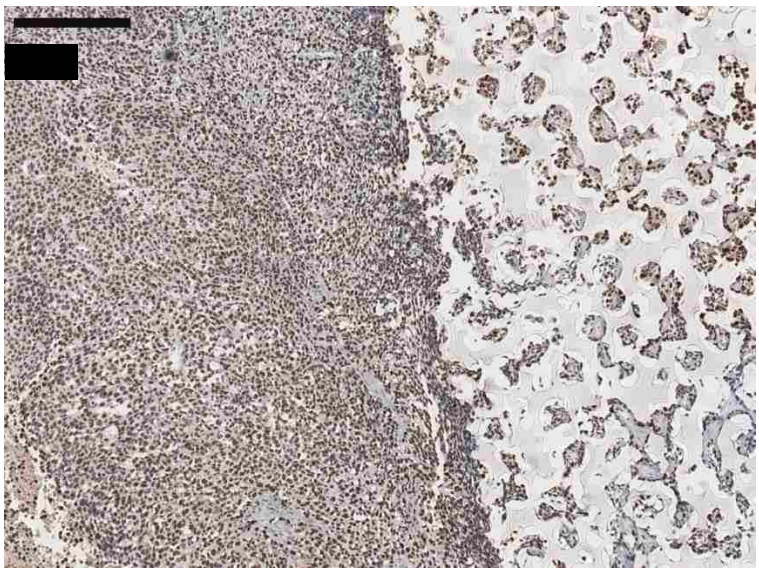

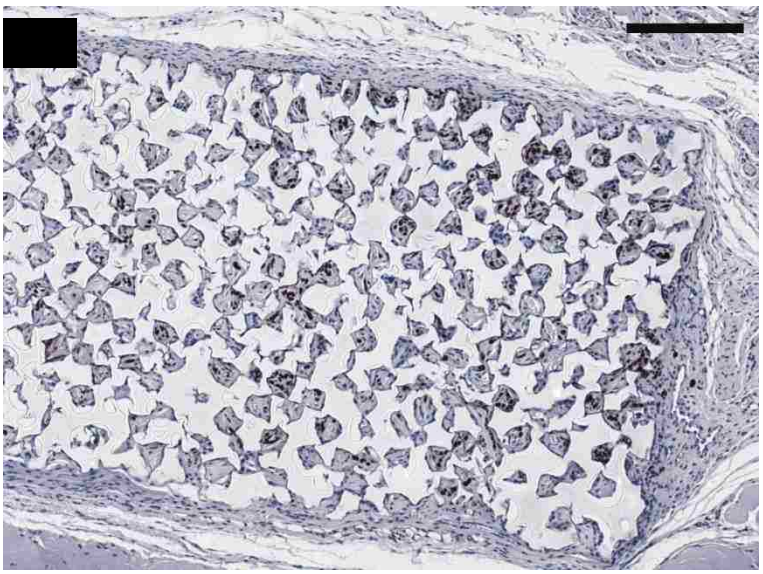

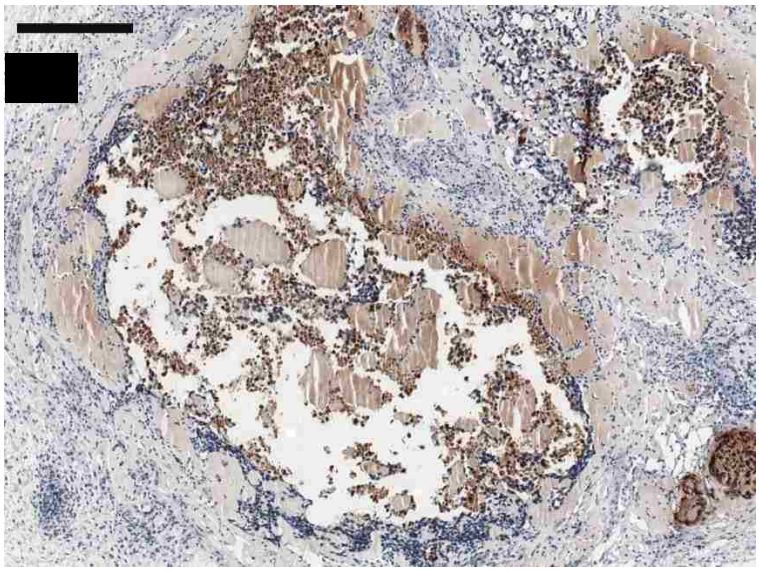

[redacted]

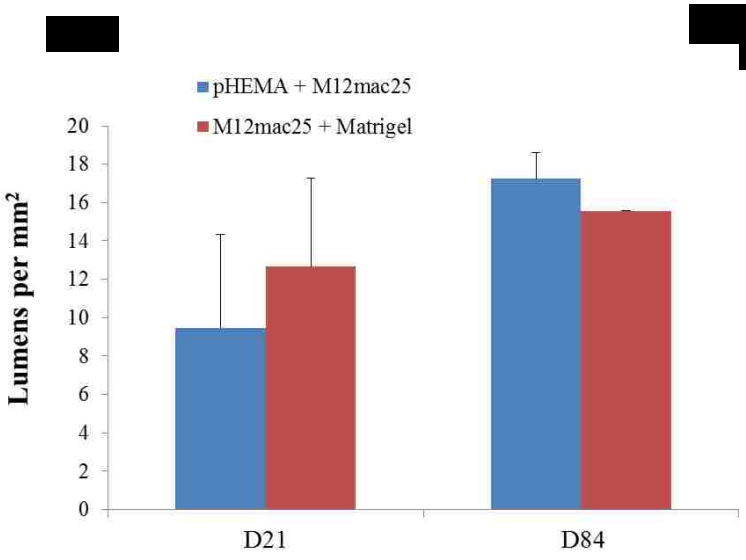

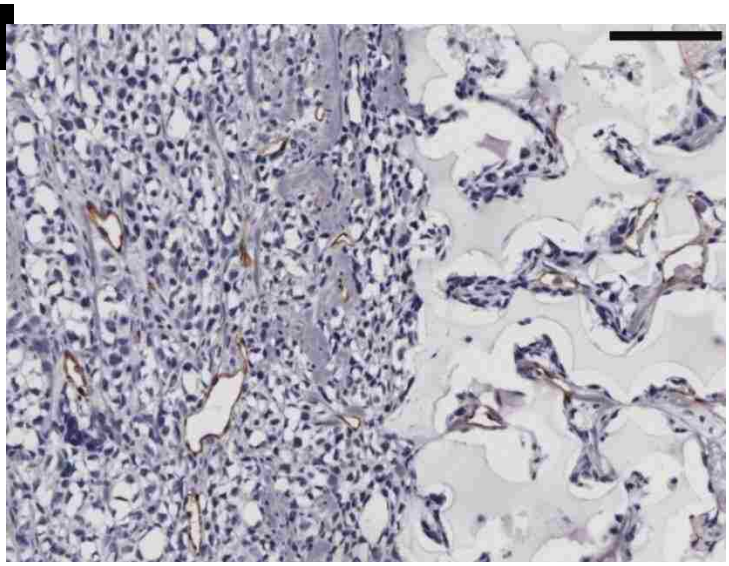

[redacted]

www.manaraa.com

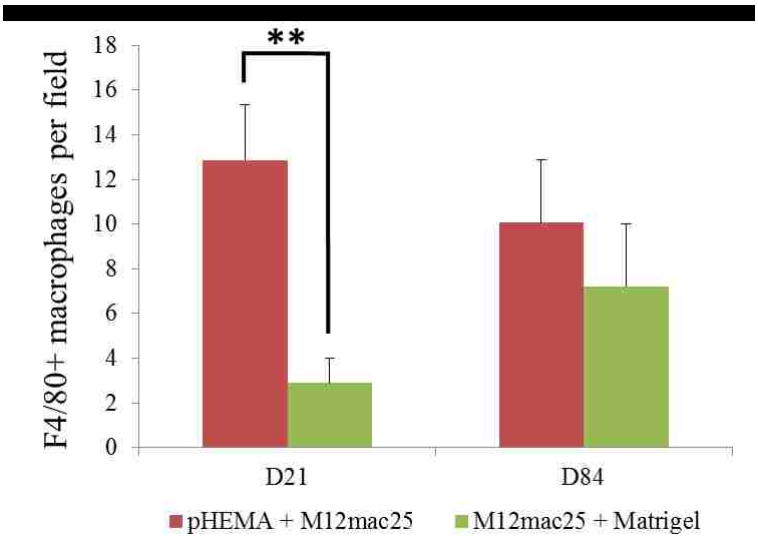

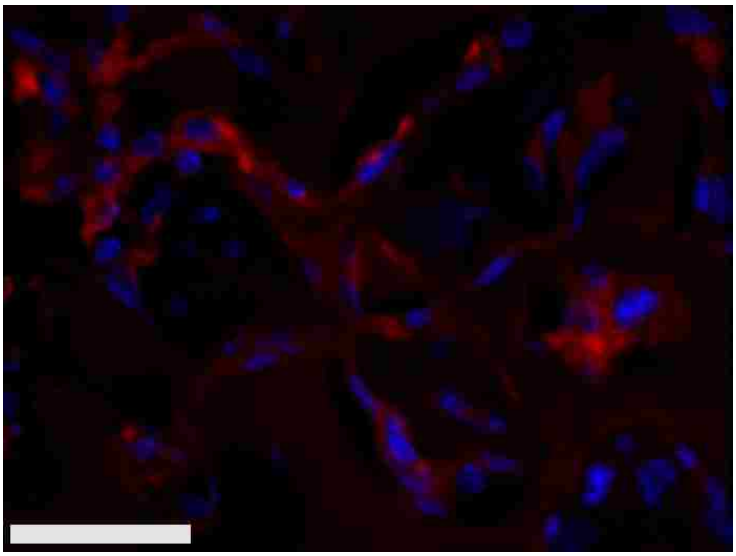

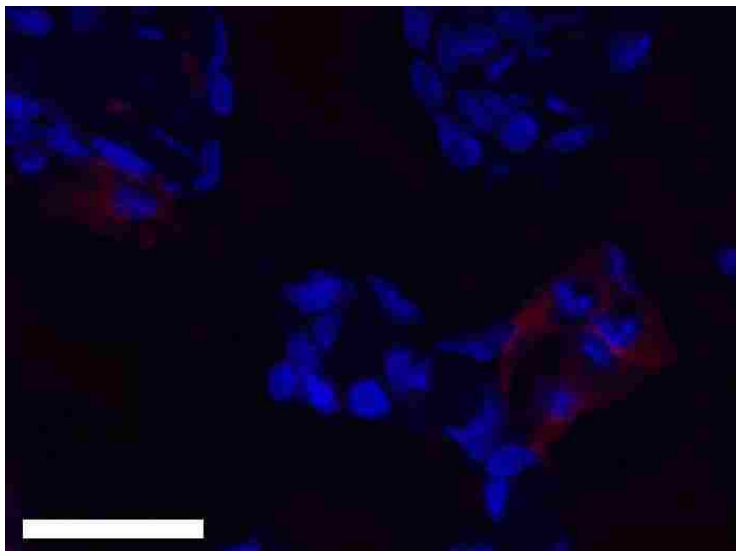

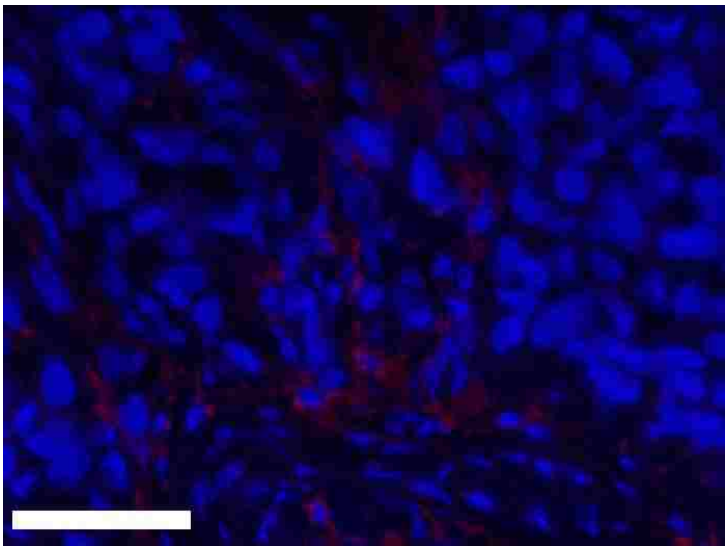

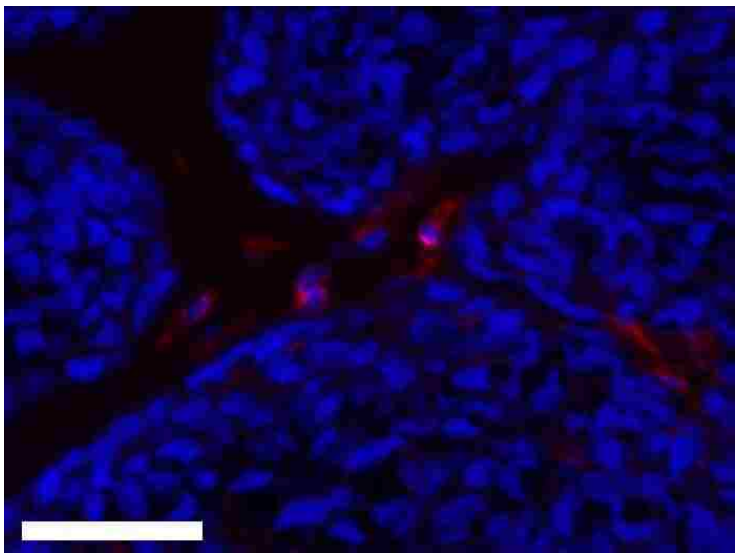

www.manaraa.com

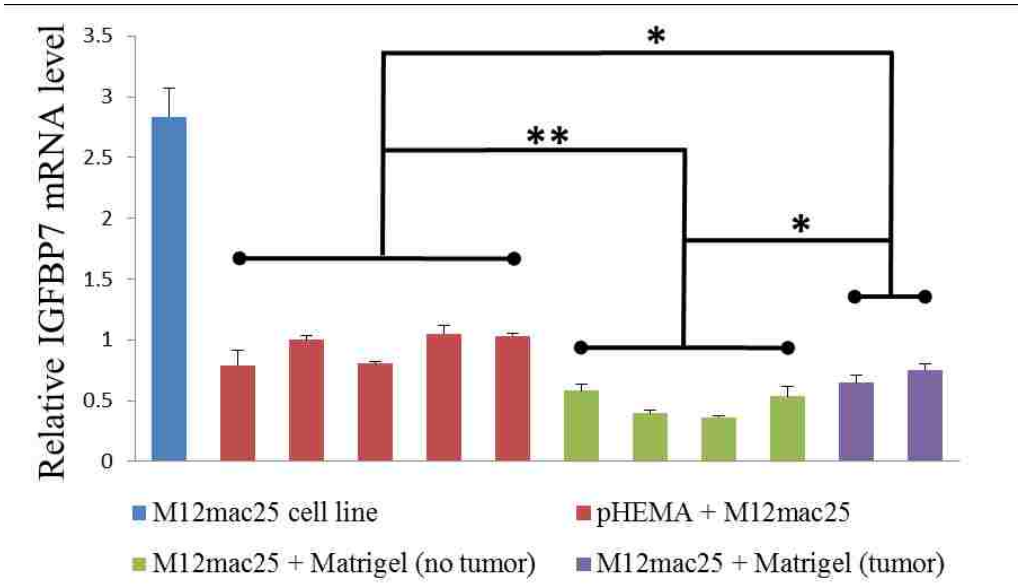

[redacted]

5.4.4 M12mac25 Explant Lysate Cytokine Arrays

Example human and mouse cytokine arrays from explants are shown in Figure 5.7. The *in vivo* explant cytokine arrays tended to have a background signal, which is especially evident when compared to the conditioned media cytokine arrays (see Figure 6.2), so spots with a density less than 2% of the positive control (densities averaged among pHEMA and Matrigel groups) were removed from consideration. Appendix 4 shows the top 20 cytokines present on both the human and mouse arrays for pHEMA explants sorted by average density. There was generally good

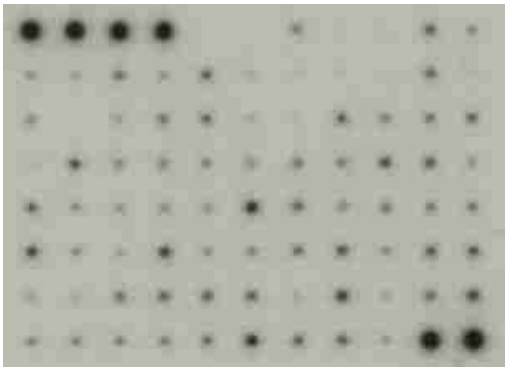

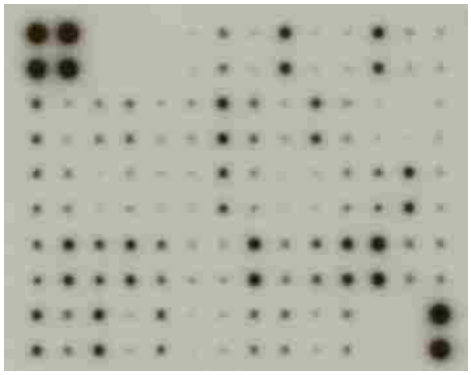

[redacted]

www.manaraa.com

agreement between the top cytokines present in the pHEMA and Matrigel explants (17 out of 20 protein agreement for the human arrays and 19 out of 20 for the mouse arrays). However, because we are interested in the *differences* between the pHEMA and Matrigel samples in an attempt to explain M12mac25 dormancy escape, the student t-test was used to determine which cytokines had statistically different expression between those groups. A list of the cytokines that showed significant difference between the pHEMA and Matrigel groups is shown in Table 5.2, and full human and mouse array significance data are shown in Appendices 5 and 6, respectively. All the cytokines listed, with the exception of IL-4 on the mouse arrays, were higher in the pHEMA-derived samples compared to those from Matrigel. Figures 5.8 and 5.9 highlight some representative proteins found to be significant in the human and mouse arrays, respectively (full data sets for significant proteins can be found in Appendices 5 and 6). In those figures, each data point represents normalized density for one spot of that particular cytokine. The data is divided into three groups: pHEMA (5 samples), Matrigel growth (2 samples) and Matrigel no growth (3 samples). It was also possible to draw statistical conclusions about cytokines with different expression levels between the Matrigel growth and Matrigel no growth groups, and those data are also summarized in Table 5.2 and shown in full in Appendix 5. At first glance it is clear that the pHEMA-derived explants show more variability in spot density for most proteins compared with Matrigel-derived explants. This is likely because the pHEMA explants were more heterogeneous in cellular content compared with the Matrigel explants.

Many of the proteins found to be up-regulated in the pHEMA samples are associated with macrophage recruitment or an inflammatory macrophage phenotype (indicated with a * in Table 5.2). IL-1β, CCL8, CCL11, CCL5, CXCL9, and CXCL10 are cytokines produced by inflammatory macrophages [100]. In addition, the IL-12^{high} IL-10^{low} phenotype is typically shown by inflammatory macrophages. In these explants, IL-12 levels were higher across all groups compared with IL-10 levels, and IL-12 was significantly higher in pHEMA explants relative to Matrigel. CCL5 is a potent chemotactic factor for macrophages, which was significantly higher in pHEMA explants compared to Matrigel in the mouse arrays. However, in the human arrays it was also one of the most highly expressed proteins (see Appendix 4), as was M-CSF, another macrophage recruitment factor. VEGF was also significantly up-regulated in pHEMA in both the mouse and human arrays. While we did not demonstrate higher vascularity

www.manaraa.com

in the pHEMA explants, macrophage recruitment can lead to an up-regulation of the factors associated with angiogenesis, including VEGF [23]. Vascular cell adhesion molecule-1 (VCAM-1) was shown to be significantly higher in the pHEMA explants by mouse array. VCAM-1 is generally expressed by endothelial cells and allows circulating immune cells such as monocytes to tether to and infiltrate tissues [124]. Finally, CXCL5 (ENA-78 on human arrays and LIX on mouse arrays) was found to be the most significantly up-regulated protein in pHEMA from the human cytokine arrays and one of the top 20 most present cytokines on the mouse arrays. CXCL5 was also significantly higher in the Matrigel growth group compared to the Matrigel no growth group.

Human Protein	**p value**		**Mouse Protein**	**p value**
ENA-78 (CXCL5)#	*0.0138*		**VEGF**	0.0006
IL-1β*#	0.0163		**IL-1β***	0.0007
IL-15	0.0169		CD30T	0.0013
MCP-2 (CCL8)*#	0.0297		IGFBP5	0.0014
IL-3	*0.0341*		Leptin	0.0035
LIGHT#	0.0348		*RANTES (CCL5)**	*0.0088*
IGFBP-1	0.0425		**Eotaxin (CCL11)***	0.0098
IL-2	*0.0427*		*SDF-1a (CXCL12)^*	*0.0143*
VEGF	0.0445		CTACK (CCL27)^	0.0146
IL12 p40p70#*	*0.0475*		*MIG (CXCL9)**	*0.0234*
PDGF-BB	0.0496		TPO	0.0248
Eotaxin (CCL11)*	0.0512		CRG-2 (CXCL10)*	0.0329
			VCAM-1	0.0385
			*IL-4 (lower expression)**	*0.0401*

Table 5.2 Proteins identified by human and mouse cytokine arrays to be significantly different between pHEMA and Matrigel (no growth)-derived M12mac25 explants. Proteins in **bold** show agreement between mouse and human arrays. Proteins in *italics* only showed significance on one out of two mouse or human arrays (note: proteins in neither bold nor italics were not present on both arrays and could not be compared). Proteins with * are associated with macrophage recruitment or the inflammatory macrophage phenotype. Proteins with ^ are associated with an alternatively activated macrophage phenotype. Proteins with # also showed significance or a trend toward significance in the Matrigel no growth vs. growth samples.

www.manaraa.com

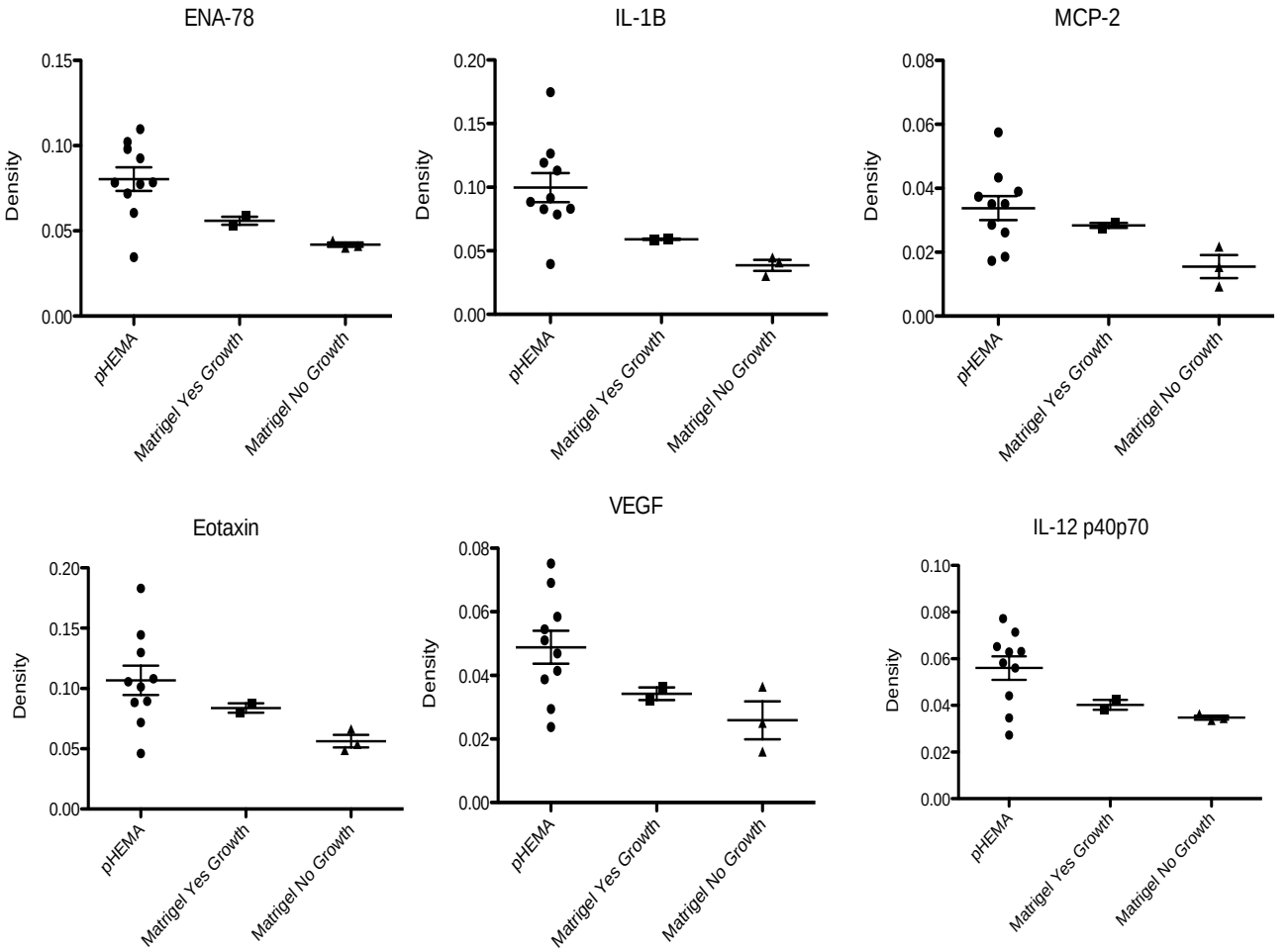

[redacted]

5.4.5 M12mac25 Explant Lysate DNA Oligonucleotide Arrays

Unsupervised clustering of the top 1000 most variable genes between the pHEMA and Matrigel-derived M12mac25 xenografts resulted in the clustering of pHEMA and Matrigel samples with each other, showing that the expression levels of those genes were distinguishable between those sample groups (see Figure 5.10). Matrigel no growth samples formed a sub-cluster separate from Matrigel growth samples, but both sets of Matrigel-derived samples clustered separately from pHEMA-derived tumors.

www.manaraa.com

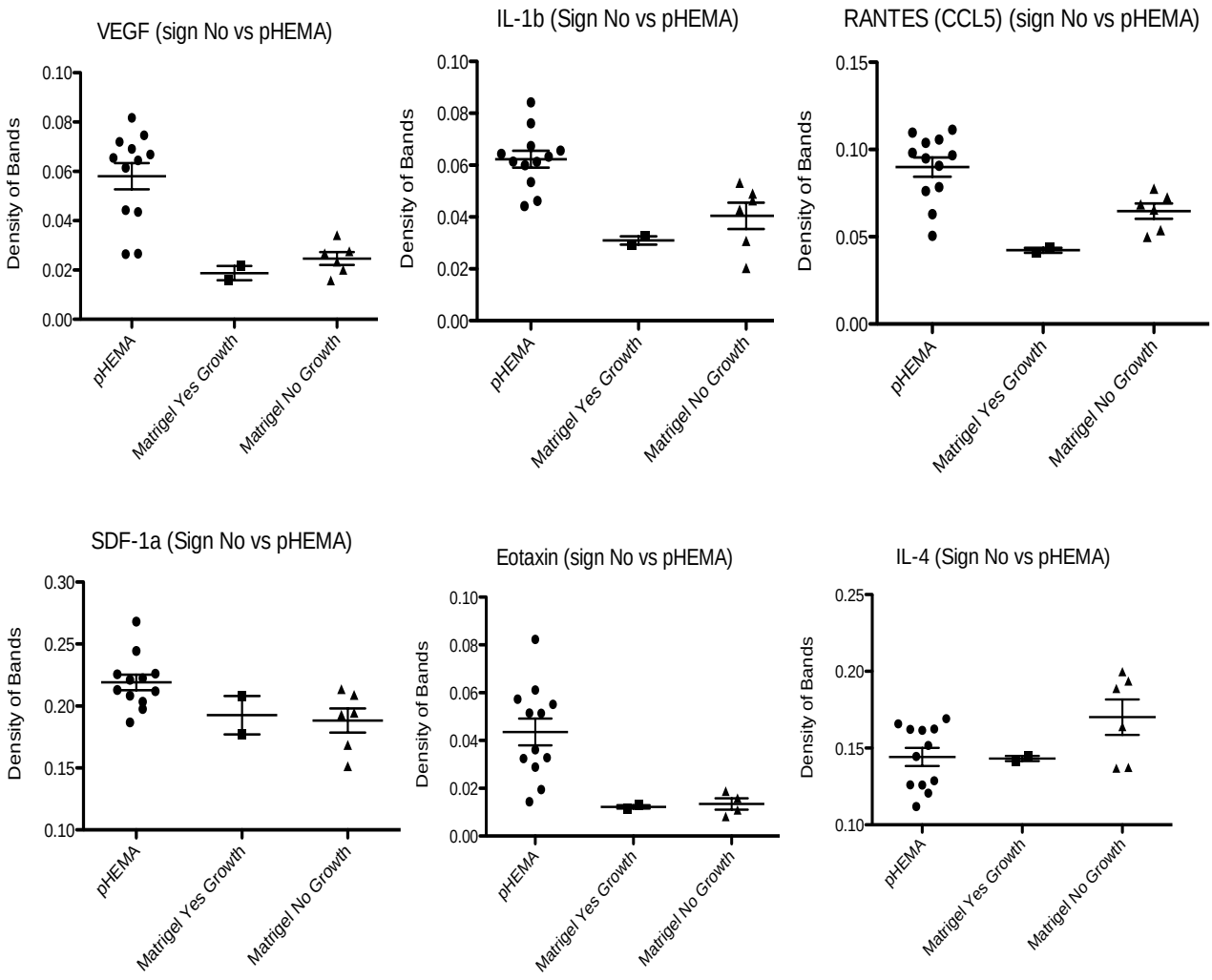

[redacted]

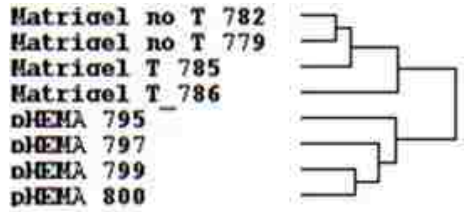

[redacted]

Gene set enrichment analysis (GSEA) was performed on all samples, and the results for gene set up-regulation and down-regulation are shown in Appendix 8. Using this analysis for guidance, it was determined that in general groups of genes associated with transcription, translation, cell cycle regulation, and cell/ECM interactions were upregulated in pHEMA compared with

www.manaraa.com

Matrigel, while groups of genes associated with mitochondrial proteins and aerobic respiration were down-regulated in pHEMA compared with Matrigel. These results are consistent with tumorigenic versus non-tumorigenic phenotypes.

The top 50 genes most up-regulated in pHEMA relative to Matrigel are shown in Appendix 8. A deeper one-by-one analysis of genes for major cytokines, chemokines, ECM proteins/receptors, intracellular signaling proteins, transcription factors, growth factors, prostate-related proteins, and those proteins previously identified from explant cytokine arrays is shown in Appendix 9 with a subset shown in Table 5.3. Full microarray data sets are available upon request. This analysis revealed several classical signaling pathways that were potentially up-regulated in pHEMA relative to Matrigel: mitogen-activated protein kinase/extracellular signal-related kinase (MAPK/ERK), phosphatidylinositol-3-kinase/protein kinase B (PI3K/AKT), transforming growth factor-β (TGF-β)/SMAD, Rho/Rock, and janus kinase/signal transducer and activator of transcription (JAK/STAT). When hyper-active, these pathways have been linked to aberrant cell proliferation and tumorigenesis. Pathway maps indicating which genes are up-regulated can be found in Appendices 10 and 11.

www.manaraa.com

Gene Name	Protein Name (if different)	SAM Rank (Fold Change pHEMA vs. Matrigel)	Replicate hit (if applicable)
CCL5	RANTES	3499 (1.58)	
CCL2	MCP-1	14731 (-1.4)	
CCL24	Eotaxin-2	13454 (-1.4)	
CXCL5	ENA-78	2079 (2.16)	2652 (1.51)
CXCL2	GRO-B	5947 (1.35)	
CXCL1	GRO-A	8859 (1.09)	
CXCL12	SDF-1	10711 (-1.2)	
IL1β		18017 (-3.7)	
IL6		4430 (1.46)	
CDH2	N-cadherin	6587 (1.21)	
CDH1	E-cadherin	16669 (-1.6)	
VIM	Vimentin	323 (1.4)	1681 (1.33)
EGFR	epidermal growth factor receptor	16969 (-1.3)	
FGF2	fibroblast growth factor 2	3 (1.84)	
FGF9	fibroblast growth factor 9	17365 (-2.8)	
VEGFC	vascular endothelial growth factor C	925 (2.56)	
VEGFA	vascular endothelial growth factor A	6806 (1.13)	
TGFB2	transforming growth factor β2	226 (1.68)	
TGFB1	transforming growth factor β1	947 (2.15)	
TGFBR2	transforming growth factor β receptor 2	1007 (1.5)	
IGFBP7	insulin-like growth factor binding protein 7	12559 (-1.3)	
HIF1α	hypoxia inducible factor 1 alpha	1910 (1.22)	
PTEN		7445 (1.06)	
mTOR	mammalian target of rapamycin	6327 (1.1)	
AKT3		15 (3.42)	
RhoA		172 (1.34)	417 (1.35)
Rock1		542 (1.4)	2593 (1.5)

Table 5.3 DNA oligonucleotide array results showing select genes of interest. More individual gene analysis can be found in Appendix 10. SAM rank indicates gene position in the full list of genes sorted by up-regulation in pHEMA (from 1 to roughly 18,000). The number in parentheses is the fold change relative to Matrigel (a negative number indicates the gene was up-regulated in Matrigel relative to pHEMA).

www.manaraa.com

Human Cytokine Array Data		Human cDNA array data	
Top 20 most present cytokines	Normalized Average Spot Intensity	Also present on the array?	Rank (fold change)
pHEMA + M12mac25			
TGF-β2	0.312406017	Y	226 (1.68)
NAP-2 (CXCL7)	0.214119718	N	N/A
FGF-9	0.211329695	Y	17365 (-2.8)
Oncostatin M (OSM)	0.186929029	N	N/A
GDNF	0.180155393	N	N/A
BDNF	0.178621145	N	N/A
TIMP-1	0.174286083	Y	11560 (-1.1)
IGFBP-2	0.163863154	Y	18038 (-5.7)
HGF	0.162091647	N	N/A
Osteopontin (SPP1)	0.15606151	N*	N/A*
RANTES (CCL5)	0.152368155	Y	3499 (1.58)
MCSF (CSF1)	0.1517563	N	N/A
GRO (CXCL1)	0.147386092	Y	8859 (1.09)
MIF	0.143576844	Y	9364 (1.01)
NT-3 (NTF3)	0.132236886	N	N/A
IP-10 (CXCL10)	0.131925894	N	N/A
GCP-2 (CXCL6)	0.12223965	N	N/A
LIF	0.113217919	N	N/A
IL-3	0.108432874	N	N/A
Eotaxin-2 (CCL24)	0.108294291	Y	13454 (-1.4)
* Gene not present on DNA oligonucleotide array			

Table 5.4 Comparison between top 20 human cytokine array results and DNA oligonucleotide array results. The top twenty most present cytokines from human cytokine arrays sorted by normalized average spot intensity are shown in column one (official gene names in parentheses if different from protein name). Column three indicates whether these genes were also present on average above background intensity on the DNA oligonucleotide arrays. If so, their SAM rank and fold up-regulation/down-regulation is shown in column 4. 19 out of the 20 proteins were also found on the DNA oligo array, and 8 showed up as present in the M12mac25 explants.

www.manaraa.com

Human Protein	cDNA rank (fold change)		Mouse Protein	cDNA rank (fold change)	Mouse/human sequence homology?
ENA-78 (CXCL5)	2079 (2.16)		VEGF	925 (2.56)	N
IL-1B	18017 (-3.7)		IL-1B	18017 (-3.7)	N
IL-15	9495 (1)		CD30T*	N/A*	
MCP-2 (CCL8)	N/A		IGFBP5	17329 (-3.7)	N
IL-3	N/A		Leptin	N/A	N
LIGHT (TNFSF14)	N/A		RANTES (CCL5)	3499 (1.58)	N
IGFBP-1	N/A		Eotaxin (CCL11)	N/A	N
IL-2	N/A		SDF-1a (CXCL12)	10711 (-1.2)	N
VEGF	925 (2.56)		CTACK (CCL27)	N/A	N
IL12 p40p70	N/A		MIG (CXCL9)	N/A	N
PDGF-BB	N/A		TPO	N/A	N
			CRG-2 (CXCL10)	N/A	N
			VCAM-1	N/A	N
			IL-4 (lower expression)	N/A	N
*Gene not present on DNA oligonucleotide array					

Table 5.5 Comparison between mouse and human cytokine array results and DNA oligonucleotide array results. Human and mouse proteins that were found to be significantly different between pHEMA and Matrigel-derived M12mac25 xenografts are listed (gene names in parentheses if applicable). If the genes were also found on the DNA oligo array, their SAM rank with fold up-regulation/down-regulation in pHEMA shown in parentheses are listed. Up-regulated genes are shown in red while down-regulated genes are shown in green. With the exception of IL-4, all significant proteins shown were up-regulated in pHEMA vs. Matrigel according to cytokine arrays. It should be noted that for all genes listed from the mouse array, there is no significant sequence homology between the mouse and human oligonucleotides.

www.manaraa.com

5.4.6 Comparisons Between DNA Oligonucleotide and Cytokine Array Results

When examining the top 20 proteins present from the human cytokine arrays, only eight of the nineteen genes that were available on the human DNA oligo array showed up as hits (see Table 5.4). However, it is not uncommon for genomic and proteomic data to not be entirely consistent [125]. The up-regulation or down-regulation of genes in pHEMA relative to Matrigel (shown in red and green in Table 5.4) is not significant in this comparison because in general the top proteins present from the cytokine arrays were the same between pHEMA and Matrigel (see Appendix 4). Where up-regulation and down-regulation becomes significant is when looking at the proteins determined to be significantly different between pHEMA and Matrigel samples (see Table 5.5). What is immediately noticeable is that again, many of the proteins identified by cytokine arrays were also not identified by the DNA oligo arrays. However, if the top proteins identified from Table 5.4 were not observed as gene hits, then it is reasonable that some proteins with less expression may also have not been gene hits. So, just looking at the proteins that were identified in both gene and protein arrays, it is clear that there is some disconnect between the up or down-regulation results. For example, IL-1β was found to be significantly up-regulated in both the human and mouse cytokine arrays but found to be significantly down-regulated in the human gene array. Mouse results can be tricky because there was no reported sequence homology between mouse and human sequences used in the oligo array. However, three proteins shown to be significantly up-regulated in pHEMA were also found to be up-regulated by the DNA oligo array: CXCL5 (ENA-78), VEGF, and CCL5 (RANTES).

5.4.7 Flow Separation of Scaffold-Derived M12mac25 Tumor Cells

Figure 5.11 shows that *in vitro* M12mac25 cells from standard 2D culture were able to be used as controls for EpCAM+ staining and 7AAD-negative viability. M12mac25 cell viability from the tumor suspension was typically around 40-45%, and approximately 60-70% of cells from the viable parent gate stained positive for EpCAM. Figure 5.12 shows representative dot plots and histograms for the disaggregated tumor samples.

5.4.8 Re-injection of Flow-Separated M12mac25 Cells in Matrigel

Of the five mice that received injections of these flow-separated M12mac25 cells with Matrigel, none grew tumors over twelve weeks. Figure 5.13 shows IHC for SV40T where M12mac25 cells

www.manaraa.com

were intact and present in the small explants, confirming that they were not sheared apart during flow separation. These staining images looked equivalent to the dormant M12mac25 explants from the pilot *in vivo* study (see Figure 5.3).

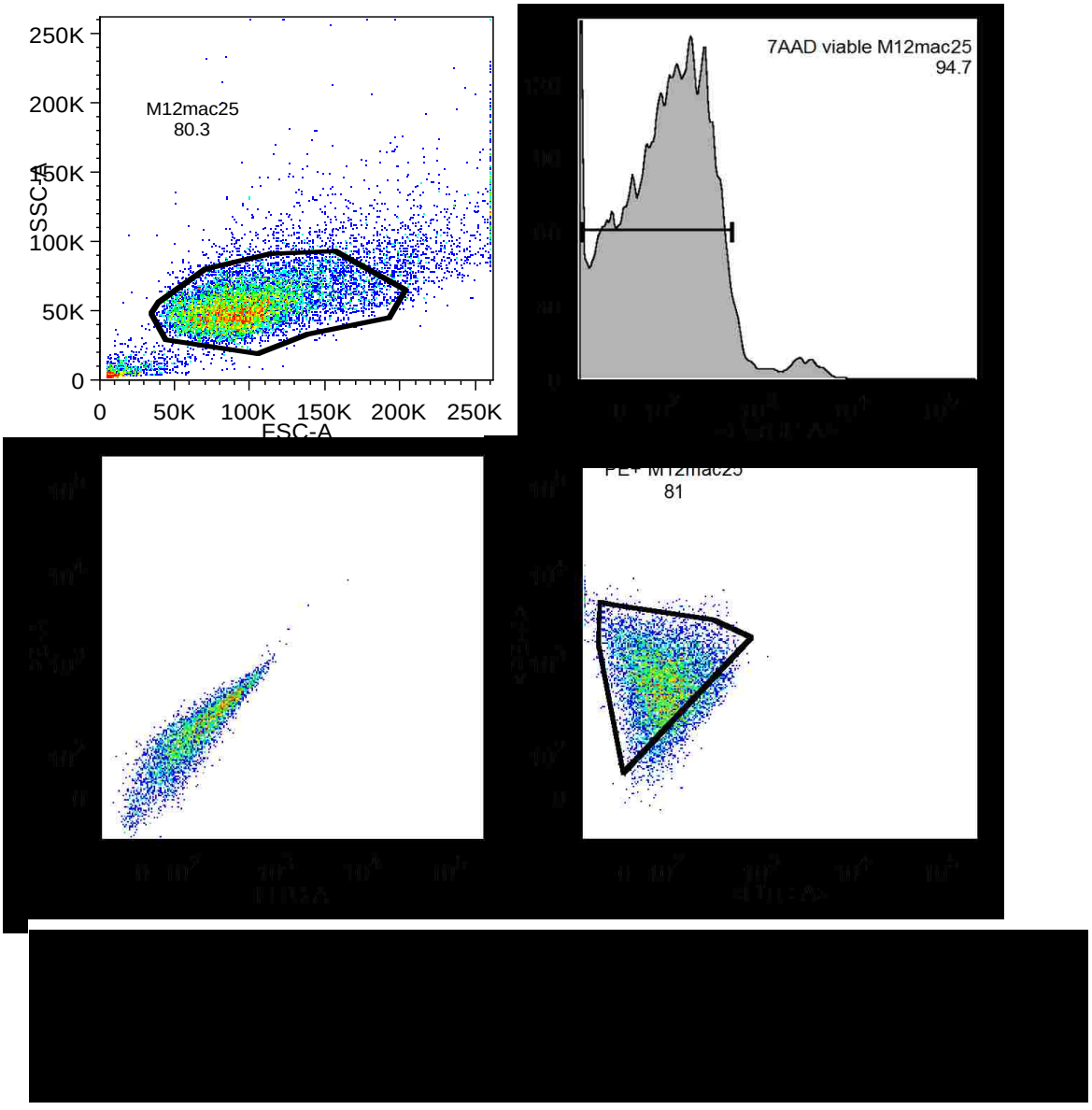

www.manaraa.com

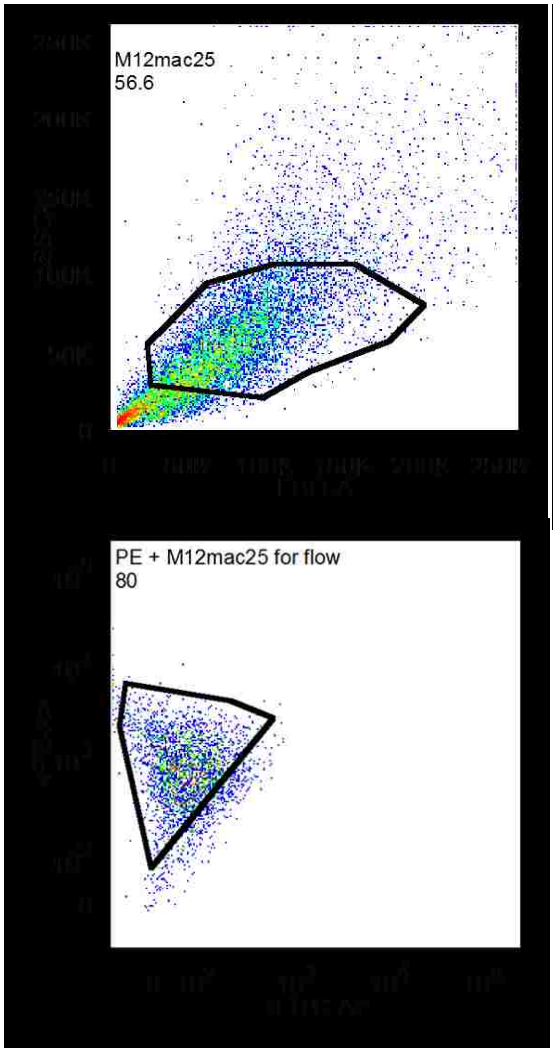

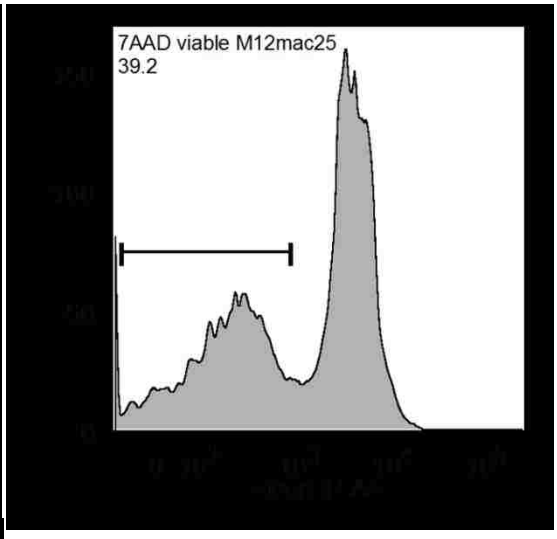

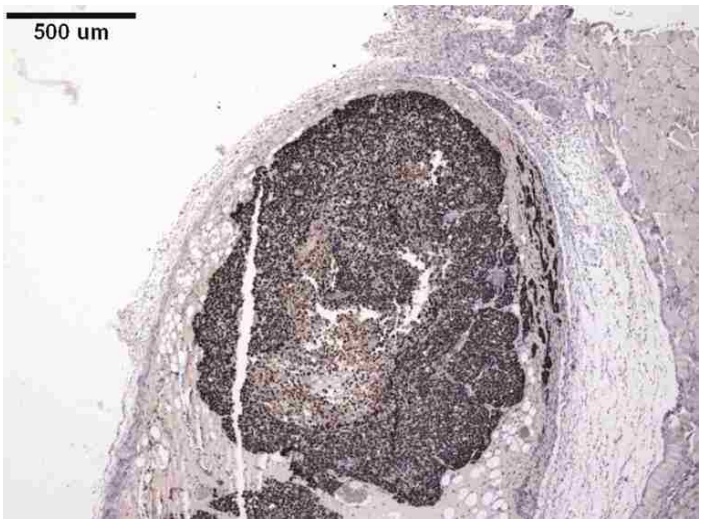

www.manaraa.com

5.4.9 Clondronate Liposome Pilot Study #1- Injection Strategy

DiI-labeled PBSLs were able to be detected by fluorescent microscopy of histological sections from subcutaneous pHEMA explants as well as spleen tissue (see Figure 5.14). Subcutaneously injected labeled PBSLs were found to be pervasive in the pHEMA scaffolds and surrounding capsule tissue. The IP-injected labeled PBSLs were seen in the spleen positive control tissue, but only a few macrophages in the subcutaneous implant stained positive with the IP injection alone, indicating that IP injection is not as effective as subcutaneous delivery for the liposome phagocytosis.

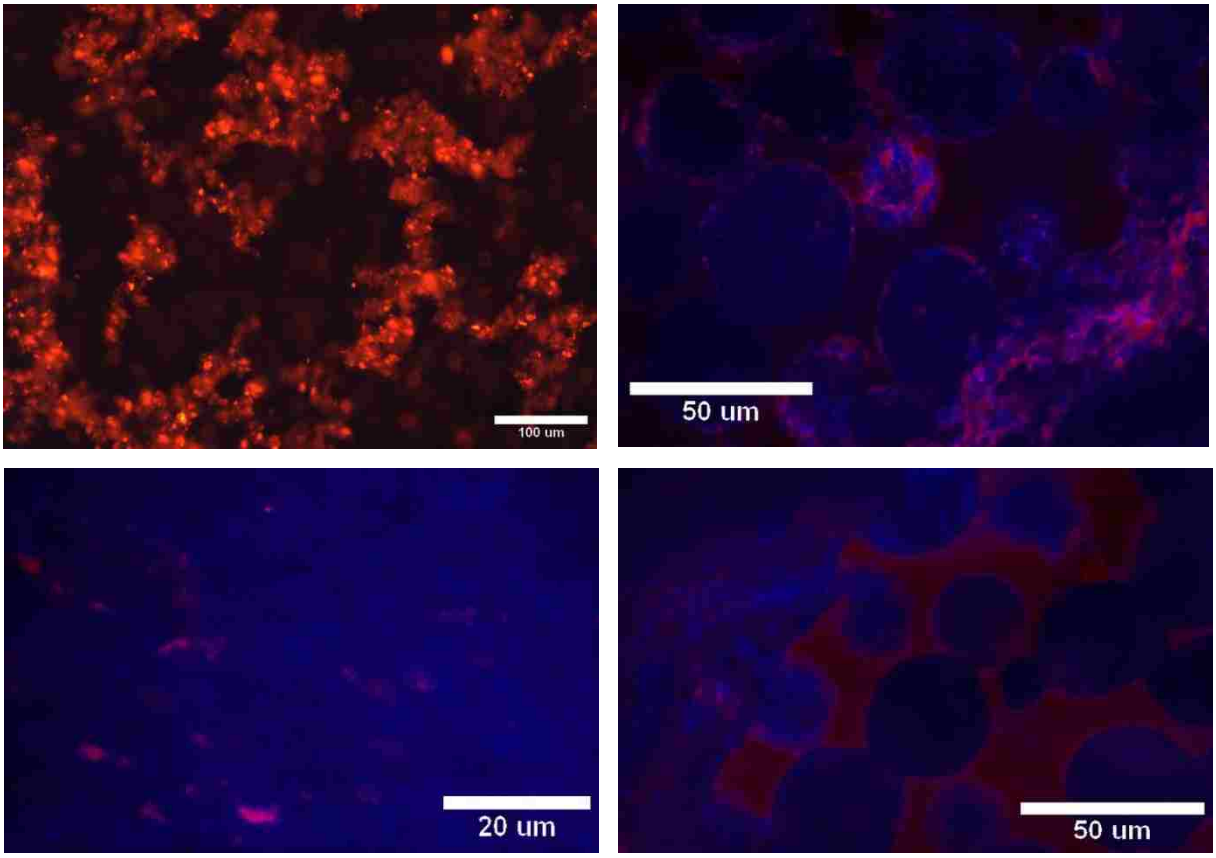

www.manaraa.com

5.4.10 Clondronate Liposome Pilot Study #2- Dosage Strategy

H+E staining of PBSL controls showed that at all time points there was significant tissue infiltration into the scaffolds. Direct comparison between the scaffolds exposed to CLs and PBSLs displayed a clear difference between the CL explants and the PBSL explants at one, two, and four days after injection and no discernible difference at day seven after injection (see Figure 5.15). This study confirmed that CLs can be used to have an effect on the FBR to implanted porous materials. However, by day seven the macrophages may have had a chance to recover. A five day dosing period was thus selected based on the results of this pilot study.

5.4.11 Clondronate Liposome Pilot Study #3- Long-Term FBR Knockdown

Figure 5.16 shows Masson's trichrome staining of D14 and D21 scaffold explants injected with CLs and PBSLs. From these results it is clear that the clondronate liposomes are having an effect on the foreign body response to the material. In the CL samples the scaffold is much less infiltrated with cellular material and the beginnings of the foreign body capsule are less densely collagenous. This pilot study indicates that repetitive liposome dosing can be used to affect macrophage activity within the scaffolds over several weeks.

www.manaraa.com

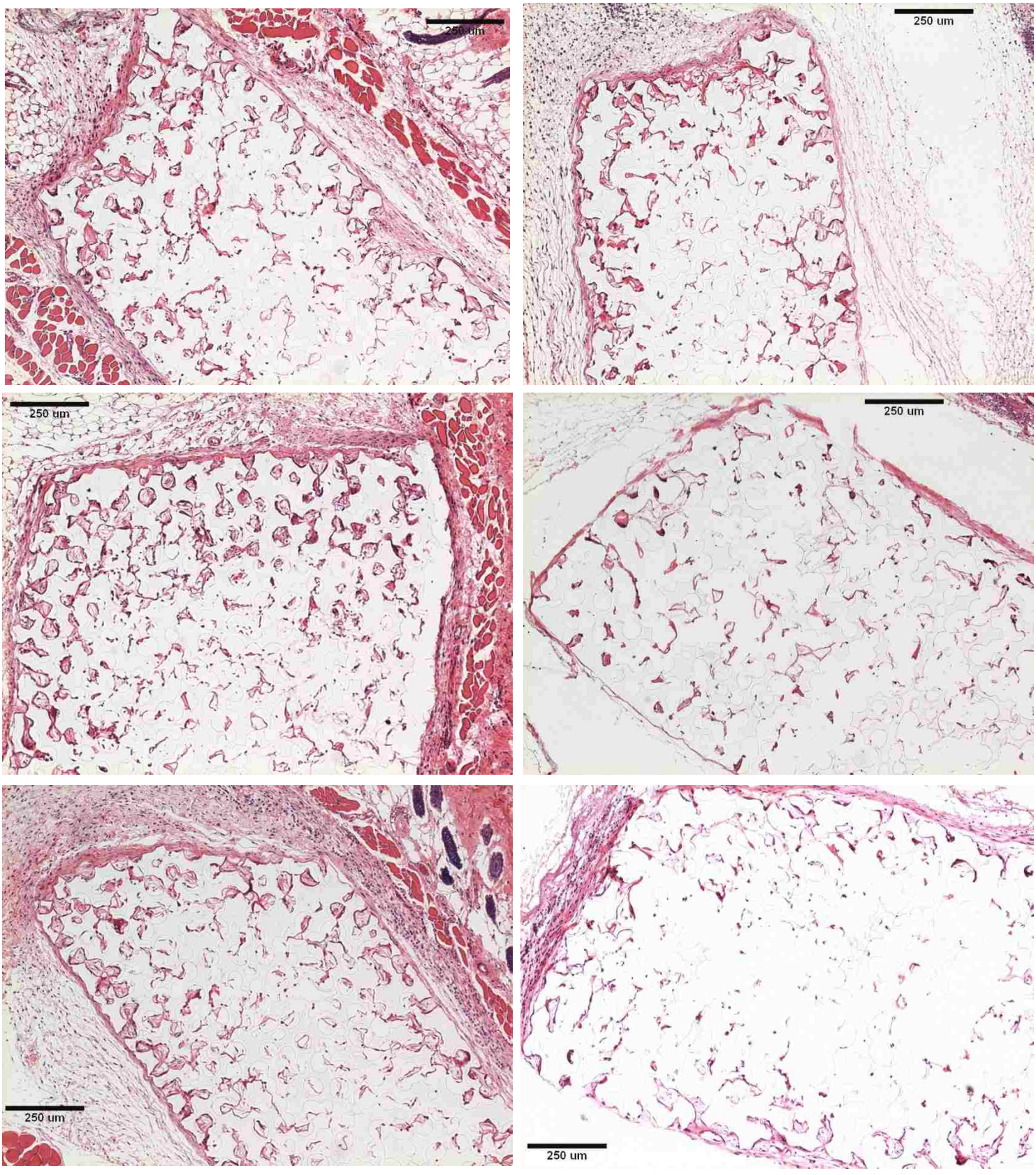

www.manaraa.com

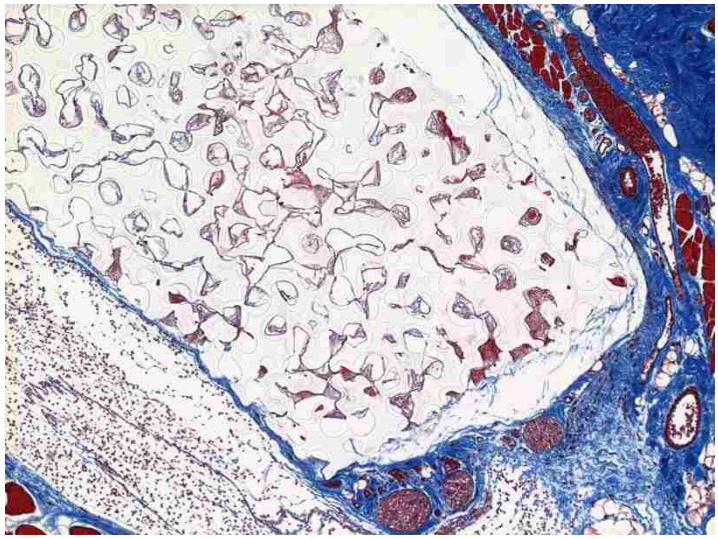
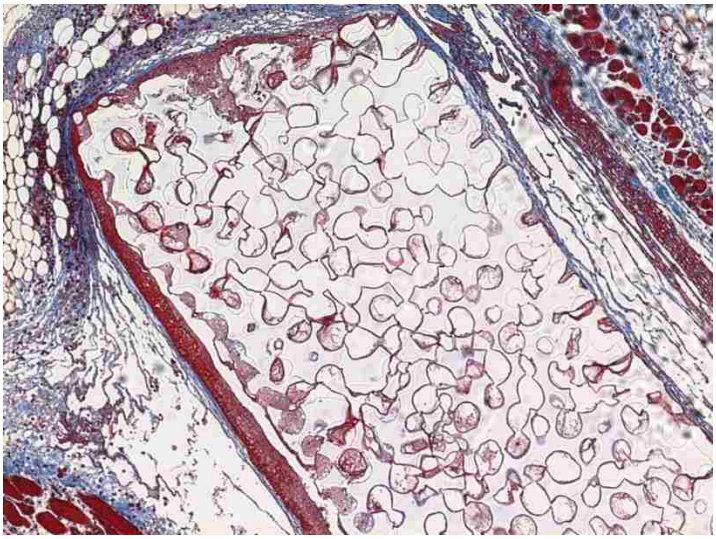
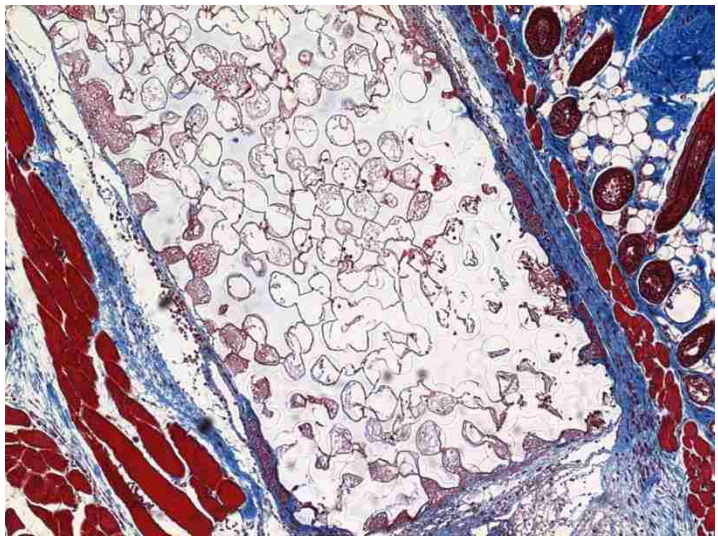
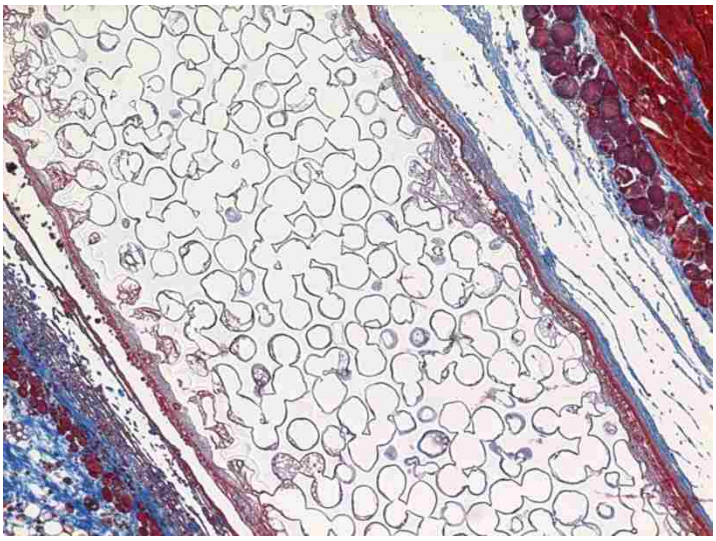

[redacted]

المنارة للاستشارات
www.manaraa.com

5.4.12 M12mac25 Clondronate Liposome Study

Figure 5.17 shows representative histological images of Masson's trichrome-stained early and late-stage M12mac25 cell-seeded pHEMA explants from PBSL, CL, and sham injection sample groups. It is clear that the clondronate has a significant effect over the long term *in vivo* response to the material. There is a general lack of nucleated cell material in the scaffolds injected with CLs compared to PBSLs, and most of the material in the scaffold appears to be cytoplasmic cell debris. There was also no significant difference between the sham PBS injections and the PBSLs, indicating that the clondronate, and not the liposomes themselves, impact the foreign body response. Figure 5.18 shows SV40T IHC of explants from this study. It was not clear from macroscopic observations and caliper measurements whether tumors were growing in any samples by the six or eight week explant time, which is consistent with previous observations (see Figure 5.1). However, it is evident from immunostaining that PBSL and sham control injections resulted in M12mac25 tumor growth while five of six CL samples had tumor growth eliminated. F4/80 IHC shows that macrophages are still heavily infiltrated into the PBSL and sham injected scaffolds and surrounding tumor, but are largely eliminated in the clondronate samples (see Figure 5.19). Interestingly, the one CL explant that did show tumor growth retained macrophages. MECA-32 IHC shows a complete lack of endothelial vessels in CL samples and statistically equivalent vessel density between PBSL and sham explants. The CL sample that displayed tumor growth had a vessel density consistent with controls (see Figure 5.20).

www.manaraa.com

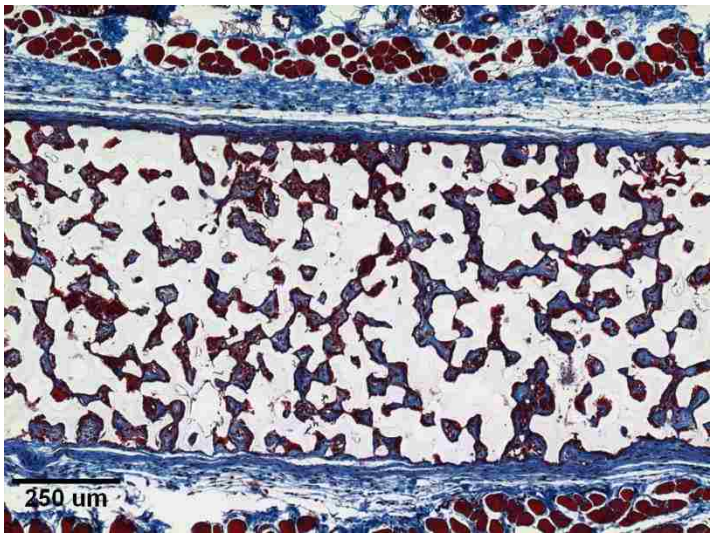

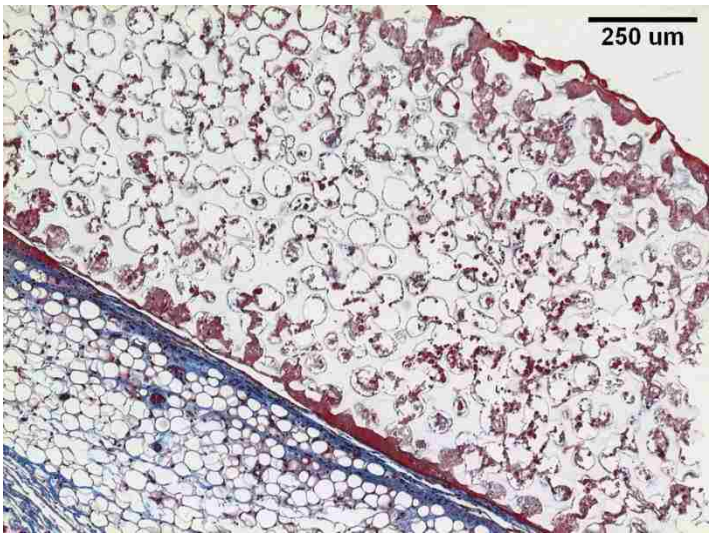

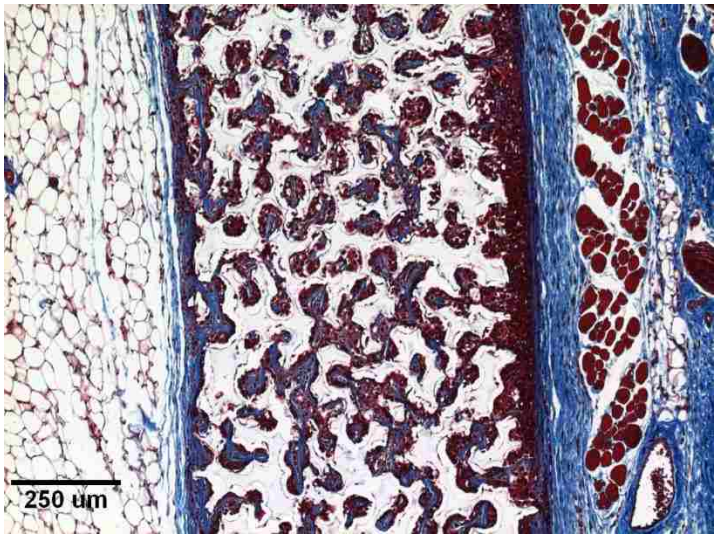

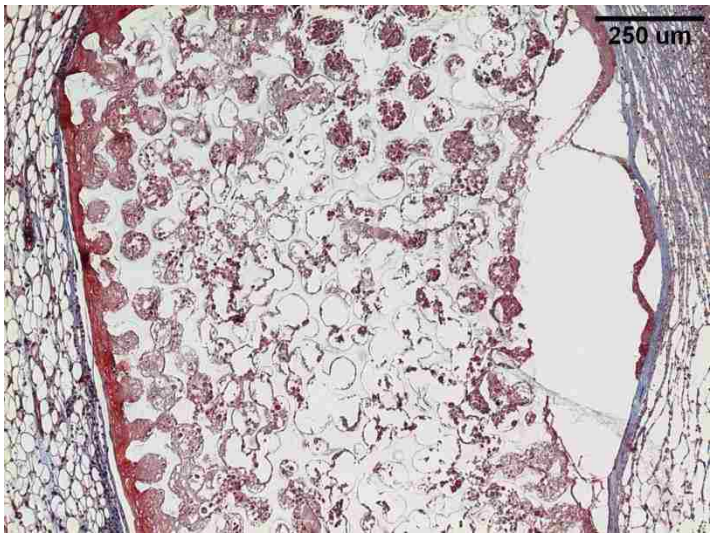

www.manaraa.com

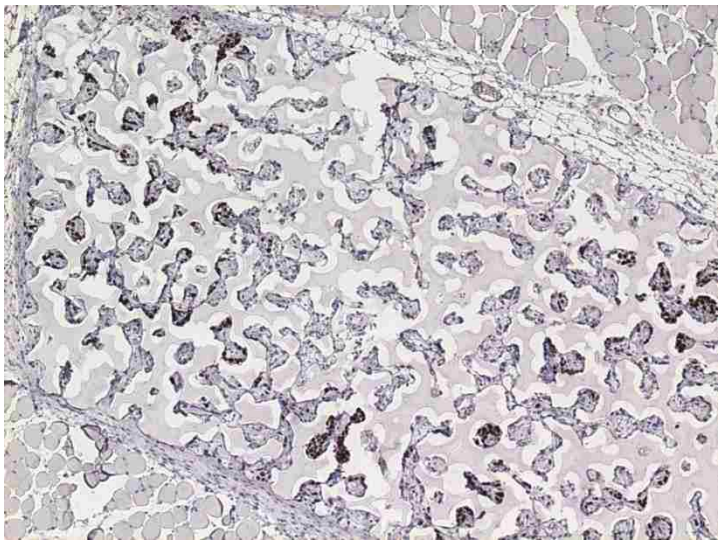

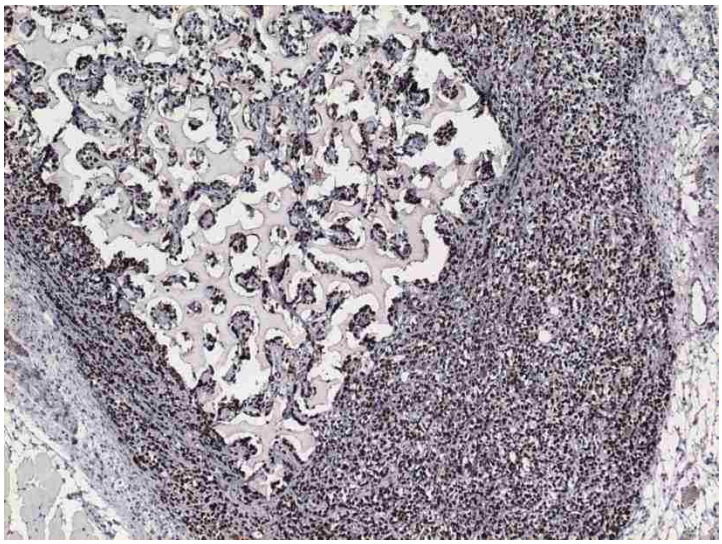

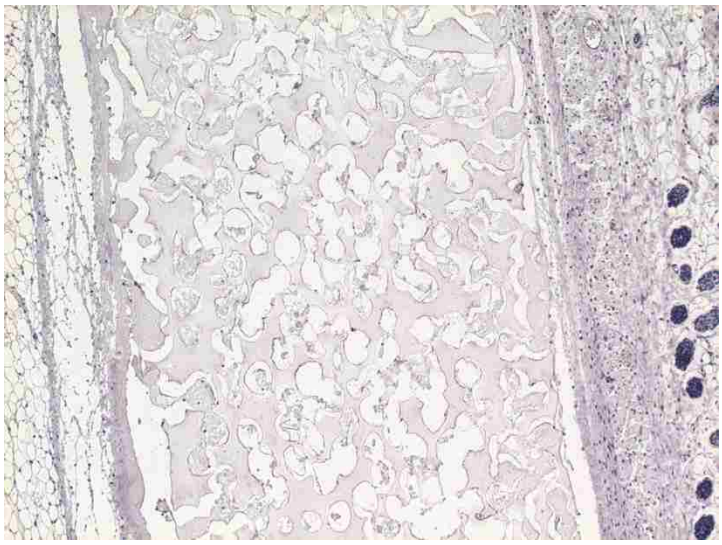

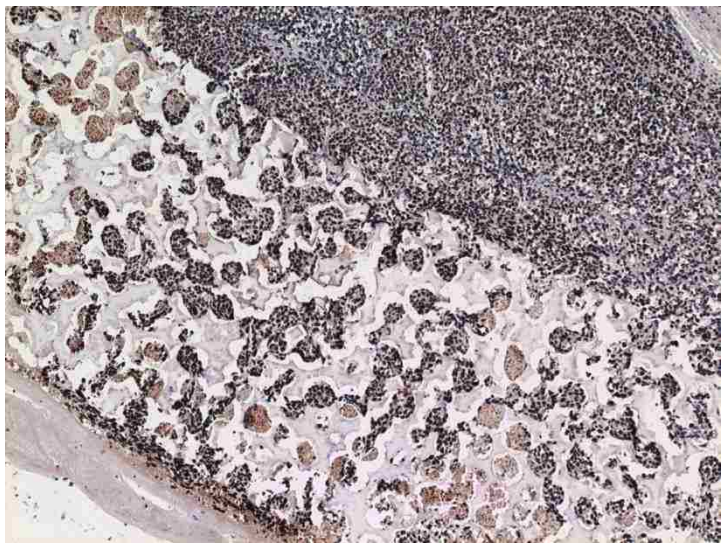

المنارة للاستشارات
www.manaraa.com

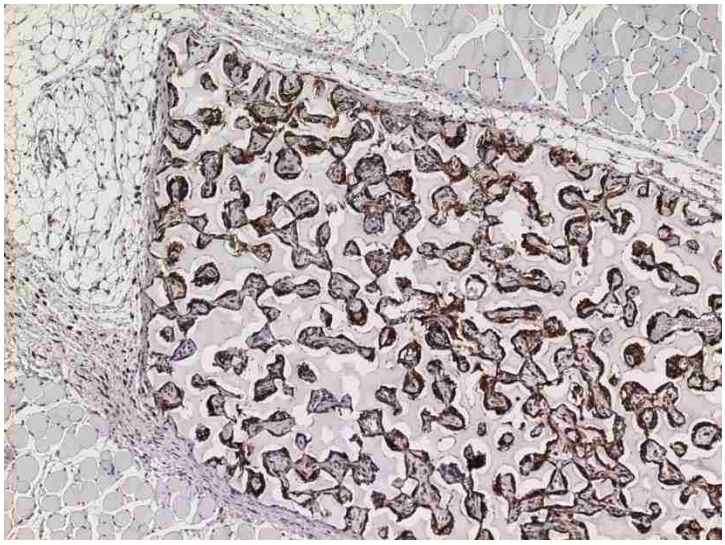
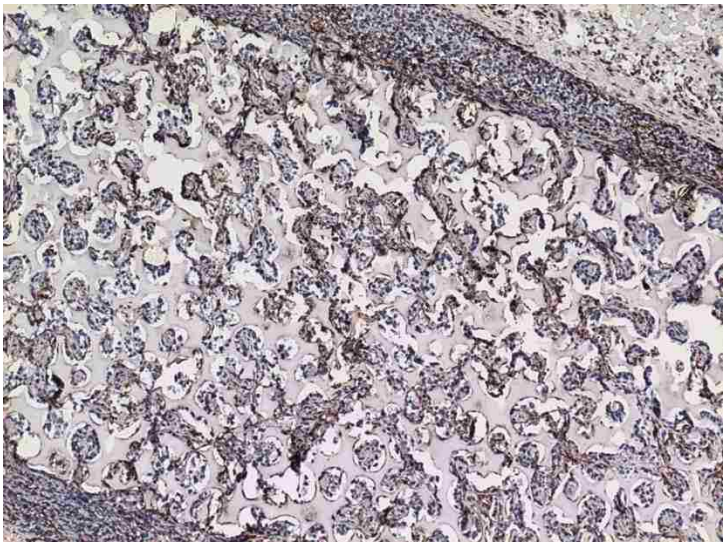
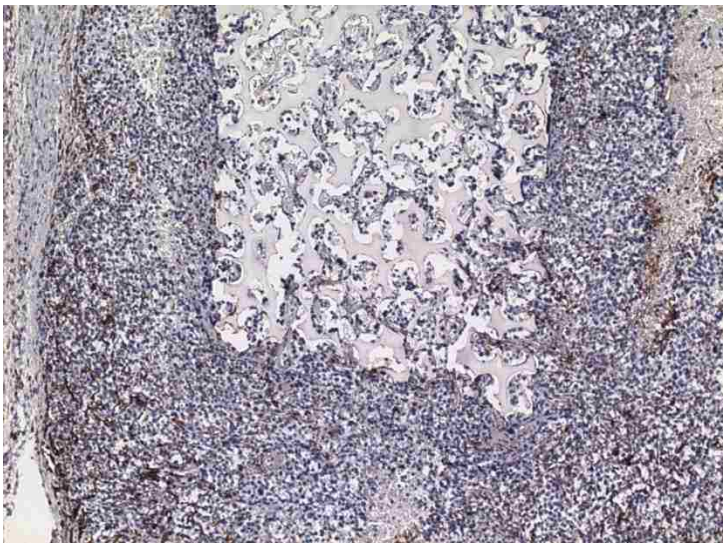
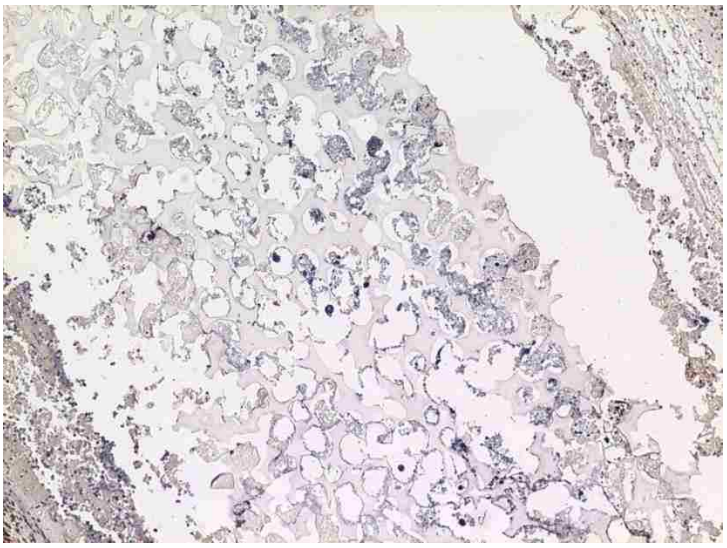
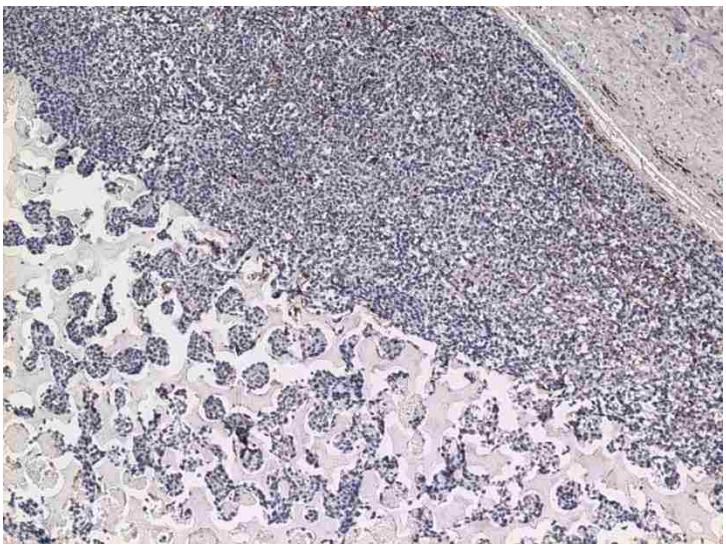


www.manaraa.com

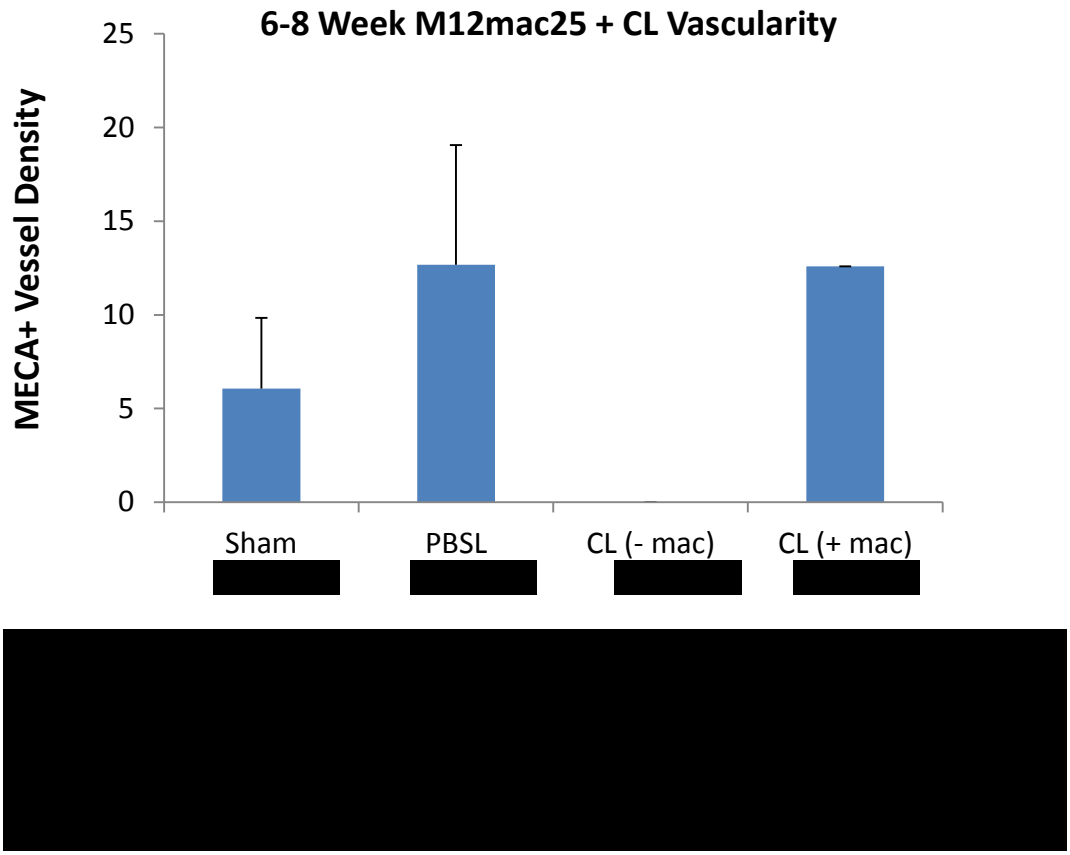

5.4.13 In Vitro *Clondronate Liposome Analysis*

Figure 5.21 shows that when applied *in vitro*, clondronate liposomes have no effect on the proliferation of M12mac25 cells over 72 hours. Bone marrow-derived primary macrophages served as a positive control and showed that a 1% (v/v) CL concentration is cytotoxic to macrophages. PBSLs had no negative effect on M12mac25 or BMDM proliferation.

www.manaraa.com

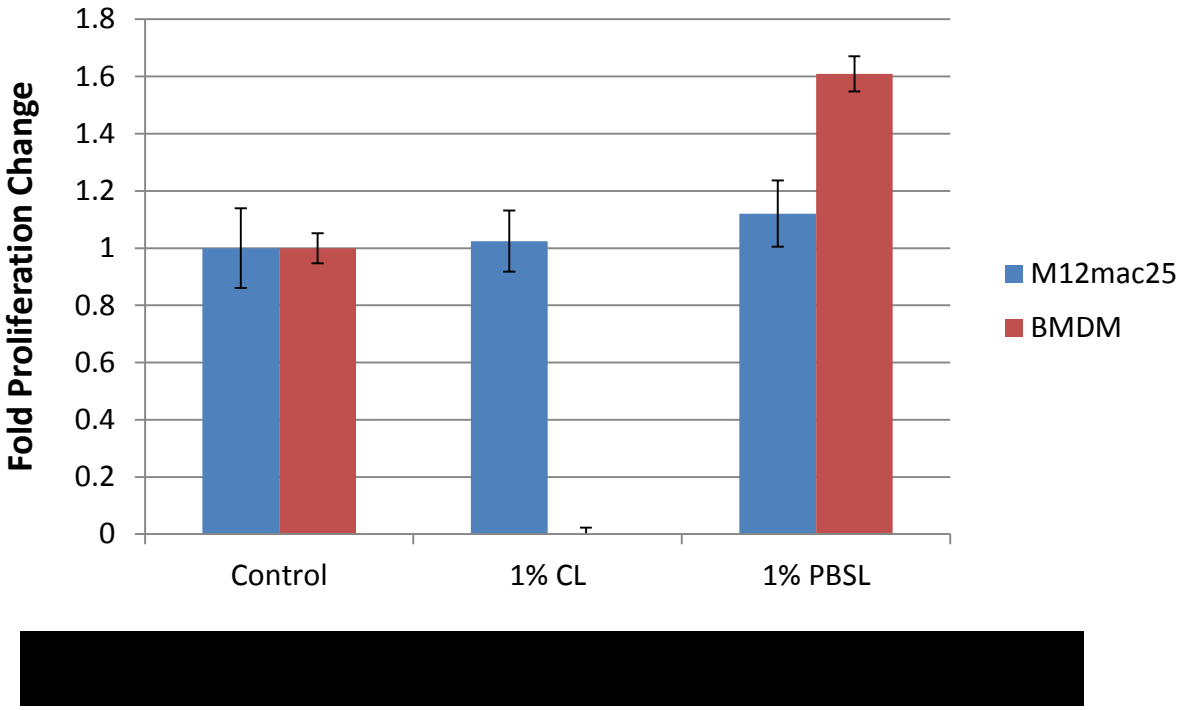

5.5 Discussion

M12mac25 cells remained largely dormant when injected with Matrigel, but grew tumors when implanted within porous pHEMA with or without Matrigel. The data presented in this chapter were designed to address the cellular and molecular mechanisms of this dormancy escape. Histological analysis confirmed that SV40T positive cells proliferated to fill the scaffolds and form most of the tumor bulk around the scaffolds. SV40T positive cells remained localized in small dormant Matrigel plugs for the standard xenograft injections. RNA analysis demonstrated that mac25 expression was retained in the explants that grew tumors, so the M12mac25 cells did not turn off the gene that induced cellular dormancy. To confirm that the M12mac25 cells themselves were not altered in the pHEMA scaffolds, M12mac25 cells derived from pHEMA tumors were flow separated and re-injected into mice with Matrigel. These cells reverted to their dormant state, indicating that the mac25 gene was still active and that the pHEMA scaffold signaling was necessary to induce tumorigenicity.

Thus, some element of the microenvironment resulting from scaffold implantation, and not mac25 loss, is responsible for M12mac25 dormancy escape. Current theories regarding tumor

www.manaraa.com

dormancy escape, such as angiogenic release and immunosurveillance evasion [81], likely do not account for these observations. MECA+ endothelial vessel density was equivalent between the pHEMA and Matrigel explants at three and twleve weeks, and athymic nude mice have a compromised adaptive immune system that does not demonstrate T cell-mediated destruction of cancer cells. Alternatively, the foreign body response to implanted biomaterials attracts activated macrophages to the implant site, and it has been established that sphere-templated materials induce substantial macrophage infiltration within their porous network [50]. Indeed, F4/80+ macrophage density was higher in the pHEMA explants at both three and twelve weeks, where at both time points macrophages in pHEMA-derived tumors were present in close proximity to M12mac25 cells as opposed to localized around clusters of M12mac25 cells. It has been well-established that tumor-associated macrophages can activate pro-tumor signaling pathways (see section 5.1.4) [23][94], and it is possible that the cell signaling mediated by macrophage interactions plays a significant role in the observed M12mac25 cell re-activation.

The potential role of macrophage signaling was demonstrated in high-throughput experiments including cytokine arrays and DNA oligonucleotide arrays that were utilized to try and gather useful information regarding the molecular differences between the pHEMA and Matrigel-derived explants. Cytokine arrays demonstrated that many most of the top 20 proteins present were similar between pHEMA and Matrigel explants; however, several proteins were found to be significantly up-regulated in the pHEMA explants including many that are associated with macrophage recruitment or an inflammatory macrophage phenotype, including CXCL5, IL-1β, IL-12, CCL8, CCL11, CCL5, CXCL9, and CXCL10 (see Table 5.2). DNA oligonucleotide arrays demonstrated validation of some of these up-regulated proteins, including CXCL5, VEGF, and CCL5. DNA arrays also showed the up-regulation of many components associated with the MAPK/ERK, PI3K/AKT, and TGF-β/SMAD pathways. The TGF-β pathway is associated with macrophage signaling. The MAPK/ERK and PI3K/AKT pathways are associated with cytokine/chemokine receptors including CXCR2, the receptor for CXCL5 (see Appendix 11 for CXCR2 pathway map). It should be noted that this analysis was performed on whole explant protein and RNA, so for molecules that are conserved between species there is no way to determine the cellular origin of individual signaling molecules, (ie whether they are from M12mac25 cells, macrophages, or other cell types).

www.manaraa.com

CXCL5 has been demonstrated to correlate to prostate cancer malignancy while stimulating proliferation in several prostate cancer cell lines and showing the potential to induce an EMT response. CXCL5 is known to be secreted by both prostate cancer immune infiltrate and the prostate cancer epithelial cells themselves [108][109]. We have demonstrated from explants that CXCL5 is the most statistically up-regulated cytokine in pHEMA from human cytokine arrays and is one of the top cytokines identified by mouse array. CXCL5 was also confirmed as up-regulated in pHEMA by DNA oligo arrays. The components of signaling pathways associated with CXCR2, the CXCL5 receptor, namely the MAPK/ERK and PI3K/AKT pathways, were shown to be up-regulated in pHEMA explants by DNA oligo arrays. In total, this data could fit a model where macrophages enter the pHEMA scaffold, produce CXCL5 and its induce its up-regulation in M12mac25 cells, which can induce a proliferative response (likely in conjunction with other signaling pathways). The potential role of CXCL5 in the M12mac25 dormancy escape process will be further explored using *in vitro* studies in chapter six.

The elimination of macrophages from the *in vivo* system using clondronate liposomes had the potential to give a final verdict on the role of these cells in the dormancy escape process. If M12mac25 tumors failed to grow in scaffolds without macrophages, then those cells are the key players in eliciting dormancy escape. A series of pilot studies demonstrated that repeated subcutaneous dosing of clondronate liposomes mitigated the foreign body response to the implanted material. When applied to M12mac25-seeded scaffolds, clondronate liposomes prevented tumor formation in most cases, but upon closer histological examination all cells in the scaffolds, including the F4/80+ macrophages, MECA+ endothelial cells, and the SV40T+ M12mac25 cells themselves, had been removed. It was demonstrated that CLs have no effect on M12mac25 cells *in vitro*, so it is likely that lack of macrophages in the scaffolds prevented the recruitment of endothelial cells and the resulting lack of vascularization caused M12mac25 cell death. So, while it was not proven that macrophages are directly responsible for M12mac25 cell dormancy escape, it was shown that they have at least an indirect effect on this process. Without macrophages, the M12mac25 cells cannot escape dormancy, but it is possible that some other cellular element involved in the foreign body response that is recruited by macrophages is actually responsible for the observed effect.

www.manaraa.com

Though not examined experimentally here, it is also possible that given the large difference in stiffness between the pHEMA scaffolds (~690 kPa) and Matrigel (~0.45 kPa [126]), mechanical cues may contribute to changes in cell behavior, something that has been observed in a variety of cell types including cancer cells involved in metastatic progression (see section 5.1.7) [64][86][87]. Synthetic biomaterials allow for the modulation of scaffold mechanics, but porous materials with sphere-templated architecture cannot be fabricated within orders of magnitude of soft tissue modulus, which prevents the full investigation of the effect of stiffness on this system.

www.manaraa.com

Chapter 6. *In Vitro* Analysis of Macrophage Signaling and CXCL5 on Dormant Prostate Cancer Cells

6.1 Motivation

Results in chapter five demonstrated a pHEMA scaffold-mediated M12mac25 cell dormancy escape *in vivo*. One of the major differences observed between the pHEMA-derived M12mac25 tumors and their dormant Matrigel counterparts was macrophage infiltration caused by the foreign body response. In this chapter, the potential effects of macrophage signaling on M12mac25 cells will be explored *in vitro* using conditioned media studies. On the molecular level, CXCL5 and the downstream signaling pathways of its CXCR2 receptor were shown to be significantly upregulated in the pHEMA explants by cytokine and DNA oligonucleotide arrays. CXCL5 has been associated with prostate cancer progression. *In vitro* follow-up studies will also be presented in this chapter to attempt to confirm the potential role of CXCL5 in the observed M12mac25 dormancy escape.

6.2 Hypothesis

It is hypothesized that macrophage conditioned media can induce *in vitro* M12mac25 proliferation and that factors found to be up-regulated in M12mac25-seeded pHEMA explants may also be up-regulated in response to macrophage media. Further, it is also hypothesized that CXCL5 can be demonstrated *in vitro* as a critical molecular player mediating M12mac25 dormancy escape

6.3 Materials and Methods

6.3.1 Primary Macrophage Isolation, Culture, and Macrophage Conditioned Media (MCM)

Bone marrow-derived macrophages were isolated from femurs of athymic nude mice as previously described [127]. Briefly, femurs were removed from euthanized mice and put on ice for no more than a half hour before use. Femurs were flushed with warm serum free RPMI 1640 to obtain myeloid progenitor cells, which were then triturated into a single cell suspension using an 18G needle and plated onto 100 mm non-TC coated polystyrene petri dishes. $4x10^6$ cells were plated per dish with 10 mL of media. Cells were cultured in RPMI containing 20% FBS and 50 ng/mL macrophage colony stimulating factor (M-CSF) (Peprotech). Cells were washed and media was replaced after four days. At seven days from harvest, adherent cells were

www.manaraa.com

differentiated to either the M0 resting, or the M1 or M2 polarized phenotypes by culturing cells for two additional days in serum free RPMI containing 50 ng/mL M-CSF, 20 ng/mL IFN-γ (Shenandoah Biotechnology) and 100 ng/mL LPS (Sigma), or 60 ng/mL IL-4 (Shenandoah Biotechnology), respectively. M0, M1, and M2 MCM was collected, sterile filtered, and frozen until use.

6.3.2 M12mac25-MCM Proliferation Study

M12mac25 cells were seeded in triplicate into a 48 well plate at a density of $1.5x10^4$ cells per well in 1 mL of either serum free media or complete media. After overnight attachment, 500 µL of media was removed from each well and 500 µL of MCM (M0, M1, or M2) or fresh serum free media was added. Proliferation measurements were taken using a 1:10 dilution of alamarBlue at 24 and 72 hours after media addition. Controls for this experiment included M12mac25 cells with serum free media alone or 50% serum free 50% complete media.

6.3.3 MCM Cytokine Arrays

Macrophage conditioned media from the M0, M1, and M2 states were used as samples for the Ray Biotech mouse cytokine array III. 1 mL of conditioned media was used per membrane for secreted factor analysis.

6.3.4 M12mac25-MCM Cytokine Arrays

M12mac25 cells were seeded in triplicate into 6 well plates at a density of $3x10^5$ cells per well in 3 mL serum free culture medium. After overnight attachment, 1.5 mL of culture medium was replaced in each well by either 1.5 mL of MCM (M0, M1, or M2) or fresh serum free media. 24 hours after media change, M12mac25-conditioned media was collected, sterile filtered, and frozen until use. 1 mL of M12mac25-conditioned media or M12mac25-MCM were run as samples on Ray Biotech human membrane cytokine array V. MCM alone controls were used to account for background from mouse proteins on the human arrays.

6.3.5 CXCL5 ELISA

An ENA-78 (hCXCL5) ELISA kit was obtained from Ray Biotech, Inc. Standards and protocols were developed according to the manufacturer's specifications. Experimental samples included

www.manaraa.com

M12mac25 conditioned media, M0 MCM, M1 MCM, M2 MCM, M12mac25 + M0 MCM, M12mac25 + M1 MCM, and M12mac25 + M2 MCM. All incubations were performed at room temperature with orbital shaking. 100 µL of hCXCL5 standards and experimental samples were incubated for 2.5 hours on 96 well plates coated with anti-hCXCL5 antibodies. After sample washing, 100 µL of biotinylated antibody was added to each well for 1 hour. Wells were washed and 100 µL of streptavidin solution was added to each well for 45 minutes. Wells were washed again and 100 µL of 3,3',5,5'- tetramethylbenzidine (TMB) substrate was added for 30 minutes. 50 µL of the stop solution (0.2 M sulfuric acid) were added to each well and absorbance at 450 nm was recorded on a plate reader.

6.3.6 rCXCL5 M12mac25 In Vitro *Proliferation Studies*

M12mac25 cells were seeded in triplicate into a 48 well plate at a density of $1.0x10^4$ cells per well in 1 mL of either serum free media or complete media (for positive control). After overnight attachment, 500 µL of media was removed from each well and 500 µL of fresh serum free media was added containing recombinant human CXCL5 (rCXCL5, R+D Systems) to a final concentration of 10 pM, 100 pM, 1 nM, 10 nM, 20 nM, or 50 nM. Proliferation measurements were taken using a 1:10 dilution of alamarBlue at 24 hours after media addition. Controls for this experiment included M12mac25 cells with serum free media alone or 50% serum free 50% complete media. For a positive control of rCXCL5 bioactivity on prostate cancer cells, PC3 cells were plated in the same format with 10 pM, 100 pM, 1 nM, and 10 nM rCXCL5 concentrations. Proliferation was measured using alamarBlue at 96 hours after media addition.

6.3.7 CXCR2 Blockade of MCM-Induced M12mac25 Proliferation

M12mac25 cells were seeded in triplicate into a 48 well plate at a density of $1.0x10^4$ cells per well in 1 mL of either serum free media or complete media (for positive control). After overnight attachment, 500 µL of media was removed from each well. Some wells were then treated with either 5 µg/mL or 10 µg/mL anti-CXCR2 mAB (R+D systems) for 1 hour. 500 µL of either serum free media (controls), M0 MCM, M1 MCM, or M2 MCM was then added. In total, sample groups included serum free control, 50% complete medium control, M0 MCM, M1 MCM, M2 MCM, 5 µg/mL anti-CXCR2 control, 10 µg/mL anti-CXCR2 control, M0 MCM + 5 µg/mL anti-CXCR2, M0 MCM + 10 µg/mL anti-CXCR2, M1 MCM + 5 µg/mL anti-CXCR2,

www.manaraa.com

and M2 MCM + 5 µg/mL anti-CXCR2. Proliferation measurements were taken using a 1:10 dilution of alamarBlue at 24 hours after media addition.

6.4 Results

6.4.1 M12mac25-MCM Proliferation Study

M12mac25 cell proliferation rate increased in the presence of MCM regardless of macrophage phenotype. Fold M12mac25 proliferation changes by AB detection are shown in Figure 6.1 where Figure 6.1A shows results in cells plated with serum-free media and Figure 6.1B shows results with cells plated in complete media. When added to serum free media, MCM induced a statistically significant ($p < 0.003$) proliferation increase over serum free controls, with average fold AB reduction increases of 2.48 +/- 0.21, 2.20 +/- 0.12, and 1.92 +/- 0.14 for M0, M1, and M2 macrophages, respectively (see Figure 6.1A). This effect is masked at 72 hours most likely because M12mac25 cells have trouble maintaining viability in the absence of serum. When added to complete media, MCM also induced a proliferation increase over the 50/50 complete/serum free control at 24 hours, with average fold AB reduction increases of 1.55 +/- 0.29, 1.45 +/- 0.39, and 1.94 +/- 0.51 for M0, M1, and M2 macrophages, respectively (see Figure 6.1B). Thus, the MCM effect on M12mac25 proliferation still is present but is slightly masked compared with the serum free case. At 72 hours there is little change between controls and M12mac25 + MCM samples because all wells containing complete media were 100% confluent by that time point.

6.4.2 MCM Cytokine Arrays

Figure 6.2 shows raw MCM mouse cytokine array results. All spots were analyzed qualitatively on a five point scale, where – indicated no spot presence, + indicated a spot that might be background, ++ indicated a spot likely present above background intensity, +++ indicated a highly expressed protein, and ++++ indicated very highly expressed protein. A full data compilation for the three macrophage phenotypes is shown in Appendix 12. Validation that phenotypic differentiation was successful can be seen in the protein spots for IL-6 (blue), RANTES (green), IL-12 (yellow), and IL-4 (purple). IL-6, RANTES, and IL-12 were clearly up-regulated in M1 MCM relative to the others, while IL-4 was up-regulated in M2 MCM (IL-4 was

www.manaraa.com

used to stimulate M2 differentiation). Proteins that showed qualitative differences in expression levels are shown in bold in Appendix 12.

However, the most relevant way to look at this data for this application is to figure out which cytokines are expressed above background intensity in all three M0, M1, and M2 phenotypes. This is because all three phenotypes induced a significant proliferative increase in M12mac25 cells. Table 6.1 shows a list of 15 cytokines that were present at ++ or above in all three phenotypes. CXCL5 (in mouse, LIX) was shown to be significant in human cytokine arrays and up-regulated in DNA oligo arrays. To follow up on this, LIX quantification is shown in Table 6.2, where normalized intensities are relatively consistent over three macrophage phenotypes, which supports the qualitative data.

www.manaraa.com

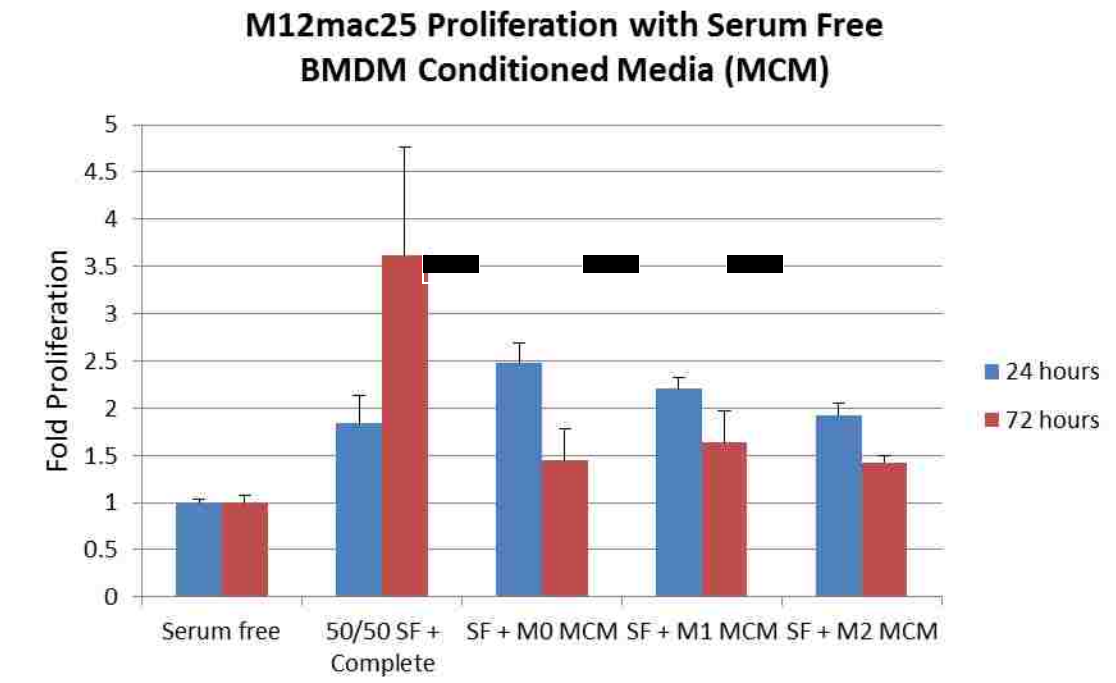

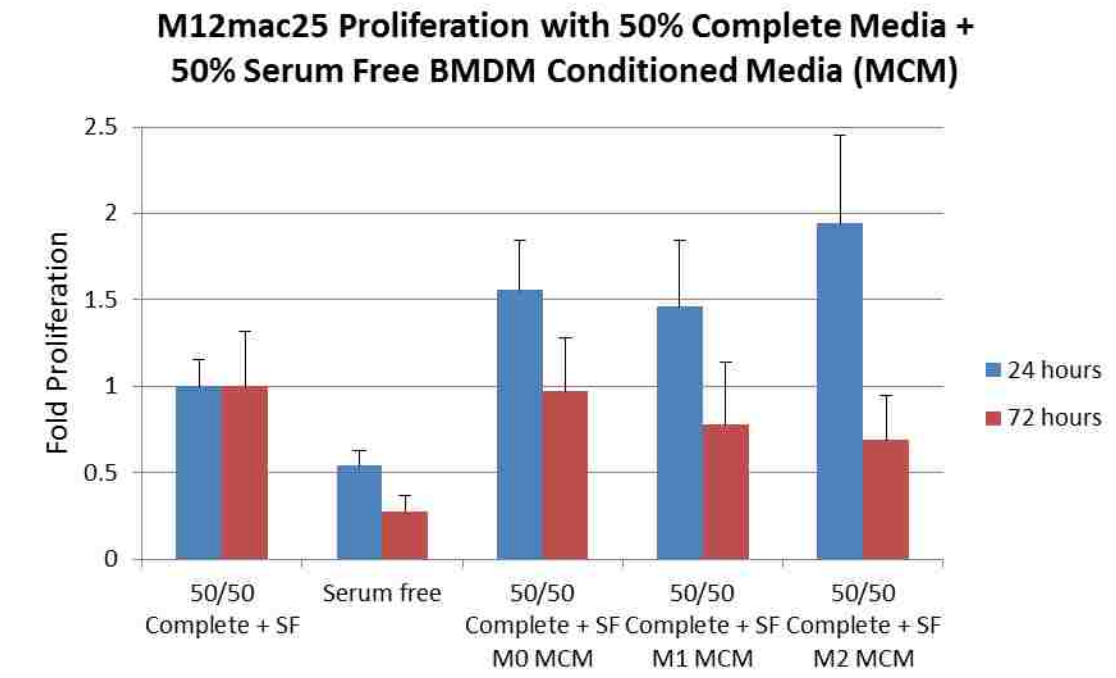

www.manaraa.com

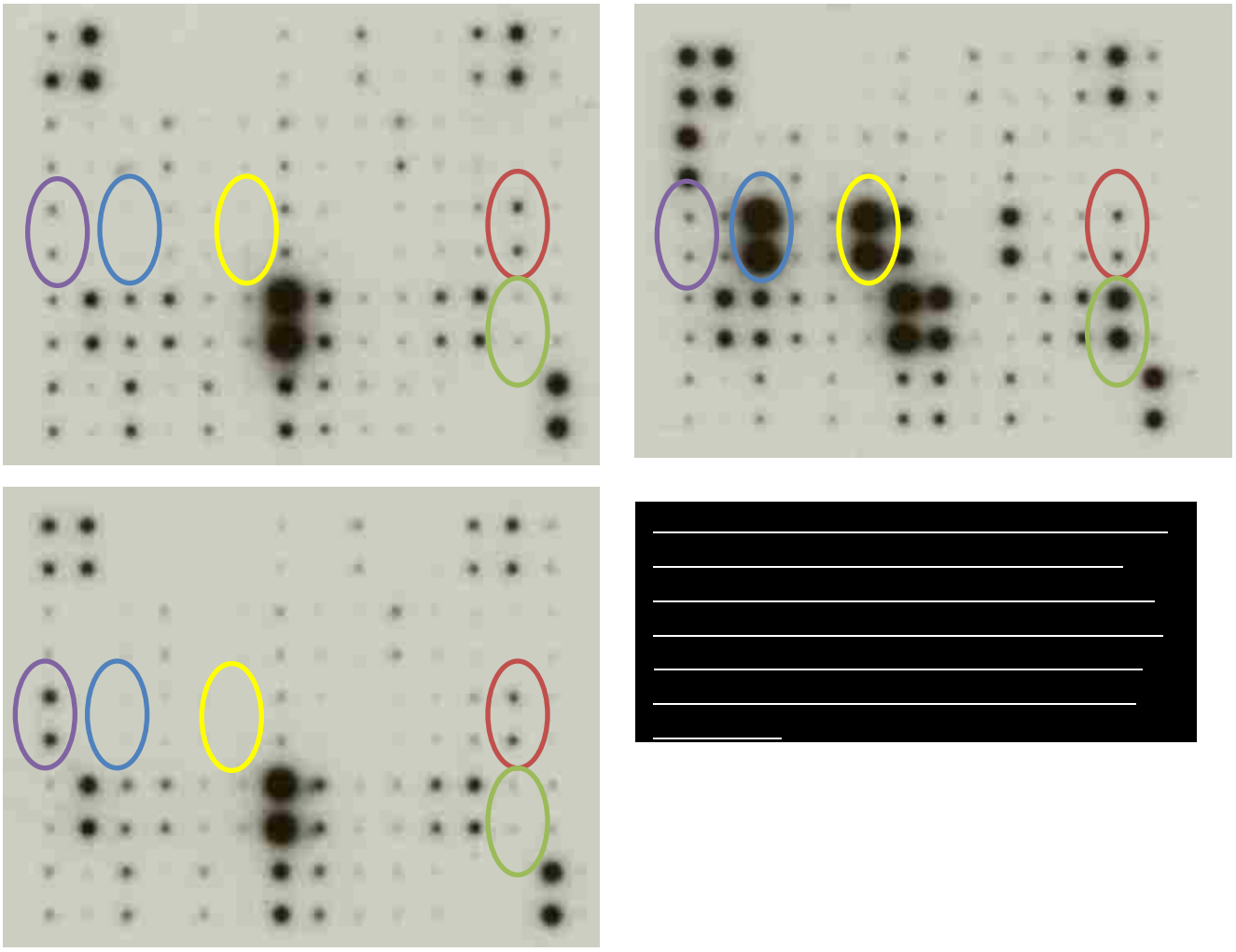

6.4.3 M12mac25-MCM Cytokine Arrays

Quantitative human cytokine arrays results for M12mac25 media stimulated by M0, M1, and M2 MCM are shown in Table 6.3 (raw results shown in Appendix 13). All numerical values represent fold increase cytokine signal over M12mac25 alone controls, and proteins are sorted by average fold increase. Table 6.1 lists only proteins that were found to be up-regulated in all three M0, M1, and M2 conditioned media. Proteins and individual data points listed in bold were also found to be up-regulated after background subtraction of the MCM controls (which compensates for mouse-human cytokine antibody cross-reactivity). These proteins (IL-6, VEGF, IL-8, GRO, CXCL5, Angiogenin, and MCP-1) likely have up-regulated secretion from the M12mac25 cells themselves after stimulation with MCM.

www.manaraa.com

Table 6.4 shows a comparison between the proteins found to be up-regulated in human cytokine arrays and the results of M12mac25-conditioned media cytokine arrays. All proteins found to be up-regulated in the *in vivo* explants were also found to be up-regulated in at least two of three M12mac25-MCM samples, with CXCL5 and VEGF from that list also showing up as significant above MCM background (shown in bold).

Protein	**M0**	**M1**	**M2**
MIP-1Y	++++	++++	++++
CXCL16	+++	+++	+++
MCP-1	+++	+++	+++
MIP-2	+++	+++	++
sTNF RI	+++	++	+++
IL-12 p70	++	+++	++
MCP-5	++	+++	++
P-selectin	++	++	+++
CTACK	++	++	++
GCSF	++	++	++
IL-1a	++	++	++
LIX	++	++	++
M-CSF	++	++	++
PF-4	++	++	++
TCA-3	++	++	++

Table 6.1 Proteins identified from macrophage conditioned media cytokine array to be expressed above background across three macrophage phenotypes.

	M0	M1	M2
Spot 1 Normalized Intensity	0.35	0.26	0.31
Spot 2 Normalized Intensity	0.31	0.22	0.31

Table 6.2 Quantification of LIX (CXCL5) spot intensity on macrophage conditioned media mouse cytokine arrays.

www.manaraa.com

	M0	M1	M2	Average Fold Increase
IL-6	**2.83**	**23.00**	**3.11**	9.645192291
VEGF	**1.57**	**5.09**	**2.02**	2.891743061
IL-8	**1.85**	**3.64**	**2.01**	2.497700718
GRO	**1.83**	**3.31**	**2.14**	2.425618924
ENA-78	1.25	**3.52**	**1.73**	2.168191202
Angiogenin	**1.91**	**2.27**	**1.55**	1.907222394
PDGF-BB	1.48	**2.36**	1.56	1.801188622
IL-12 p40p70	1.41	1.49	**2.17**	1.686030737
MCP-1	**1.37**	**2.10**	**1.22**	1.565296706
GCP-2	1.01	**2.17**	1.37	1.517705947
IL-15	1.28	1.36	1.88	1.505490062
GM-CSF	1.13	**1.92**	1.45	1.499213194
Fractalkine	1.18	1.78	1.39	1.448269218
RANTES	1.18	1.98	1.15	1.438979991
IFN-γ	1.28	1.40	1.55	1.40946006
IGF-1	1.29	1.67	1.12	1.359561339
Ck β 8-1	1.30	1.39	1.28	1.322760174
MDC	1.29	1.15	1.39	1.27871977
MCP-2	1.03	1.04	**1.70**	1.257175497
NT-3	1.19	1.43	1.14	1.252960662
BLC	1.03	1.29	1.40	1.240010386
TIMP-2	1.21	1.06	1.36	1.210273503
EGF	1.17	1.31	1.15	1.208927745
IGFBP-2	1.19	1.43	1.01	1.206942748
MIF	1.02	1.45	1.12	1.193653176
NAP-2	1.05	1.44	1.01	1.165471784
TNF-α	1.13	1.11	1.20	1.145576764
IL-3	1.10	1.10	1.18	1.129163954
TGF-β3	1.07	1.05	1.20	1.108318977

Table 6.3 Fold up-regulation for proteins identified by human cytokine array to be up-regulated in M12mac25-conditioned media stimulated by M0, M1, and M2 MCM. Cytokines listed were proteins that were up-regulated in all three M0, M1, and M2 states. Proteins listed in bold were up-regulated after mouse MCM background subtraction. Proteins with low signal (<4% of background) were eliminated.

www.manaraa.com

	M0	M1	M2
ENA-78 (CXCL5)	1.25	**3.52**	**1.73**
IL-1B	1.08	0.92	1.47
IL-15	1.28	1.36	1.88
MCP-2 (CCL8)	1.03	1.04	**1.70**
IL-3	1.10	1.10	1.18
LIGHT	1.22	1.83	0.77
IGFBP-1	1.12	1.44	0.89
IL-2	1.09	0.82	1.60
VEGF	**1.57**	**5.09**	**2.02**
IL12 p40p70	1.41	1.49	**2.17**
PDGF-BB	1.48	**2.36**	1.56

Table 6.4 List of proteins that were up-regulated in human cytokine arrays from *in vivo* explants. Proteins listed in red were also found to be up-regulated in M12mac25-conditioned media for all M0, M1, and M2 states. All other proteins were up-regulated in two of the three macrophage phenotypes. Samples listed in bold were up-regulated after background subtraction.

6.4.4 CXCL5 ELISA

Figure 6.3 shows hCXCL5 ELISA results on MCM, M12mac25 conditioned media, and conditioned media from M12mac25 cells stimulated with MCM. Standards included in the kit and developed according to the manufacturer's specifications showed linear signal through 666 pg/mL (data not shown), and all experimental samples fell below that range. The ELISA results corroborate those from the *in vitro* cytokine array data in section 6.4.1, where M0, M1, and M2 MCM stimulate the secretion of human CXCL5 from M12mac25 cells and M1 MCM induces the highest levels of CXCL5. Background from M0, M1, and M2 MCM was negligible.

www.manaraa.com

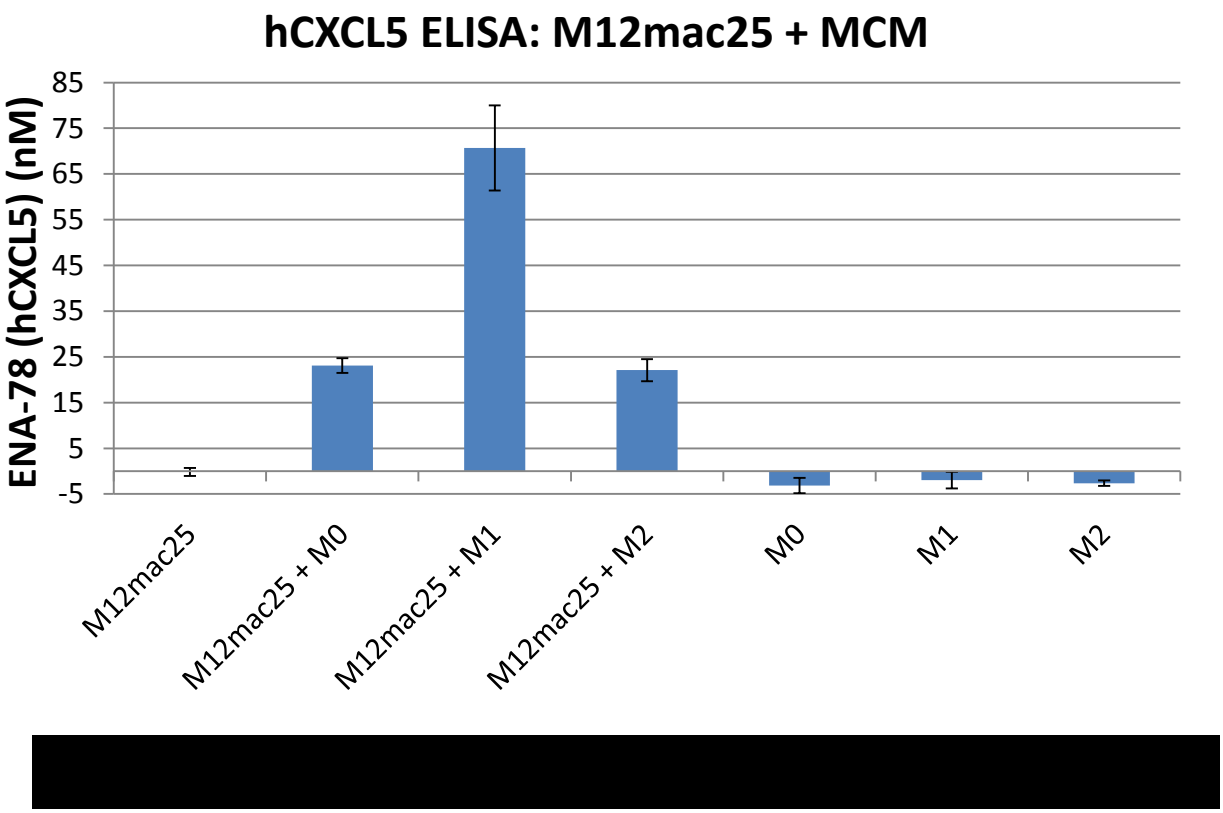

[redacted]

6.4.5 rCXCL5 M12mac25 In Vitro *Proliferation Study*

The ELISA data presented in section 6.4.4 established a relative concentration range of CXCL5 stimulated from MCM *in vitro,* approximately 20 – 70 nM, which falls into the range of rCXCL5 previously used to stimulate PC3 prostate cancer cell proliferation [108][109]. A study with rCXCL5 was used to determine if CXCL5 can act alone to stimulate M12mac25 proliferation in the absence of other factors present in MCM. Figure 6.4 shows these results, where the addition of rCXCL5 failed at all concentrations to induce proliferation. To confirm the bioactivity of the rCXCL5 itself, we replicated previously reported proliferation increases in PC3 cells in the presence of rCXCL5 over 96 hours (see Figure 6.5). CXCL5 was confirmed bioactive with a dose-dependent PC3 cell proliferation increase over complete media control through 100 pM.

www.manaraa.com

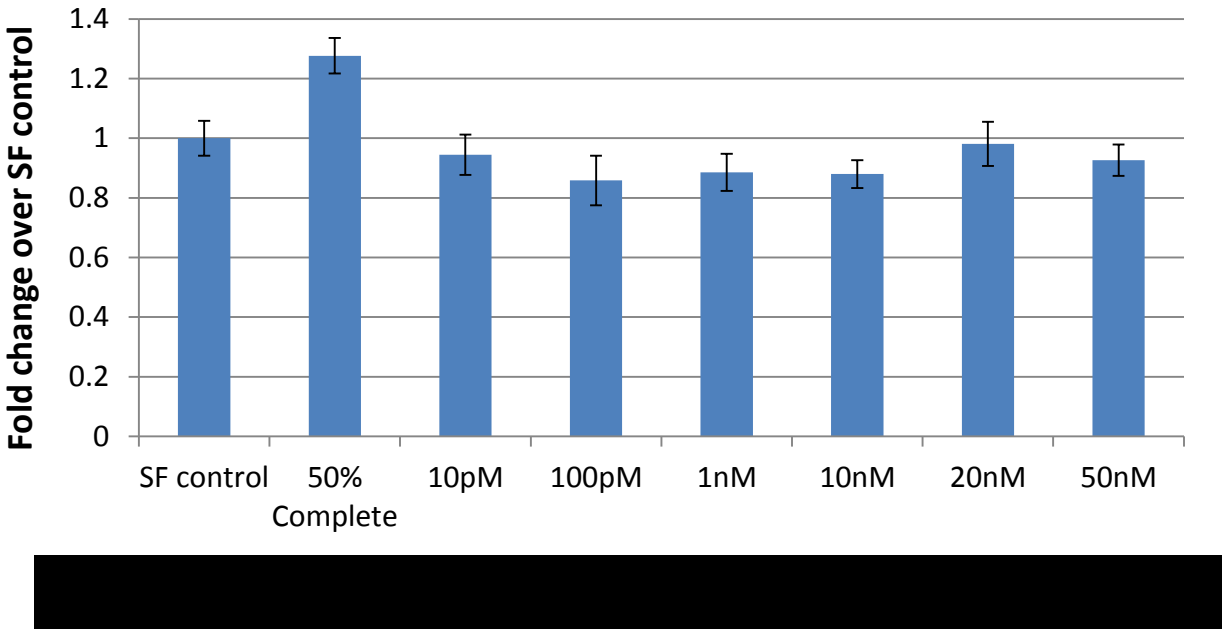

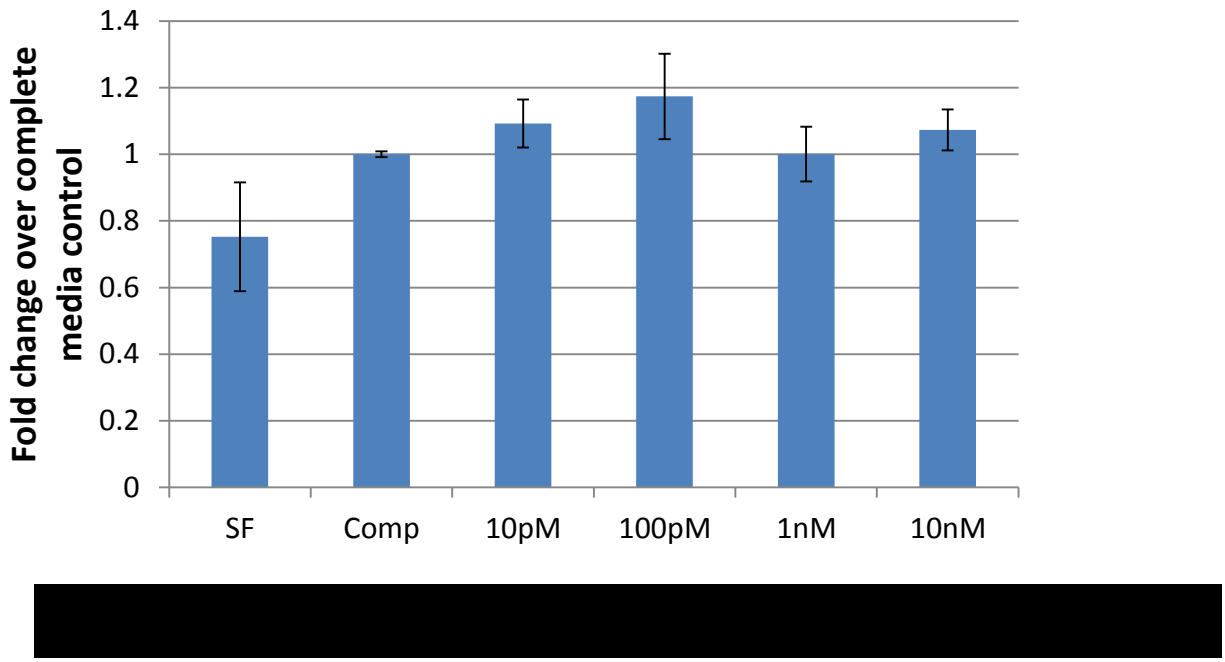

6.4.6 CXCR2 Blockade of MCM-Induced M12mac25 Proliferation

To determine whether the CXCL5 receptor plays a role in MCM-mediated M12mac25 proliferation, an anti-CXCR2 blocking antibody was used in an attempt to abrogate the MCM proliferation increase. Figure 6.6 shows 24 hour proliferation results, where M0, M1, and M2 MCM alone stimulate M12mac25 proliferation (in agreement with the results presented in section 5.4.7). However, CXCR2 mAB blocking decreases this proliferation only slightly: 3%

www.manaraa.com

for M0 with 5 µg/mL mAB, 11% for M0 with 10 µg/mL mAB, 14% for M1 with 5 µg/mL mAB, and 11% for M2 with 5 µg/mL mAB. Decreases of 37%, 45%, and 34% would be requires for complete knockdown of M0, M1, and M2-mediated M12mac25 proliferation increases, respectively.

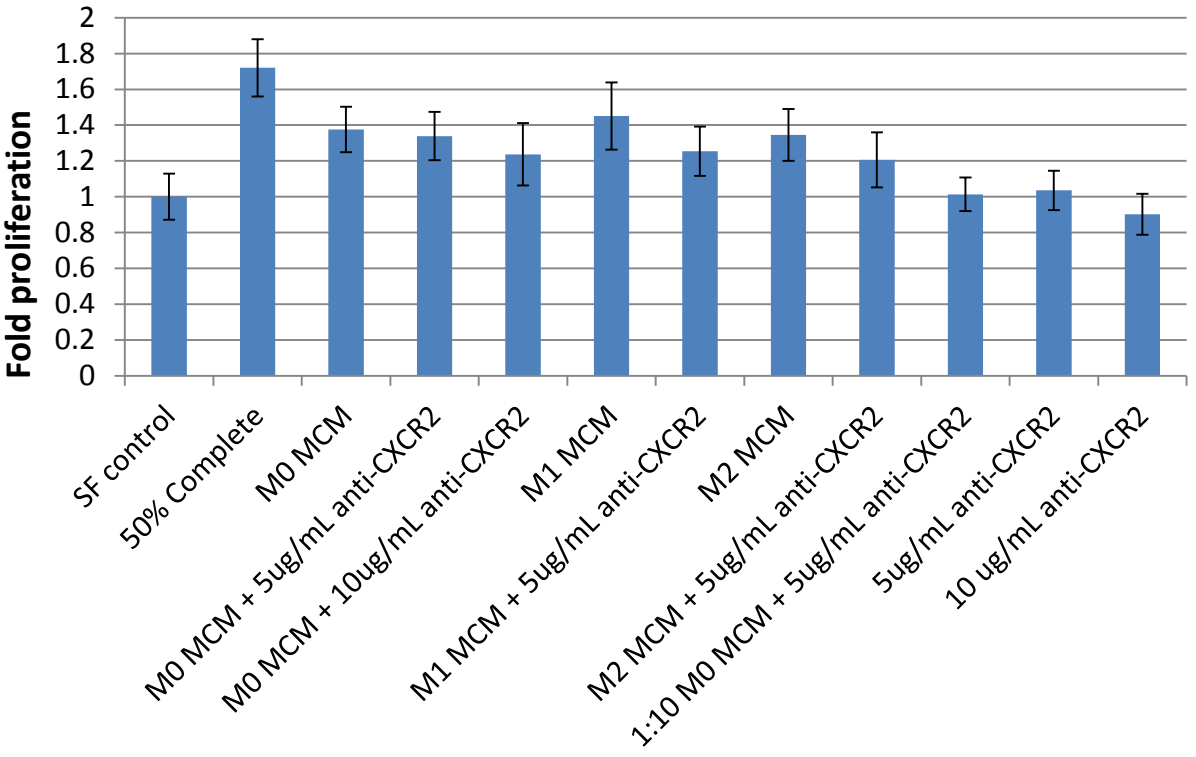

[redacted]

6.5 Discussion

M12mac25 cells remained largely dormant when injected with Matrigel, but grew tumors when implanted within porous pHEMA with or without Matrigel. The data presented in this chapter were designed to address potential cellular and molecular mechanisms of this dormancy escape *in vitro*. In chapter five, it was demonstrated that *in vivo*, there was significant macrophage infiltration into the scaffolds and that this response was necessary to induce the signaling that elicited the M12mac25 dormancy escape response. Here, follow-up studies were presented to explore the potential role of macrophage signaling on M12mac25 cells was explored *in vitro*.

www.manaraa.com

Macrophage conditioned media studies were designed to specifically probe the effects of various macrophage phenotypes on M12mac25 cells and determine whether these interactions could explain the results seen at the protein level on the explant cytokine arrays. MCM induced a significant increase in M12mac25 proliferation regardless of M0/M1/M2 macrophage phenotype (see Figure 6.1). Cytokine arrays on MCM identified a set of factors that is consistently present in all three phenotypes (see Table 6.1). Of these, MCP-1 [128], CXCL16 [129], M-CSF [130], and CXCL5 [108][109] have been associated with prostate cancer in the literature. However, MCP-1 was not shown to be significant in the explant cytokine arrays, CXCL16 has been associated with T cell response to prostate cancer while the athymic nude mouse system is T cell-deficient, and M-CSF was one of the top 20 cytokines present in both the pHEMA and Matrigel cytokine arrays (so it was not significantly different between the two groups). CXCL5, on the other hand, was shown to be up-regulated in pHEMA explants by cytokine array and DNA oligo array.

To address what might be up-regulated by M12mac25 cells when they are exposed to macrophages, human cytokine arrays were run on conditioned media from M12mac25 cells exposed to MCM. A set of proteins was found to be up-regulated across all three macrophage phenotypes, and that set included CXCL5. When comparing the whole explant human cytokine array data to this list, all proteins found to be up-regulated in the explants were up-regulated in response to at least two of three macrophage phenotypes, which lends *in vitro* evidence to the idea that macrophage signaling could be responsible for M12mac25 dormancy escape.

In chapter five, it was demonstrated that CXCL5 and the signaling pathways downstream of its CXCR2 receptor were significantly up-regulated in the pHEMA explants compared to Matrigel. To further examine the role of CXCL5 on M12mac25 cells *in vitro*, a proliferation study was run using recombinant human CXCL5 in the absence of all other factors in MCM. It was found that in the concentration range of CXCL5 in the M12mac25 MCM as demonstrated by ELISA, no significant proliferation increase was observed in M12mac25 cells. In addition, blocking the CXCR2 pathway only partially abrogated the increase in proliferation mediated by MCM. This indicates that the mechanism for M12mac25 proliferation increase *in vitro* occurs, at least in part, through another signaling pathway.

www.manaraa.com

However, it is important to note that all the *in vitro* conditioned media studies presented in this chapter were performed using standard two-dimensional tissue culture. Because caution is warranted whenever applying 2D results to 3D situations (see section 1.3), it is reasonable to question whether these 2D results are applicable to the *in vivo* scenario. The consistency between *in vitro* and *in vivo* cytokine array results should limit these concerns. *In vivo* we observed a set number of proteins that were up-regulated in pHEMA explants containing elevated numbers of macrophages. *In vitro* we see that same set of proteins up-regulated in M12mac25 cells after being exposed to macrophage conditioned media. Just because CXCL5 does not act on its own *in vitro* doesn't necessarily mean it isn't the main actor *in vivo*, though it seems highly likely that the signaling events *in vivo* that result in dormancy escape are not mediated by one protein or pathway but rather are the result of complex cellular interactions.

www.manaraa.com

Chapter 7. Conclusions, Limitations, and Future Directions

Biomaterials are becoming more widely used as the basis for engineering cancer model systems as research groups move toward more complex and physiologically relevant 3D pre-clinical models. This effort is necessary because traditional model systems fail to adequately control cellular and molecular interactions and ultimately can provide data that might not be representative of the human disease state. Biomaterials-based cancer model systems have the potential for both basic biological discovery studies and drug screening. The advantages of biomaterials-based models include a tight control over cellular microenvironment *in vitro* and the ability to create orthotopic tissue niches *in vivo* including the cancer tissue xenografts themselves or engineered metastatic sites. Synthetic biomaterials are tunable systems where researchers have control over surface chemistry, mechanics, degradation, fabrication architecture, and factor release. Because of this, synthetic systems are more adaptable for some studies over naturally-derived materials such as Matrigel, which is currently used as the gold standard for the generation of xenografts for numerous cancer cell lines.

The studies presented in this dissertation established that sphere-templated porous pHEMA scaffolds can be used to engineer human prostate cancer xenografts and that these tissues demonstrated unique properties *in vivo* including the induction of cellular dormancy escape. First, methods were developed for the *in vitro* cell culture of prostate cancer cells within the pHEMA scaffolds. To seed cells within the interconnected porous structure, a capillary force-based technique was introduced that improved the cell number and distribution within the scaffolds compared to other established seeding methods. Dynamic culture conditions limited necrotic zone formation during 3D cell culture, and a PicoGreen DNA assay quantitatively demonstrated the proliferation of prostate cancer cells within the 3D scaffold.

The capacity for porous pHEMA to be used as a vehicle for xenograft generation was demonstrated using M12 cells, a tumorigenic human prostate epithelial cancer cell line. While pHEMA-derived M12 tumors did not display significant differences in growth kinetics or vascularity compared to their Matrigel counterparts, this is not necessarily surprising because the cells are naturally tumorigenic in the subcutaneous space even without Matrigel. A similar effect has been observed for other highly malignant cell lines [38], so it is possible that going forward,

www.manaraa.com

the advantages of biomaterials-based *in vivo* tumor models could be limited in cell lines that display high inherent tumorigenicity in the environment in which they are implanted.

In contrast, pHEMA could not be used as a reliable basis for the generation of xenografts from LNCaP C4-2 cells, which ordinarily require Matrigel or stromal cell support to form tumors *in vivo*. Both pHEMA alone and pHEMA-co-MAA with surface-conjugated collagen I only yielded tumors from one out of six implants over twelve weeks, yielding a designation of these constructs as poorly tumorigenic. It is important to note that Matrigel contains numerous growth factors and ECM proteins involved in stimulating cell proliferation, and these factors were missing from the pHEMA microenvironment. However, it is possible that in future studies the synthetic scaffold could be adaptable to present one or more of these factors to enhance tumorigenesis. This could mean conjugating laminin I or collagen IV to polymer surface, as these are the main ECM constituents of Matrigel, or this could mean controllably releasing growth factors from the polymer. It is also possible that enhanced vascularity would allow for tumor growth, which could be accomplished by modulating pore size.

Finally, M12mac25 cells, which remain dormant when injected in Matrigel due to the transfection of the tumor suppressor gene mac25, re-activated to form tumors when implanted within porous pHEMA scaffolds. This is an important result because currently there are few model systems for studying cancer dormancy escape. It was demonstrated that relative to the dormant Matrigel samples, the pHEMA implants recruited a significantly higher number of macrophages, which are important cells in ordinary tumor development but have not been established as a player in dormancy escape. High-throughput protein analysis indicated that many of the significant differences between the pHEMA and Matrigel samples were related to macrophage signaling, and conditioned media from macrophages, regardless of polarization, stimulated the proliferation of M12mac25 cells *in vitro*. There was good agreement between the proteins up-regulated by M12mac25 cells in the presence of MCM and the significantly increased proteins in the pHEMA explants. CXCL5, which has been previously associated with prostate cancer progression [108][109], was identified as a potential actor in these *in vitro* and *in vivo* cytokine arrays, but further *in vitro* analysis could not conclusively demonstrate a role for CXCL5 or the CXCR2 receptor in MCM-mediated M12mac25 proliferation. However, this does

www.manaraa.com

not necessarily discount CXCL5 as an actor *in vivo*. It is likely that multiple signaling pathways are at work to re-activate M12mac25 cells in the complex microenvironment created by scaffold implantation. Blocking antibodies for CXCR2 applied *in vivo* to M12mac25-seeded scaffolds or rCXCL5 applied *in vivo* to M12mac25-Matrigel xenografts would be potential future strategies to confirm the potential role of CXCL5 in M12mac25 dormancy escape.

Clondronate liposomes were used to attempt to elucidate the role of macrophages in scaffold-mediated M12mac25 dormancy escape. It was demonstrated that CLs effectively eliminated macrophages in most cases *in vivo*, but along with that the other cell types involved in the foreign body response, including endothelial cells. With the loss of vascularity, the M12mac25 cells themselves could not survive in the scaffolds. So, it was demonstrated that while the microenvironment created by the scaffolds is necessary for dormancy escape, we could not establish with the CL studies that the macrophages have a direct role in that process. Macrophages do, however, have at least an indirect role because they orchestrate the entire response to the implanted material. A potential avenue to confirm the role of macrophages in this dormancy escape process would be to use a model system such as the macrophage-null transgenic macrophage FAS-induced apoptosis (MAFIA) mouse alone along with thinner scaffolds that allow the M12mac25 cells to survive without the vascularity induced by the macrophage.

In general, the immunocompromised mouse model system used for these studies presents a potential limitation to fully recapitulating the tumor microenvironment. Athymic nude mice lack the adaptive immune response, which is known to play roles in cancer development and dormancy escape, and T cells also represents a potential therapeutic target in the field of immune-oncology. Human tumor xenografts in mice have been used for many years in a variety of applications because it is desirable to study actual human tumor biology rather than use an immune-competent system that involves mouse-derived cancer cells. This is a trade-off that must be kept in mind for future studies. In the dormancy model presented here, the development of mouse cell lines expressing mac25 could be used in an immune-competent setting. In addition, subcutaneous xenografts have been used ubiquitously in cancer research labs due to their simplicity, but the potential relevance of an ectopic tumor developing in the subcutaneous space

www.manaraa.com

remains in question. Biomaterials-based systems present an attractive way to mimic tissue microenvironments ectopically, but the studies presented here really only utilized the subcutaneous microenvironment. For future prostate cancer development studies, it is possible to inject biomaterials directly into the prostate, or to study metastatic progression or dormancy in a more relevant tissue setting, it is possible to design materials to mimic a bone marrow-like microenvironment (see section 1.6).

In conclusion, the studies in this dissertation have demonstrated that synthetic biomaterial scaffolds can produce unique and interesting results when applied to the generation of cancer model systems. In the coming years there is no doubt that more sophisticated *in vitro* and *in vivo* tumor models will be developed with control over the tumor microenvironment mediated by biomaterial scaffolds. I predict that future collaborations between bioengineers and cancer biologists will yield technologies that will impact pre-clinical therapeutics development and ultimately will influence clinical outcomes.

www.manaraa.com

Appendix 1: P69, M12, and M12mac25 Cell Line Generation

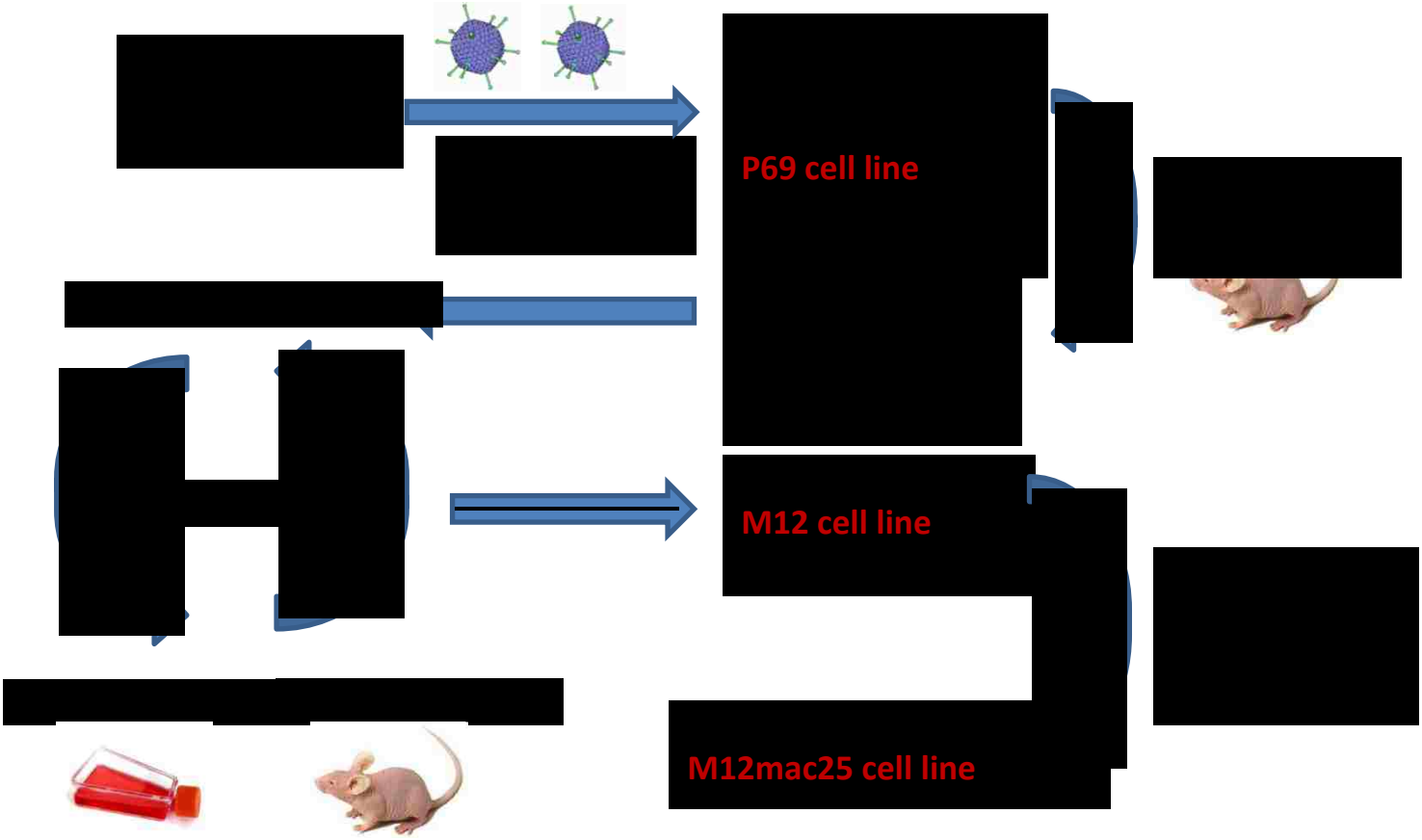

www.manaraa.com

Appendix 2: LNCaP C4-2 Cell Line Generation

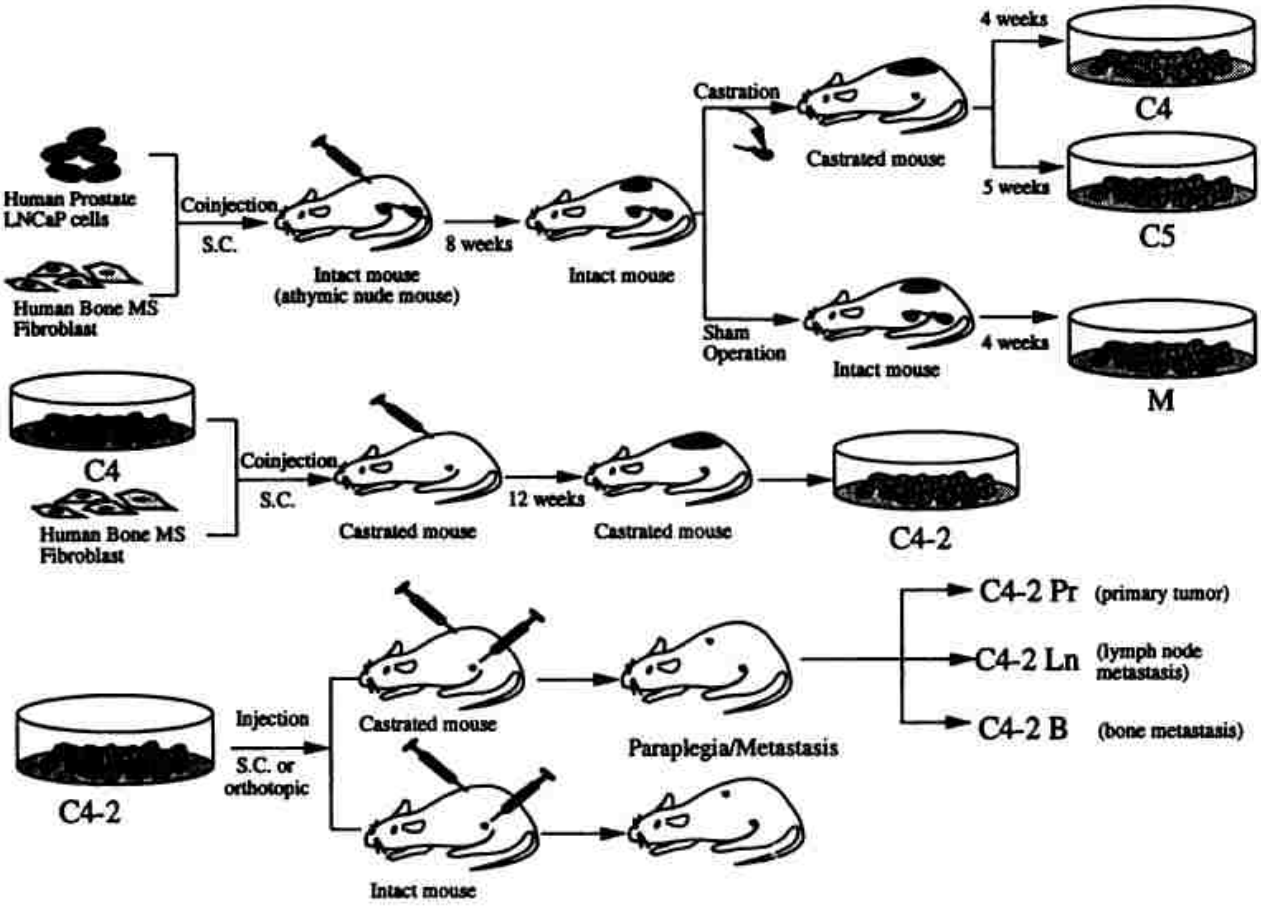

Source: [70]

www.manaraa.com

Appendix 3: Cytokine Antibody Array Maps

RayBio® Human Cytokine Antibody Array 5 Map

	A	B	C	D	E	F	G	H	I	J	K
1	Pos	Pos	Pos	Pos	Neg	Neg	ENA-78	GCSF	GM-CSF	GRO	GRO-α
2	I-309	IL-1α	IL-1 β	IL-2	IL-3	IL-4	IL-5	IL-6	IL-7	IL-8	IL-10
3	IL-12 p40p70	IL-13	IL-15	IFN- γ	MCP-1	MCP-2	MCP-3	MCSF	MDC	MIG	MIP-1β
4	MIP-1δ	RANTES	SCF	SDF-1	TARC	TGF-β1	TNF-α	TNF-β	EGF	IGF-I	Angiogenin
5	Oncostatin M	Thrombopoietin	VEGF	PDGF-BB	Leptin	BDNF	BLC	Ck β 8-1	Eotaxin	Eotaxin-2	Eotaxin-3
6	FGF-4	FGF-6	FGF-7	FGF-9	Flt-3 Ligand	Fractalkine	GCP-2	GDNF	HGF	IGFBP-1	IGFBP-2
7	IGFBP-3	IGFBP-4	IL-16	IP-10	LIF	LIGHT	MCP-4	MIF	MIP-3 α	NAP-2	NT-3
8	NT-4	Osteopontin	Osteoprotegerin	PARC	PIGF	TGF- β 2	TGF- β 3	TIMP-1	TIMP-2	Pos	Pos

RayBio® Mouse Cytokine Antibody Array 3 (62)

	A	B	C	D	E	F	G	H	I	J	K	L	M	N
1	POS	POS	NEG	NEG	Blank	Axl	BLC	CD30 L	CD30 T	CD40	CRG-2	CTACK	CXCL16	Eotaxin
2	POS	POS	NEG	NEG	Blank	Axl	BLC	CD30 L	CD30 T	CD40	CRG-2	CTACK	CXCL16	Eotaxin
3	Eotaxin-2	Fas Ligand	Fractalkine	GCSF	GM-CSF	IFN γ	IGFBP-3	IGFBP-5	IGFBP-6	IL-1α	IL-1 beta	IL-2	IL-3	IL-3 Rb
4	Eotaxin-2	Fas Ligand	Fractalkine	GCSF	GM-CSF	IFN γ	IGFBP-3	IGFBP-5	IGFBP-6	IL-1α	IL-1 beta	IL-2	IL-3	IL-3 Rb
5	IL-4	IL-5	IL-6	IL-9	IL-10	IL-12 p40/p70	IL-12 p70	IL-13	IL-17	KC	Leptin R	Leptin	LIX	L-Selectin
6	IL-4	IL-5	IL-6	IL-9	IL-10	IL-12 p40/p70	IL-12 p70	IL-13	IL-17	KC	Leptin R	Leptin	LIX	L-Selectin
7	Lymphotactin	MCP1	MCP-5	M-CSF	MIG	MIP-1α	MIP-1γ	MIP-2	MIP-3 β	MIP-3α	PF-4	P-Selectin	RANTES	SCF
8	Lymphotactin	MCP1	MCP-5	M-CSF	MIG	MIP-1α	MIP-1γ	MIP-2	MIP-3 β	MIP-3α	PF-4	P-Selectin	RANTES	SCF
9	SDF-1α	TARC	TCA-3	TECK	TIMP-1	TNFα	sTNF RI	sTNF RII	TPO	VCAM-1	VEGF	Blank	Blank	POS
#	SDF-1α	TARC	TCA-3	TECK	TIMP-1	TNFα	sTNF RI	sTNF RII	TPO	VCAM-1	VEGF	Blank	Blank	POS

www.manaraa.com

Appendix 4: Top Proteins Present in M12mac25 Explants Identified by Cytokine Arrays

Human Cytokine Array Data			**Mouse Cytokine Array Data**	
Top 20 most present cytokines	Normalized Average		Top 20 most present cytokines	Normalized Average
TGF-β2	0.312406017		P-Selectin	0.413548
NAP-2 (CXCL7)	0.214119718		MIP-2	0.337668
FGF-9	0.211329695		CD30 T	0.292457
Oncostatin M	0.186929029		CTACK	0.287407
GDNF	0.180155393		TCA-3	0.283367
BDNF	0.178621145		IGFBP-3	0.27711
TIMP-1	0.174286083		MCP-1	0.274381
IGFBP-2	0.163863154		PF-4	0.270757
HGF	0.162091647		LIX (CXCL5)	0.263582
Osteopontin	0.15606151		M-CSF	0.258866
RANTES (CCL5)	0.152368155		SDF-1α	0.229357
MCSF	0.1517563		IL-1α	0.210563
GRO (CXCL1)	0.147386092		MCP-5	0.198346
MIF	0.143576844		IL-12 p70	0.190637
NT-3	0.132236886		TIMP-1	0.183167
IP-10 (CXCL10)	0.131925894		MIP-3a	0.153063
GCP-2	0.12223965		Eotaxin-2	0.149965
LIF	0.113217919		IL-4	0.149035
IL-3	0.108432874		Lymphotactin	0.13977
Eotaxin-2 (CCL24)	0.108294291		TARC	0.129858

The above lists are for pHEMA-derived explants, but in general there was good agreement between pHEMA and Matrigel explants in terms of the top proteins identified (17/20 similarity for the human arrays and 19/20 similarity for the mouse arrays).

www.manaraa.com

Appendix 5: Full Human Cytokine Array Significant Results

Human Cytokine Array Data

Significant differences ($p < 0.05$) (student t-test)

pHEMA (n=10) vs. Matrigel No Growth (n=3)

Protein	p value	Matrigel No vs. Yes also significant?	Higher or lower expression in pHEMA	Agreement with mouse array?
ENA-78 (CXCL5)	0.0138	Yes, p = 0.0098	Higher	N/A
IL-1B	0.0163	Yes, p = 0.0359	Higher	Yes, p = 0.0007
IL-15	0.0169	No	Higher	N/A
MCP-2 (CCL8)	0.0297	Trending, p = 0.0702	Higher	N/A
IL-3	0.0341	No	Higher	No, mouse not significant
LIGHT	0.0348	Yes, p = 0.0171	Higher	N/A
IGFBP-1	0.0425	No	Higher	N/A
IL-2	0.0427	No	Higher	No, mouse not significant
VEGF	0.0445	No	Higher	Yes, p = 0.0006
IL12 p40p70	0.0475	Trending, p = 0.0669	Higher	No, mouse not significant
PDGF-BB	0.0496	No	Higher	N/A

N/A: protein not present on mouse array

Matrigel Growth (n=2) vs. No Growth (n=3)

Protein	p value	pHEMA vs. Matrigel No also significant?	Higher or lower expression in Matrigel growth	Agreement with mouse array?
ENA-78 (CXCL5)	0.0098	Yes, p = 0.0138	Higher	N/A
LIGHT	0.0171	Yes, p = 0.0348	Higher	N/A
PARC	0.0189	No	Higher	N/A
IL-8	0.0208	Trending, p = 0.0579	Higher	N/A
IGF-1	0.0249	No	Higher	N/A
LIF	0.0251	No	Higher	N/A
IL-4	0.0315	No	Higher	Trend doesn't agree
PIGF	0.0338	No	Higher	N/A
Eotaxin (CCL11)	0.0343	Trending, p = 0.0512	Higher	Yes, p = 0.0098 (pHEMA)
IL-1B	0.0359	Yes, p = 0.0163	Higher	Yes, p = 0.0007 (pHEMA)
MDC (CCL22)	0.0418	No	Higher	N/A
TGF-B	0.0436	No	Higher	N/A

N/A: protein not present on mouse array

www.manaraa.com

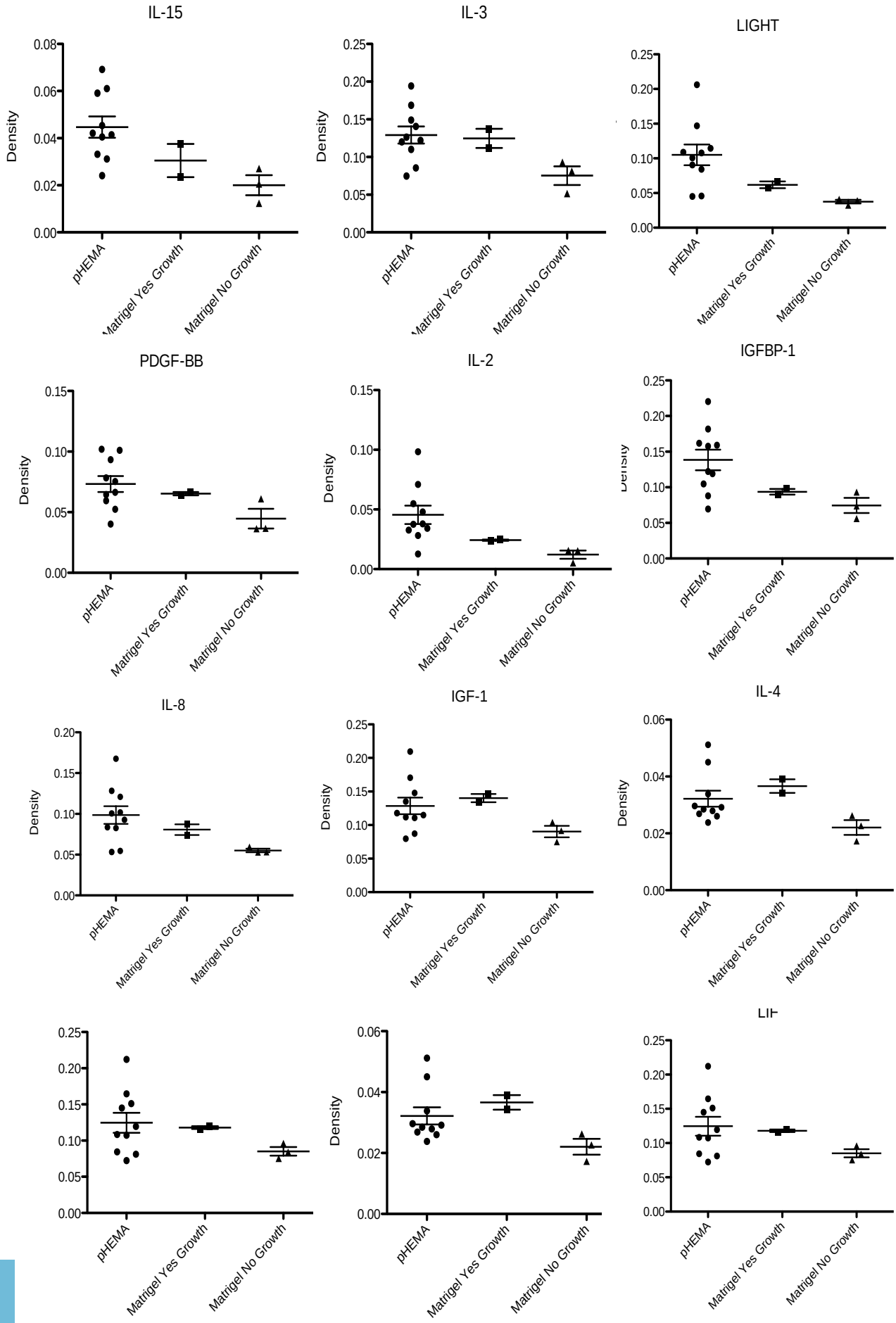

www.manaraa.com

Appendix 6: Full Mouse Cytokine Array Significant Results

Mouse Cytokine Array Data

Significant differences ($p < 0.05$) (student t-test)

pHEMA (n=6) vs. Matrigel No Growth (n=4)

Protein	p value	Higher or lower expression in pHEMA	Agreement with human array?
VEGF	0.0006	Higher	Yes, p = 0.0445
IL-1B	0.0007	Higher	Yes, p = 0.0163
CD30T	0.0013	Higher	N/A
IGFBP5	0.0014	Higher	N/A
Leptin	0.0035	Higher	N/A
RANTES (CCL5)	0.0088	Higher	No, human not significant
Eotaxin (CCL11)	0.0098	Higher	Yes, p = 0.0343 (human Matrigel)
SDF-1α (CXCL12)	0.0143	Higher	No, human not significant
CTACK (CCL27)	0.0146	Higher	N/A
MIG (CXCL9)	0.0234	Higher	No, human not significant
TPO	0.0248	Higher	N/A
CRG-2 (CXCl10)	0.0329	Higher	No, human IP-10 not significant
VCAM-1	0.0385	Higher	N/A
IL-4	0.0401	Lower	Trend doesn't agree

N/A: protein not present on human array

www.manaraa.com

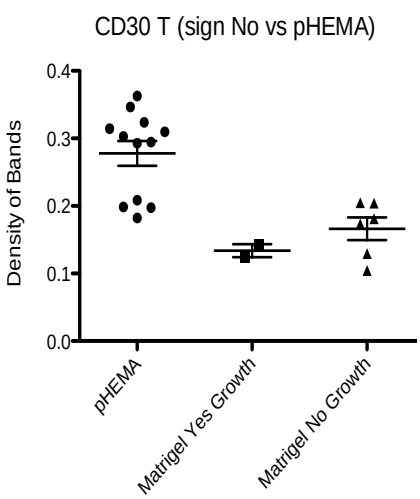

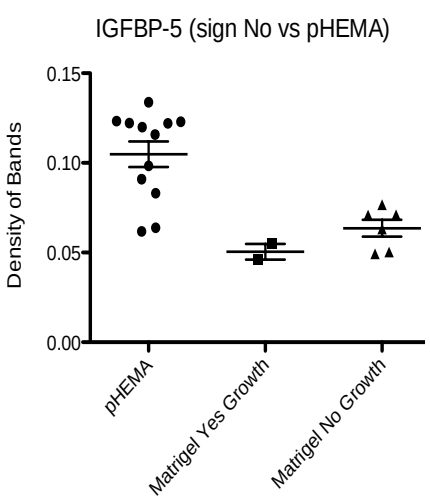

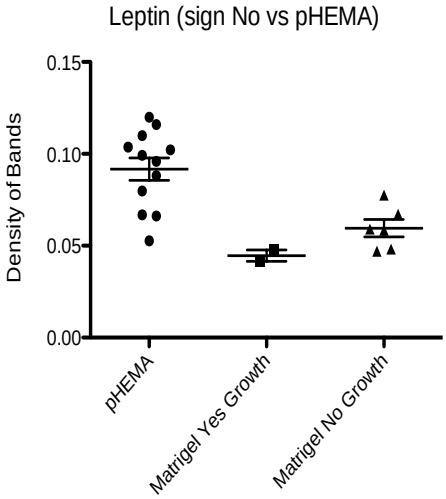

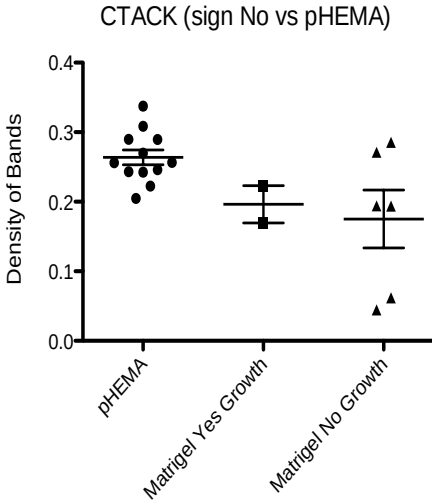

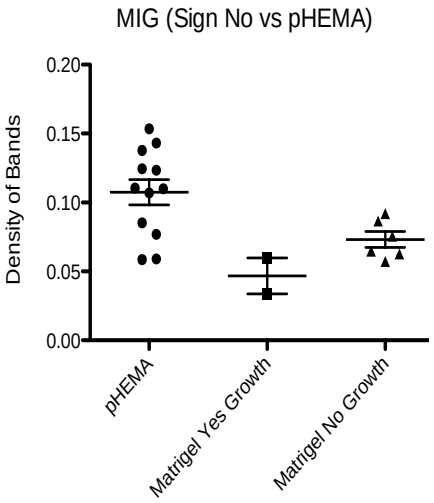

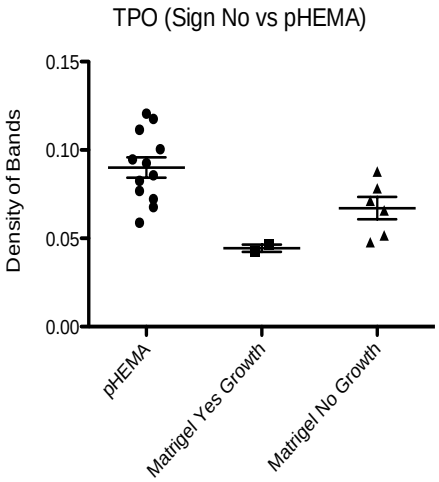

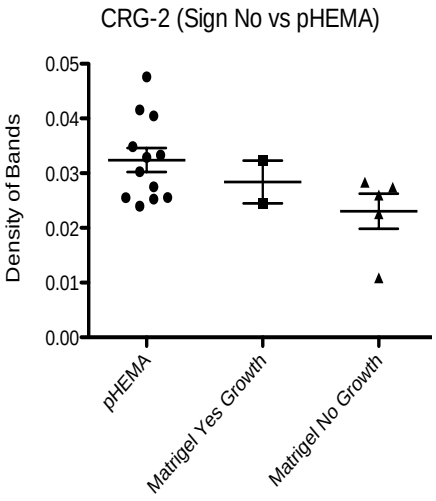

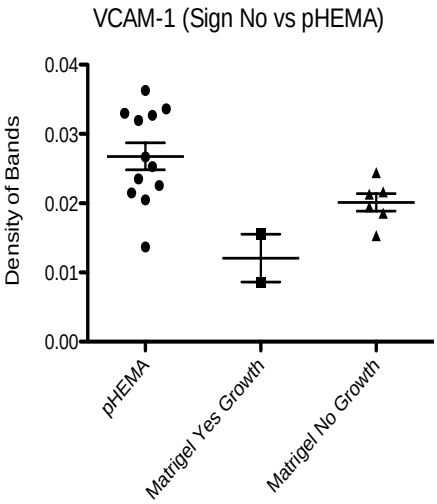

www.manaraa.com

Appendix 7: DNA Oligonucleotide Array Gene Set Enrichment Analysis Results

CS2 Canonical Pathways
Positive upregulation in pHEMA vs. Matrigel no growth
24 gene sets significant at false discovery rate (FDR) < 25%
Sorted by normalized enrichment score (NES)

Cholesterol biosynthesis
Steroid biosynthesis
Steroid metabolism
snRNP assembly
Metabolism of RNA
Cell-ECM interactions
Purine metabolism
Nuclear import of REV protein
Cytosolic tRNA aminoacylation
Transport of SLBP independent mature mRNA
REV mediated nuclear export of HIV RNA
Terpenoid backbone biosynthesis
E coli infection
NEP NS2 interacts with cellular export machinery
P53 signaling
Cell cycle
Regulation of APC activators between G1, S, anaphase
Regulation of glucokinase
Cyclin E events during G1/S transition
G2 and M phases
APC mediated degradation of cyclin A
VEGF signaling
Cell cycle checkpoints
Transport of ribonucleoproteins to nucleus

Negative down-regulation in pHEMA vs. Matrigel no growth
8 gene sets significant at FDR < 25%
Sorted by NES

Electron transport chain
Oxidative phosphorylation
Glucose regulation of insulin secretion
Regulation of insulin secretion
Cardiac muscle contraction
Parkinsons disease
Alzheimers disease

www.manaraa.com

CS5 Gene Ontology
Positive upregulation in pHEMA vs. Matrigel no growth
28 gene sets significant at FDR < 25%
Sorted by NES

Oxidoreductase activity
Cofactor biosynthetic process
Unfolded protein binding
Tissue development
T cell proliferation
DNA helicase activity
Behavior
Nucleotidyltransferase activity
Epidermis development
Locomotory behavior
Regulation of cyclin dependent protein kinase activity
Regulation of cytokine production
Apical plasma membrane
Tissue morphogenesis
Rho protein signal transduction
Regulation of T cell proliferation
Steroid binding
Exonuclease activity
Hydrolase activity acting on carbon nitrogen cyclic amidines
Helicase activity
Cell matrix junction

Negative down-regulation in pHEMA vs. Matrigel no growth
25 gene sets significant at FDR < 25%
Sorted by NES

Lipase activity
Phospholipase activity
Regulation of cellular pH
RNA Pol II Transcription factor activity
Cellular monovalent inorganic cation homeostasis
Protein import into nucleus translocation
Regulation of pH
Monovalent inorganic cation homeostasis
Mitochondrial respiratory chain
NADH dehydrogenase complex
Respiratory chain complex

www.manaraa.com

Mitochondrial respiratory chain complex
Phosphoinositide mediated signaling
ATPase activity coupled to transmembrane ion transport
Phosphotransferase activity
Nucleotide kinase activity
Nuclear replication fork
Substrate specific channel activity
Regulation of growth
Growth
G protein signaling coupled to IP3
Mitotic sister chromatid segregation
Nuclear chromosome part
Sister chromatid segregation
Cofactor transport

www.manaraa.com

Appendix 8: Top 50 Genes Most Up-Regulated in pHEMA-Derived M12mac25 Explants

Gene	Description	Fold Change
CAV2	caveolin 2	2.637
SERPINE1	serpin peptidase inhibitor, clade E (nexin, plasminogen activator inhibitor type 1), member 1	5.321
UBE2E2	ubiquitin-conjugating enzyme E2E 2 (UBC4/5 homolog, yeast)	1.781
FGF2	fibroblast growth factor 2 (basic)	1.843
STAC	SH3 and cysteine rich domain	3.723
PHLDA2	pleckstrin homology-like domain, family A, member 2	2.501
KRT7	keratin 7	3.929
CDKN2B	cyclin-dependent kinase inhibitor 2B (p15, inhibits CDK4)	2.072
CCND1	cyclin D1	3.078
CAV1	caveolin 1, caveolae protein, 22kDa	2.77
UBTD1	ubiquitin domain containing 1	1.631
AKT3	v-akt murine thymoma viral oncogene homolog 3 (protein kinase B, gamma)	3.423
SCD	stearoyl-CoA desaturase (delta-9-desaturase)	2.889
PROCR	protein C receptor, endothelial	1.987
ITGAV	integrin, alpha V (vitronectin receptor, alpha polypeptide, antigen CD51)	2.082
CAV1	caveolin 1, caveolae protein, 22kDa	2.611
EDIL3	EGF-like repeats and discoidin I-like domains 3	6.858
TNFSF9	tumor necrosis factor (ligand) superfamily, member 9	2.47
SFTA1P	surfactant associated 1 (pseudogene)	7.4
AHNAK2	AHNAK nucleoprotein 2	1.815
C2CD2	C2 calcium-dependent domain containing 2	2.528
IREB2	iron-responsive element binding protein 2	1.581
FSTL5	follistatin-like 5	24.06
HMGCS1	3-hydroxy-3-methylglutaryl-CoA synthase 1 (soluble)	2.204
CCND1	cyclin D1	2.451
F3	coagulation factor III (thromboplastin, tissue factor)	3.891
MATN3	matrilin 3	3.09
SC4MOL	sterol-C4-methyl oxidase-like	2.53
CHORDC1	cysteine and histidine-rich domain (CHORD)-containing 1	1.776
C9orf30	chromosome 9 open reading frame 30	1.588
FBN2	fibrillin 2	2.764
PRSS23	protease, serine, 23	2.603
COL5A2	collagen, type V, alpha 2	6.281
HEATR5A	HEAT repeat containing 5A	1.68
SCD	stearoyl-CoA desaturase (delta-9-desaturase)	3.123
CDC42SE1	CDC42 small effector 1	1.59
TBL1XR1	transducin (beta)-like 1 X-linked receptor 1	1.543
PCDH9	protocadherin 9	5.116
HMGCS1	3-hydroxy-3-methylglutaryl-CoA synthase 1 (soluble)	2.486
HERC4	hect domain and RLD 4	1.637
SPRED1	sprouty-related, EVH1 domain containing 1	2.903
CCNJ	cyclin J	1.612
E2F5	E2F transcription factor 5, p130-binding	1.831
SLC39A10	solute carrier family 39 (zinc transporter), member 10	1.977
SEC23A	Sec23 homolog A (S. cerevisiae)	1.474
TES	testis derived transcript (3 LIM domains)	1.588

www.manaraa.com

Appendix 9: DNA Oligonucleotide Array Individual Gene Analysis

Gene Category	Gene Name	Protein Name	SAM Rank (Fold Change pHEMA vs. Matrigel)	Replicate (if applicable)	Replicate (if applicable)	Comments
Chemokine Ligands and Receptors	CCL5	RANTES	3499 (1.58)			All CCL, CCR, CXCL, CXCR, CX3C that are present in gene list are listed here
	CCL2	MCP-1	14731 (-1.4)			
	CCL24	Eotaxin-2	13454 (-1.4)			
	CXCL5	ENA-78	2079 (2.16)	2652 (1.51)		
	CXCL2	GRO-B	5947 (1.35)			
	CXCL1	GRO-A	8859 (1.09)			
	CXCL12	SDF-1	10711 (-1.2)			
	CXCL14	BRAK	13346 (-1.4)			
	CCR7		9563 (-1)			
	CXCR7		7250 (1.06)			
Interleukins and Interleukin Receptors	IL1b		18017 (-3.7)			All IL and ILR that are present in gene list are listed here
	IL18		106 (2.43)			
	IL6		4430 (1.46)			
	IL7		7828 (1.11)			
	IL15		9495 (1)			
	IL27		9861 (-1)			
	IL1R		3357 (1.24)			
	IL4R		14875 (-1.4)			
	IL10R		9519 (1)			
	IL15R		2194 (1.43)			
	IL27R		2506 (1.32)			
	IL17R		3209 (1.25)			
	IL13R		5419 (1.24)	15444 (-1.2)		
	IL20R		9420 (1.01)			
	IL7R		12331 (-1.5)			
	IL11R		15130 (-1.2)			
	IL6R		17254 (-1.7)			
Extracellular Matrix Proteins	COL5A2	Collagen V alpha 2	37 (6.28)	1372 (2.45)		Too many collagens to list, representative only
	COL5A1	Collagen V alpha 1	12883 (-1.2)	15449 (-1.3)		
	COL1A1	Collagen I alpha 1	85 (1.68)			
	COL1A2	Collagen I alpha 2	12017 (-1.2)			
	COL12A1	Collagen XII alpha 1	2228 (1.63)	2486 (1.51)		
	COL9A3	Collagen IX alpha 3	4681 (1.21)			
	COL7A1	Collagen VII alpha 1	4915 (1.28)			

www.manaraa.com

	COL3A1	Collagen III alpha 1	5041 (1.38)	11480 (-1.2)		
	COL4A1	Collagen IV alpha 1	6279 (1.24)			
	COL4A2	Collagen IV alpha 2	14396 (-1.4)			
	COL4A4	Collagen IV alpha 4	18000 (-2.2)			
	LAMC1	Laminin gamma 1	299 (1.45)			All laminins listed
	LAMA1	Laminin alpha 3	490 (1.64)	1909 (1.27)		
	LAMC2	Laminin gamma 2	3807 (1.69)			
	LAMB3	Laminin beta 3	5081 (1.61)			
	LAMA5	Laminin alpha 5	11006 (-1.1)			
	LAMA4	Laminin alpha 4	13740 (-1.2)			
	LAMB4	Laminin beta 2	14077 (-1.2)			
	LAMB1	Laminin beta 1	17087 (-1.4)			
	FN1	Fibronectin 1	17816 (-2.5)	17944 (-5)		
Integrins	ITGA5	Integrin alpha 5	14 (2.08)	129 (3.08)	4913 (1.16)	
	ITGB1	Integrin beta 1	402 (1.47)	951 (1.57)	1733 (1.36)	
	ITGB5	Integrin beta 5	1318 (1.41)			
	ITGA3	Integrin alpha 3	2198 (1.34)			
	ITGB8	Integrin beta 8	14408 (-1.4)			
	ITGA6	Integrin alpha 6	15774 (-1.3)			
	ITGB4	Integrin beta 4	16033 (-1.3)			
	ITGA7	Integrin alpha 7	17455 (-1.8)			
Epithelial-Mesenchymal Transition	CDH2	N-cadherin	6587 (1.21)			Trends as expected for EMT
	CDH1	E-cadherin	16669 (-1.6)			
	VIM	Vimentin	323 (1.4)	1681 (1.33)		
	CLDN3	Claudin-3	9531 (1)	16568 (-1.4)		
	EGR1		16367 (-1.4)			
	ACTA2	Alpha smooth muscle actin	9811 (-1)			
Growth Factors	EGF	epidermal growth factor	N/A			
	EGFR	epidermal growth factor receptor	16969 (-1.3)			
	FGF2	fibroblast growth factor 2	3 (1.84)			
	FGF4	fibroblast growth factor 4	N/A			
	FGF6	fibroblast growth factor 6	N/A			
	FGF7	fibroblast growth factor 7	N/A			
	FGF9	fibroblast growth factor 9	17365 (-2.8)			
	VEGFC	vascular endothelial growth factor C	925 (2.56)			
	VEGFA	vascular endothelial growth factor A	6806 (1.13)			
	VEGFB	vascular endothelial growth factor B	10771 (-1)			
	TGFB2	transforming growth factor B2	226 (1.68)			

www.manaraa.com

	TGFB1	transforming growth factor B1	947 (2.15)			
	TGFBR2	transforming growth factor B receptor 2	1007 (1.5)			
	CTGF	connective tissue growth factor	197 (2.69)			
	PDGFC	platelet derived growth factor C	347 (1.65)	2678 (2.01)		
	PDGFR	platelet derived growth factor receptor	4753 (1.31)			
	BDNF		N/A			
	GDNF		N/A			
	HGF		N/A			
Search Term: Prostate	STEAP1	6 transmembrane epithelial prostate antigen 1	373 (2.16)	443 (1.95)		
	PMEPA	prostate transmembreane protein, androgen-induced	447 (2.54)	2762 (1.77)	676 (1.72)	
	PTOV1	prostate tumor overexpressed 1	11016 (-1.1)	15140 (-1.2)		
	KLK3	prostate specific antigen	12602 (-1.3)			
	STEAP2	6 transmembrane epithelial prostate antigen 2	11943 (-1.1)			
	PRAC	prostate cancer susceptibility candidate	13054 (-1.8)			
	PSCA	prostate stem cell antigen	15227 (-2.3)			
Transcription Factors	E2F1		16606 (-1.4)			
	E2F2		16458 (-1.2)			
	E2F3		5360 (1.16)			
	E2F4		2261 (1.18)	9087 (1.01)		
	E2F5		47 (1.83)			
	E2F6		1386 (1.38)	2076 (1.21)	9235 (1.02)	
	E2F7		16065 (-1.3)			
	E2F8		14633 (-1.2)			
	SMAD2		885 (1.46)	1431 (1.31)	3864 (1.19)	
	SMAD3		1810 (1.39)	3005 (1.26)		
	SMAD1		3259 (1.29)	12187 (-1.1)		
	SMAD4		3831 (1.19)			
	SMAD5		13013 (-1.1)			
	TWIST1		12920 (-1.1)			
	SNAIL		N/A			
	STAT5		14900 (-1.4)			
	STAT3		1777 (1.23)	2291 (1.22)		
	STAT1		1220 (1.37)			
	NFkB1		5281 (1.17)			
	JUN		17703 (-2.2)			
Cell Cycle Regulation	p53		N/A			
	MDM2		552 (1.54)			

www.manaraa.com

	p21	cyclin-dependent kinase inhibitor 1	435 (1.51)	663 (1.55)	5102 (1.2)	
	PAK2	p21 activated kinase 2	90 (1.54)	7900 (1.06)		
	PAK1	p21 activated kinase 1	1031 (1.29)			
	CDK1	cyclin-dependent kinase 1	4856 (1.15)			Too many cyclin dependent kinases and cyclin kinase inhibitors upregulated to list
	CDK2	cyclin-dependent kinase 2	2558 (1.22)			
	CDK3	cyclin-dependent kinase 3	10151 (-1)			
	CDK4	cyclin-dependent kinase 4	11395 (-1)			
	CDK5	cyclin-dependent kinase 5	11082 (-1)			
	CDK6	cyclin-dependent kinase 6	6804 (1.11)			
	CDK7	cyclin-dependent kinase 7	2763 (1.25)			
	CDK8	cyclin-dependent kinase 8	629 (1.46)			
	CDK9	cyclin-dependent kinase 9	2312 (1.54)			
	CCND1	cyclin D1	12 (3.08)	29 (2.45)	190 (2.01)	Too many cyclins upregulated to list
	CCNJ	cyclin J	46 (1.61)			
	CCNC	cyclin C	1614 (1.3)			
	CCND3	cyclin D3	1727 (1.37)			
	CCNA2	cyclin A2	3075 (1.22)			
Miscellaneous	AKT1		4727 (1.26)			
	AKT2		15454 (-1.2)			
	AKT3		15 (3.42)			
	MAPK1	ERK	1010 (1.39)	2530 (1.29)		
	MAPK2		N/A			
	MAPK3		11697 (-1)			
	MAPK4		N/A			
	MAPK5		N/A			
	MAPK6	ERK3	181 (1.85)	929 (1.4)		
	MAP2K2	MEK2	1138 (1.3)			
	MAP2K1	MEK1	3411 (1.17)			
	MAP2K3		3662 (1.18)	11725 (-1.1)		
	MAP2K5		6240 (1.15)			
	PRKCD	Protein kinase C delta	6684 (1.06)			
	PRKCA	Protein kinase C alpha	7396 (1.08)			
	PTK2	Focal adhesion kinase (FAK)	16984 (-1.3)	17397 (-1.4)	14909 (-1.2)	
	PLC	Phospholipase C	1183 (1.52)			
	PLCG1		13790 (-1.2)			
	PLCB3		10769 (-1)			
	PLCD1		16808 (-1.3)			
	PLCE1		17859 (-1.6)			
	PTEN		7445 (1.06)			
	mTOR		6327 (1.1)			
	HRas		14228 (-1.2)			

www.manaraa.com

	KRas		15627 (-1.4)	737 (1.59)	4998 (1.13)	
	NRas		284 (1.52)			
	RRas		4917 (1.21)	8165 (1.06)		
	RRas2		496 (1.45)			
	Raf1		7834 (1.04)			
	Braf		6021 (1.15)			
	RhoA		172 (1.34)	417 (1.35)	1412 (1.2)	
	Rho		12764 (-1.4)			
	RhoV		575 (1.84)	1017 (1.61)		
	RhoD		1980 (1.51)			
	RhoQ		2344 (1.22)	2909 (1.23)		
	RhoC		5112 (1.09)	17555 (-1.3)	4413 (1.15)	
	Rock1		542 (1.4)	2593 (1.5)		
	Notch1		12236 (-1.2)			
	Notch 2		14623 (-1.1)			
	Wnt5b		821 (1.73)			
	Wnt7b		4660 (1.45)			
	Wnt5a		10016 (-1)			
	Wnt10a		14475 (-1.4)	15077 (-1.4)		
	Wnt3		16094 (-1.6)			
	Wnt6		17355 (-2)			
	Wnt4		17758 (-2.2)	17890 (-1.7)		
	GNAi3		2224 (1.22)			
	GNAi1		3069 (1.21)			
	GNAi2		15396 (-1.2)			
	FOXO1		1783 (1.33)			
	FOXO3		6825 (1.07)			
	PIK3R4	PI3K, regulatory subunit 4	765 (1.33)			
	PIK3CB	PI3K, catalytic beta polypeptide	1077 (1.45)			
	PIK3CD	PI3K, catalytic delta polypeptide	4341 (1.21)			
	PIK3C2A	PI3K class 2 alpha polypeptide	4930 (1.23)			
	PIK3C3	PI3K class 3	6143 (1.07)	13538 (-1.2)		
	PIK3CA	PI3K catalytic alpha polypeptide	7453 (1.06)			
	PIK3C2B		14920 (-1.2)			
	PIK3R1	PI3K regulatory subunit 1 alpha	17198 (-1.8)			
	PIK3R3		17551 (-1.9)			
	CTNNB1	Beta catenin	4032 (1.17)	5937 (1.09)	7494 (1.07)	
	JAK1		6069 (1.11)	17741 (-1.9)		
	SRC		9083 (1.01)			
	SHC1		3631 (1.33)			
	GRB2		5847 (1.08)			

www.manaraa.com

	SOS2		2802 (1.22)			
	SOS1		14548 (-1.2)			
	IFN-Y	interferon gamma	N/A			
	IFNYR2		693 (1.35)			
	TNFa	Tumor necrosis factor alpha	N/A			
	HIF1a	hypoxia inducible factor 1 alpha	1910 (1.22)			
	ANG	Angiogenin	15530 (-1.2)			
	CAV2	Caveolin 2	1 (2.64)	280 (1.9)		
	CAV1	Caveolin 1	9 (2.77)	15 (2.61)		
	CAV3	Caveolin 3	179 (2.17)			
	GLB1	Beta1 galactosidase	6128 (1.08)	11492 (-1)		
	IGFBP1	insulin-like growth factor binding protein 1	N/A			
	IGFBP2	insulin-like growth factor binding protein 2	18038 (-5.7)			
	IGFBP3	insulin-like growth factor binding protein 3	5510 (1.19)			
	IGFBP4	insulin-like growth factor binding protein 4	11053 (-1.1)			
	IGFBP5	insulin-like growth factor binding protein 5	17329 (-3.7)			
	IGFBP6	insulin-like growth factor binding protein 6	11642 (-1.1)			
	IGFBP7	insulin-like growth factor binding protein 7	12559 (-1.3)			*opposite trend of RT-PCR
	IGF1	insulin-like growth factor 1	N/A			
	IGF1R	insulin-like growth factor 1 receptor	16250 (-1.5)			
	IGF2	insulin-like growth factor 2	2990 (1.52)			
	IGF2R	insulin-like growth factor 2 receptor	3400 (1.24)			
	FOSL1	FOS-like antigen 1	382 (2.02)			
	FOSL2	FOS-like antigen 2	7973 (1.13)	12076 (-1.1)		
	FOS	FBJ murine osteosarcoma viral oncogene	17070 (-1.4)			
	KLF4	kruppel-like factor 4	1719 (1.32)			
	KLF5	kruppel-like factor 5	855 (1.84)	5106 (1.29)		
	SLIT2	slit homolog 2	2001 (1.86)			
	SLIT3	slit homolog 3	12458 (-1.2)			
	PLAU	plasminogen activator, urokinase	290 (1.79)			
	PLAUR	plasminogen activator, urokinase receptor	1987 (1.33)			
	MET	met proto-oncogene (hepatocyte growth factor receptor)	1663 (1.75)	2916 (1.56)	10405 (-1)	

www.manaraa.com

Appendix 10: DNA Oligonucleotide Array Signaling Analysis

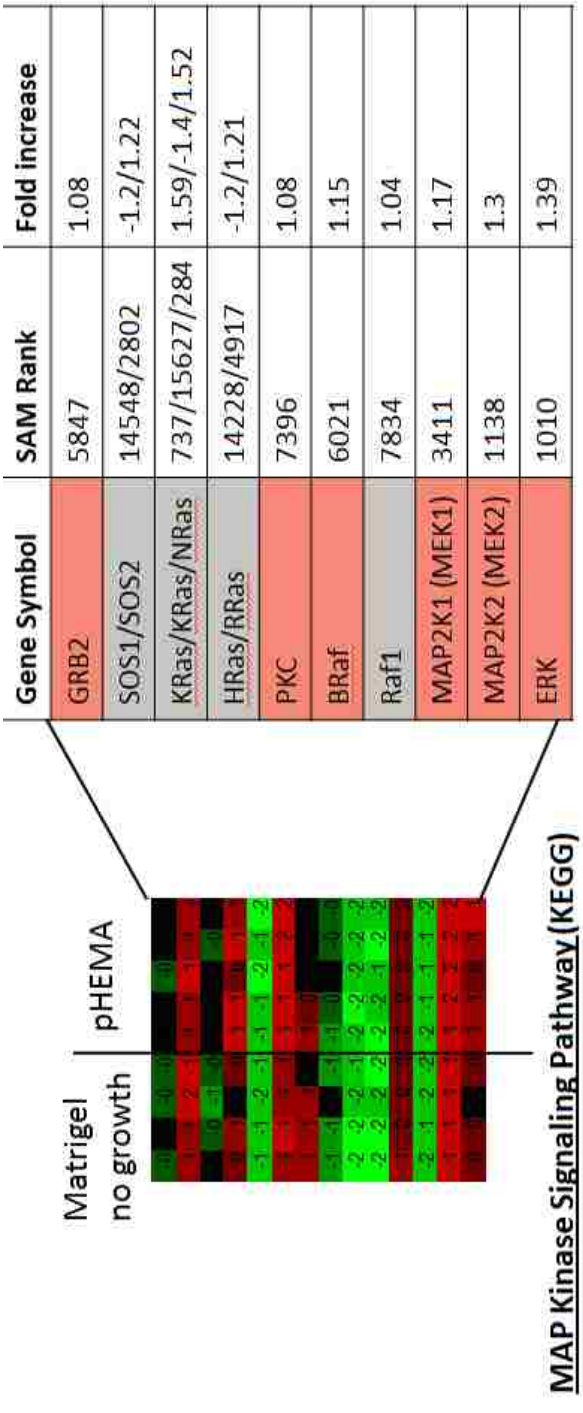

Gene Symbol	SAM Rank	Fold increase
GRB2	5847	1.08
SOS1/SOS2	14548/2802	-1.2/1.22
KRas/KRas/NRas	737/15627/284	1.59/-1.4/1.52
HRas/RRas	14228/4917	-1.2/1.21
PKC	7396	1.08
BRaf	6021	1.15
Raf1	7834	1.04
MAP2K1 (MEK1)	3411	1.17
MAP2K2 (MEK2)	1138	1.3
ERK	1010	1.39

Matrigel
no growth
pHEMA

MAP Kinase Signaling Pathway (KEGG)

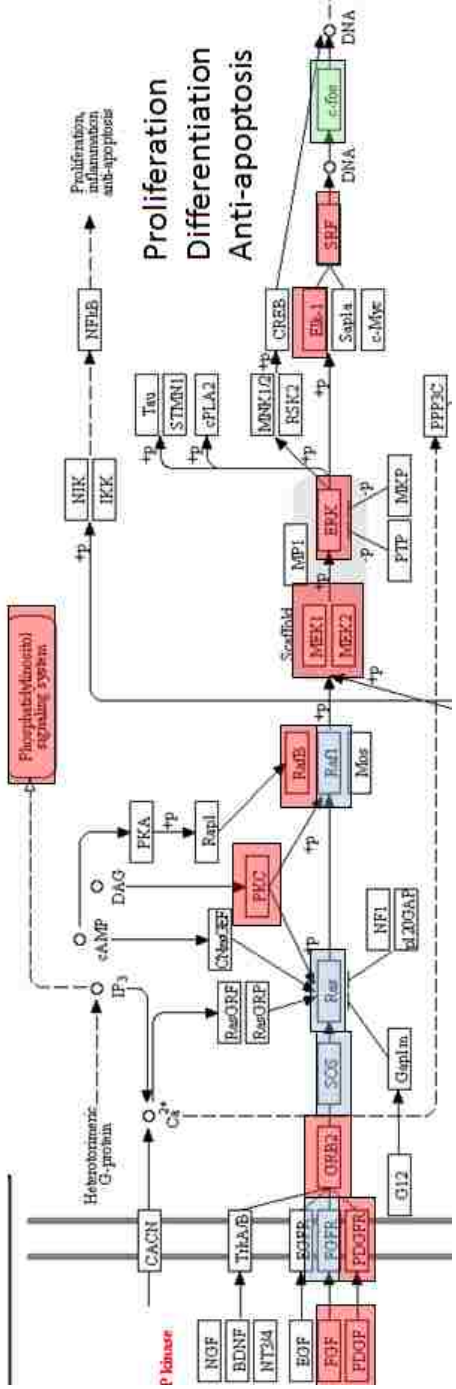

www.manaraa.com

المنارة للاستشارات

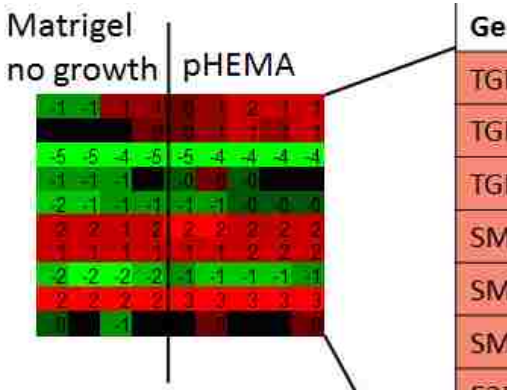

Gene Symbol	SAM Rank	Fold increase
TGFB1	947	2.15
TGFB2	226	1.68
TGFBR2	1007	1.5
SMAD2	885	1.46
SMAD3	1810	1.39
SMAD4	3831	1.19
E2F4	2261	1.18
E2F5	47	1.83
RhoA	172	1.34
Rock1	542	1.4

TGF-B Signaling Pathway (KEGG)

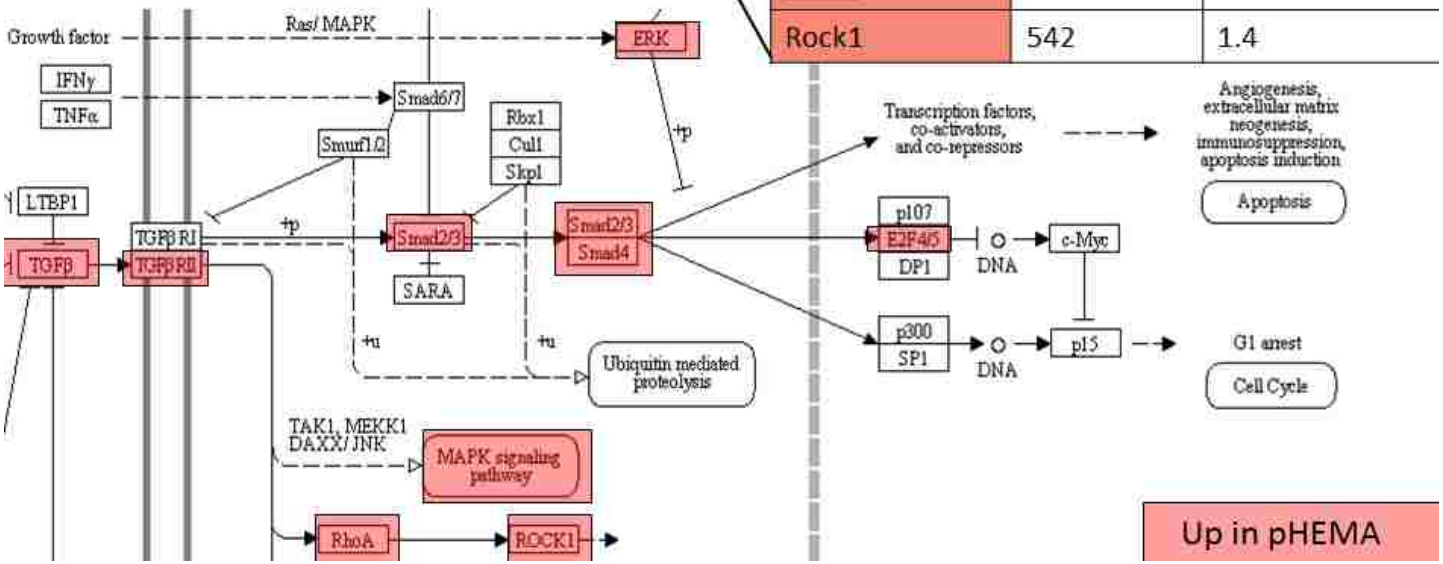

Up in pHEMA

www.manaraa.com

Cell-ECM Interactions

	Gene Symbol	SAM Rank	Fold increase
Laminins (alpha, beta, gamma chains)	LAMC2	3807	1.69
	LAMA3	490	1.64
	LAMB3	5081	1.61
	LAMC1	299	1.45
	LAMA5	11006	-1.1
	LAMA4	13740	-1.2
	LAMB2	14077	-1.2
	LAMB1	17087	-1.4
Integrins (alpha, beta chains)	ITGA5	129	3.08
	ITGB1	951	1.57
	ITGA3	2198	1.34
	ITGA6	15774	-1.3
	ITGB4	16033	-1.3
	ITGA2	17621	-2.4
Fibronectin	FN1	17816	-2.5

Heat map relative to cell line pool reference

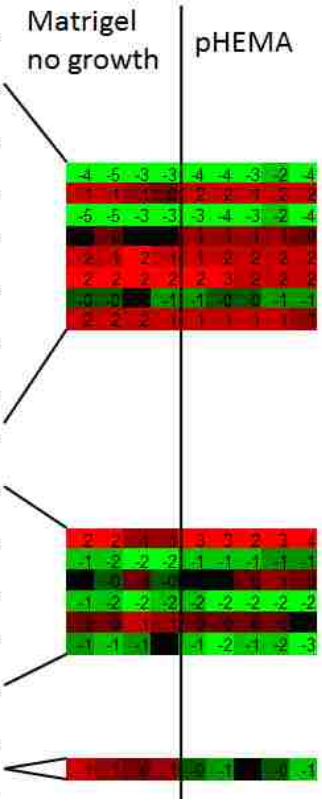

www.manaraa.com

Appendix 11: CXCL5/CXCR2 Signaling Pathway

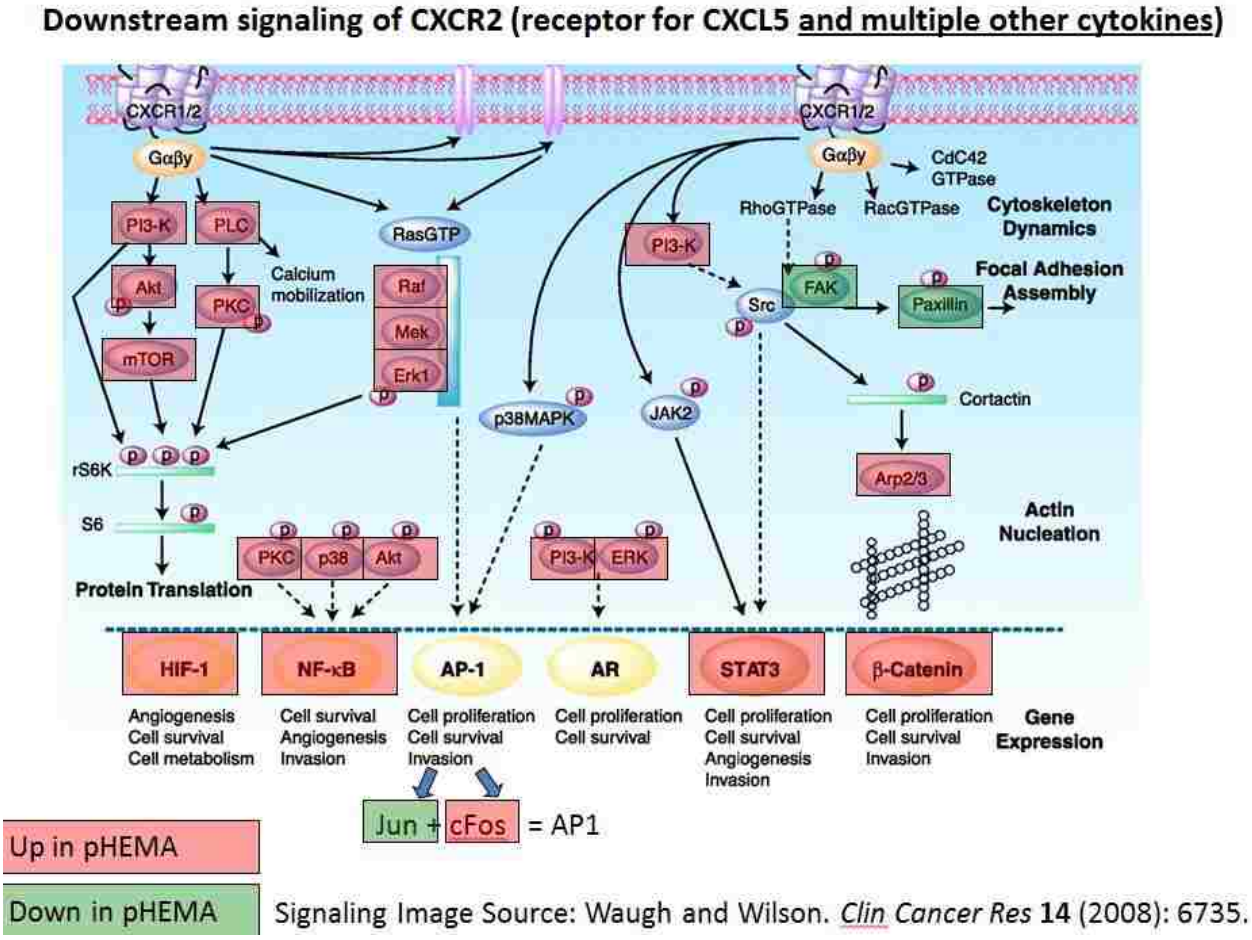

Signaling Image Source: Waugh and Wilson. *Clin Cancer Res* **14** (2008): 6735.

www.manaraa.com

Appendix 12: Mouse Macrophage Conditioned Media Cytokine Array Results

Protein	**M0**	**M1**	**M2**
Axl	-	-	-
BLC	+	+	+
CD30L	-	-	-
CD30T	++	++	+
CD40	-	-	-
CRG-2	-	-	-
CTACK	++	++	++
CXCL16	+++	+++	+++
Eotaxin	+	++	+
Eotaxin-2	++	+++	+
Fas ligand	-	-	-
Fractalkine	-	-	-
GCSF	++	++	++
GM-CSF	-	-	-
IFNY	-	+	-
IGFBP-3	++	++	++
IGFBP-5	-	-	-
IGFBP-6	-	-	-
IL-1a	++	++	++
IL-1b	-	-	-
IL-2	-	-	-
IL-3	-	-	-
IL-3 Rb	-	-	-
IL-4	++	++	+++
IL-5	-	++	-
IL-6	-	++++	-
IL-9	+	++	+
IL-10	-	++	-
IL-12 p4070	-	++++	-
IL-12 p70	++	+++	++
IL-13	-	-	-
IL-17	-	-	-
KC	-	+++	-
Leptin R	-	-	-
Leptin	+	+	+
LIX	++	++	++
L-selectin	-	-	-
Lymphotactin	++	++	+

www.manaraa.com

MCP-1	**+++**	**+++**	**+++**
MCP-5	**++**	**+++**	**++**
M-CSF	++	++	++
MIG	**+**	**++**	**+**
MIP-1a	+	+	+
MIP-1Y	++++	++++	++++
MIP-2	**+++**	**+++**	**++**
MIP-3B	+	+	+
MIP-3a	+	+	+
PF-4	++	++	++
P-selectin	**++**	**++**	**+++**
RANTES	**+**	**+++**	**+**
SCF	+	+	+
SDF-1a	**++**	**++**	**+**
TARC	-	-	-
TCA-3	++	++	++
TECK	-	-	-
TIMP-1	**+**	**++**	**+**
TNF-a	-	-	-
sTNF RI	**+++**	**++**	**+++**
sTNF RII	**++**	**++**	**++**
TPO	+	+	+
VCAM-1	**+**	**++**	**+**
VEGF	+	+	+

Proteins in bold showed some qualitative difference in expression levels between macrophage phenotypes.

www.manaraa.com

Appendix 13: M12mac25 + MCM Cytokine Array Raw Results

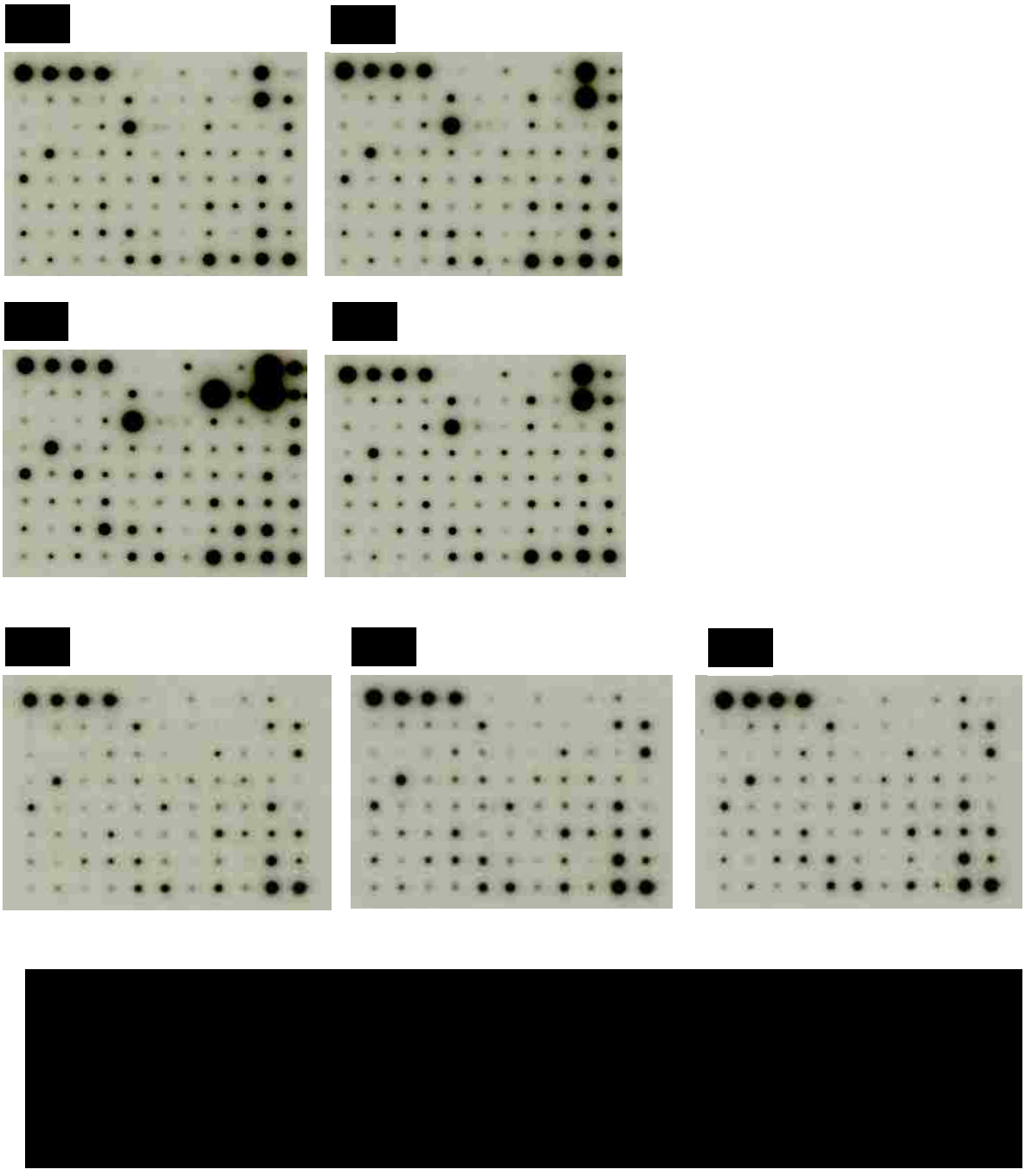

www.manaraa.com

Appendix 14: Vertebrate Animals

All protocols involving vertebrate animals have been approved by the University of Washington Institutional Animal Care and Use Committee (IACUC) under protocol 2797-04 (PI: Dr. Stephen Plymate). All animal studies have been completed in a facility managed by the University of Washington Department of Comparative Medicine, which is accredited by the Association for Assessment of Laboratory Animal Care (AALAC).

.

www.manaraa.com

Bibliography

[1] Kola, et al. Can the pharmaceutical industry reduce attrition rates? Nat Rev Drug Discov 2004;3:711.
[2] Siegel, et al. Cancer Statistics, 2013. CA Cancer J Clin 2013;63:11-30.
[3] American Cancer Society. Detailed Guide: Prostate Cancer. 2012.
[4] Bissell, et al. How does the extracellular matrix direct gene expression? J Theoretical Biology 1982;99:31-68.
[5] Cukierman, et al. Cell interactions with three-dimensional matrices. Cur Op Cell Bio 2002;14:633-9.
[6] Pampaloni, et al. The third dimension bridges the gap between cell culture and live tissue. Nat Rev Mol Bio 2007;8:839-45.
[7] Ghosh, et al. Three-dimensional culture of melanoma cells profoundly affects gene expression profile: a high density oligonucleotide array study. J Cell Phys 2005;204:522-31.
[8] Abbott A. Biology's new dimension. Nature 2003;424:870-72.
[9] Lee, et al. Three-dimensional cell culture matrices: state of the art. Tissue Eng Part B 2008;14:61-86.
[10] Lin, et al. Recent advances in three-dimensional multicellular spheroid culture for biomedical research. Biotechnology 2008;3:1172-84.
[11] Kunz-Schughart, et al. Multicellular tumor spheroids: intermediates between monolayer culture and in vivo tumor. Cell Bio Int 1999;23:157-61.
[12] Sharpless, et al. The mighty mouse: genetically engineered mouse models in cancer drug development. Nat Rev Drug Discov 2006;5:741-54.
[13] Stephenson, et al. Metastatic model for human prostate cancer using orthotopic implantation in nude mice. J Natl Cancer Inst 1992;84:951-57.
[14] Lopez-Barcons. Human prostate cancer heterotransplants: a review on this experimental model. Asian J Andrology 2010;12:509-18.
[15] Pienta, et al. The current state of preclinical prostate cancer animal models. The Prostate 2008;68:629-39.
[16] Kleinman, et al. Matrigel: basement membrane matrix with biological activity. Semin Cancer Biol 2005;15:378-86.
[17] Hughes, et al. Matrigel: a complex protein mixture required for optimal growth of cell culture. Proteomics 2010;10:1886-90.
[18] Chung, et al. Molecular insights into prostate cancer progression: the missing link of the tumor microenvironment. J Urol 2005;173:10-20.
[19] Bissell, et al. Putting tumors in context. Nat Rev Cancer 2001;1:46-54.
[20] Hanahan, et al. The hallmarks of cancer. Hormone Research 2000;100:57-70.
[21] Kalluri, et al. Fibroblasts in cancer. Nat Rev Cancer 2006;6:392-401.
[22] Olumi, et al. Carcinoma-associated fibroblasts direct tumor progression of initiated human prostatic epithelium. Cancer Res 1999;59:5002-11.
[23] Mantovani, et al. Role of tumor-associated macrophages in tumor progression and invasion. Cancer Metastasis Rev 2006;25:315-22.
[24] Papetti, et al. Mechanisms of normal and tumor-derived angiogenesis. Amer J Physiol. 2002;282:947-70.
[25] Hutmacher, et al. Can tissue engineering concepts advance tumor biology research? Trends Biotechnol 2010;28:125.

www.manaraa.com

[26] Hutmacher, D.W. Biomaterials offer cancer research the third dimension. Nat Mater 2010;9: 90.
[27] Ghajar, et al. Tumor engineering: the other face of tissue engineering. Tissue Eng Part A 2010;16:2153.
[28] Burdett, et al. Engineering tumors: a tissue engineering perspective in cancer biology. Tissue Eng Part B 2010;16:351.
[29] Debnath, et al. Modeling glandular epithelial cancers in three-dimensional cultures. Nat Rev Cancer 2005;5:675-88.
[30] Kim JB. Three-dimensional tissue culture models in cancer biology. Semin Cancer Biol 2005;15:365-77.
[31] Hutmacher, et al. Translating tissue engineering technology platforms into cancer research. J Cell Mol Med 2009;13:1417-27.
[32] Fischbach, et al. Engineering tumors with 3D scaffolds. Nat Methods 2007;4:855.
[33] Sahoo, et al. Characterization of porous PLGA/PLA microparticles as a scaffold for three dimensional growth of breast cancer cells. Biomacromolecules 2005;6:1132-39.
[34] Horning, et al. 3-D tumor model for in vitro evaluation of anticancer drugs. Mol Pharm 2008;5:849-862.
[35] Weiss, et al. The impact of adhesion peptides within hydrogels on the phenotype and signaling of normal and cancerous mammary epithelial cells. Biomaterials 2012;33:3548-59.
[36] Boxberger, et al. A new method for the 3-D in vitro growth of human RT112 bladder carcinoma cells using the alginate culture technique. Biol Cell 1994;82:109-19.
[37] Zhang, et al. Development of an in vitro multicellular tumor spheroid model using microencapsulation and its application in anticancer drug screening and testing. Biotechnol Prog 2005;21:1289-96.
[38] Kievit, et al. Chitosan-alginate 3D scaffolds as a mimic of the glioma tumor microenvironment. Biomaterials 2010;31:5903-10.
[39] Leung, et al. Chitosan-alginate scaffold culture system for hepatocellular carcinoma increases malignancy and drug resistance. Pharm Res 2010;27:1939-48.
[40] Dhiman, et al. Characterization and evaluation of chitosan matrix for in vitro growth of MCF-7 breast cancer cell lines. Biomaterials 2004;25:5147-54.
[41] Tan, et al. Three-dimensional porous silk tumor constructs in the approximation of in vivo osteosarcoma physiology. Biomaterials 2011;32:6131-37.
[42] Liu, et al. Tumor engineering: orthotopic cancer models in mice using cell-loaded, injectable, cross-linked hyaluronan-derived hydrogels. Tissue Engineering 2007;13:1091-1101.
[43] Gurski, et al. Hyaluronic acid-based hydrogels as 3D matrices for in vitro evaluation of chemotherapeutic drugs using poorly adherent prostate cancer cells. Biomaterials 2009;30:6076-85.
[44] Szot, et al. 3D in vitro bioengineered tumors based on collagen I hydrogels. Biomaterials 2011;32:7905-12.
[45] Dhiman, et al. Three-dimensional chitosan scaffold-based MCF-7 cell culture for the determination of the cytotoxicity of tamoxifen. Biomaterials 2005;26:979-86.
[46] Moreau, et al. Tissue-engineered bone serves as a target for metastasis of human breast cancer in a mouse model. Cancer Res 2007;67:10304-8.
[47] Pathi, et al. Hydroxyapatite nanoparticle-containing scaffolds for the study of breast cancer bone metastasis. Biomaterials 2011;32:5112-22.

www.manaraa.com

[48] Ko, et al. The use of chemokine-releasing tissue engineering scaffolds in a model of inflammatory response-mediated melanoma cancer metastasis. Biomaterials 2012;33:876-85.
[49] Lee, et al. Implantable microenvironments to attract hematopoetic stem/cancer cells. PNAS 2012;109:19638-43.
[50] Madden, et al. Proangiogenic scaffolds as functional templates for cardiac tissue engineering. Proc Natl Acad Sci USA 2010;107:15211.
[51] Osathanon, et al. Microporous nanofibrous fibrin-based scaffolds for bone tissue engineering. Biomaterials 2008;29:4091.
[52] Isenhath, et al. A mouse model to evaluate the interface between skin and a percutaneous device. J Biomed Mat Res Part A 2007;83:915.
[53] Marshall, et al. Biomaterials with tightly controlled pore size that promote vascular in-growth. ACS Polymer Preprints 2004;45:100.
[54] Villalona, et al. Cell-seeding techniques in vascular tissue engineering. Tissue Eng Part B 2010;16:341.
[55] Burg, et al. Comparative study of seeding methods for three-dimensional polymeric scaffolds. J Biomed Mater Res 2000;52:642.
[56] Wendt, et al. Oscillating perfusion of cell suspensions through three-dimensional scaffolds enhances cell seeding efficiency and uniformity. Biotechnol Bioeng 2003;84:205.
[57] Thevenot, et al. Method to analyze three-dimensional cell distribution and infiltration in degradable scaffolds. Tissue Eng Part C 2008;14:319.
[58] Dar, et al. Optimization of cardiac cell seeding and distribution in 3D porous alginate scaffolds. Biotechnol Bioeng 2002;80:305.
[59] Li, et al. Effects of filtration seeding on cell density, spatial distribution, and proliferation in nonwoven fibrous matrices. Biotechnol Prog 2001;17:935.
[60] Ng, et al. The challenge to measure cell proliferation in two and three dimensions. Tissue engineering 2005;11:182.
[61] Bae, et al. Metastatic sublines of an SV40 large T antigen immortalized human prostate epithelial cell line. The Prostate 1998;34:275.
[62] Ewald, et al. Surface imaging microscopy, an automated method for visualizing whole embryo samples in three dimensions at high resolution. Dev Dyn 2002;225:369.
[63] Galperin, et al. Degradable, thermo-sensitive poly)N-isopropyl acrylamide)-based scaffolds with controlled porosity for tissue engineering applications. Biomacromolecules 2010;11:2583.
[64] Galperin, et al. Adaptive tissue engineering scaffold. US Appl 20110256628, 2011.
[65] Suresh, S. Biomechanics and biophysics of cancer cells. Acta Biomater 2007;3:413.
[66] Shanbhag, et al. Cell distribution profiles in three-dimensional scaffolds with inverted-colloidal-crystal geometry: modeling and experimental investigations. Small 2005;1:1208.
[67] Anderson, et al. Foreign body reaction to biomaterials. Seminars in Immunology 2008;20:86-100.
[68] Ratner, et al. Biomaterials: where we have been and where we are going. Annual Review of Biomedical Engineering 2004;6:41-75.
[69] Thalmann, et al. LNCaP progression model of human prostate cancer: androgen-independence and osseous metastasis. Prostate 2000;44:91-103.
[70] Thalmann, et al. Androgen-independent cancer progression and bone metastasis in the LNCaP model of human prostate cancer. Cancer Res 1994;54:2577-81.
[71] Uhr, et al. Controversies in clinical cancer dormancy. Proc Nat Aca Sci USA 2011;108:12396-400.

www.manaraa.com

[72] Morgan, et al. Disseminated tumor cells in prostate cancer patients after radical prostatectomy and without evidence of disease predicts biochemical recurrence. Clin Cancer Res 2009;15:677-83.
[73] Pantel, et al. Detection, clinical relevance and specific biological properties of disseminating tumour cells. Nat Rev Cancer 2008;8:329-40.
[74] Meng et al. Circulating tumor cells in patients with breast cancer dormancy. Clinical cancer research AACR 2004;10:8152-62.
[75] Folkman, et al. Cancer without disease. Nature 2004;427:787.
[76] Aguirre-Ghiso JA. Models, mechanisms and clinical evidence for cancer dormancy. Nat Rev Cancer 2007;7:834-46.
[77] Weaver et al. Reversion of the malignant phenotype of human breast cells in three-dimensional culture and in vivo by integrin blocking antibodies. Journal Cell Bio 1997;137:231-45.
[78] White et al. Targeted disruption of B1-integrin in a transgenic mouse model of human breast cancer reveals an essential role in mammary tumor induction. Cancer Cell 2004;6:159-70.
[79] Sprenger, et al. Senescence-induced alterations of laminin chain expression modulate tumorigenicity of prostate cancer cells. Neoplasia 2008;10:1350-61.
[80] Swisshelm, et al. Enhanced expression of an insulin growth factor like-binding protein (mac25) in senescent human mammary epithelial cells and induced expression with retinoic acid. Proc Natl Acad Sci USA 1995;92:4472-4476.
[81] Burger, et al. Down-regulation of T1A12/mac25, a novel insulin-like growth factor binding protein related gene, is associated with disease progression in breast carcinomas. Oncogene 1998;16:2459-2467.
[82] Komatsu, et al. Methylation and downregulated expression of mac25/insulin-like growth factor binding protein-7 is associated with liver tumorigenesis in SV40T/t antigen transgenic mice, screened by restriction landmark genomic scanning for methylation (RLGS-M). Biochem Biophys Res Commun 2000;267:109-17.
[83] Sato, et al. Strong suppression of tumor growth by insulin-like growth factor-binding protein-related protein 1/tumor-derived cell adhesion factor/mac25. Cancer Sci 2007;98:1055-63.
[84] Wajapeyee, et al. Oncogenic BRAF induces senescence and apoptosis through pathways mediated by the secreted protein IGFBP7. Cell 2008;132:363-374.
[85] Sprenger, et al. Insulin-like growth factor binding protein related protein 1 (IGFBP-rp1) is a potential tumor suppressor for prostate cancer. Cancer Res 1999;59:2370-75.
[86] Hwa, et al. Characterization of insulin-like growth factor binding protein related protein-1 in prostate cells. J Clin Endocrinol Metab 1998;83:4355-62.
[87] Sprenger, et al. Over-expression of insulin-like growth factor binding protein-related protein-1 (IGFBP-rP1/mac25) in the M12 prostate cancer cell line alters tumor growth by a delay in G1 and cyclin A associated apoptosis. Oncogene 2002;21:140-47.
[88] Goss PE, et al. Does tumor dormancy offer a therapeutic target? Nat Rev Cancer 2010;10:871-77.
[89] Klein CA. Framework models of tumor dormancy from patient-derived observations. Curr Opin Genet Dev 2011;21:42-9.
[90] Shih, et al. Tumor-associated macrophage : its role in cancer invasion and metastasis. J Cancer Mol 2006;2:101-6.
[91] Lissbrant, et al. Tumor associated macrophages in human prostate cancer- relation to clinical pathological variables and survival. Int J Oncol 2000;17:445-41.

www.manaraa.com

[92] Shimura, et al. Reduced infiltration of tumor-associated macrophages in human prostate cancer: association with cancer progression. Cancer Res 2000;60:5857-61.
[93] Murdoch, et al. Mechanisms regulating the recruitment of macrophages into hypoxic areas of tumors and other ischemic tissues. Blood 2004;104:2224-34.
[94] Coffelt, et al. Tumor-associated macrophages: effectors of angiogenesis and tumor progression. Biochim Biophys Acta 2009;1796:11-18.
[95] Sica, et al. Tumour-associated macrophages are a distinct M2 polarised population promoting tumour progression: potential targets of anti-cancer therapy. European journal of cancer 2006;42:717-27.
[96] Wahl, et al. Tumor-associated macrophages as targets for cancer. 1998;90:1583-1584.
[97] Luo et al. Targeting tumor-associated macrophages as a novel strategy against breast cancer. J Clin Investigation 2006;116:2132-2141.
[98] Bingle, et al. The role of tumour-associated macrophages in tumour progression: implications for new anticancer therapies. J Path 2002;196:254-65.
[99] Stout, et al. Macrophages sequentially change their functional phenotype in response to changes in microenvironmental influences. J Immunology 2005;175:342-349.
[100] Sica et al. Macrophage polarization in tumour progression. Seminars in Cancer Biology 2008;18:349-55.
[101] Brown, et al. Macrophage polarization: an opportunity for improved outcomes in biomaterials and regenerative medicine. Biomaterials 2012;33:3792-802.
[102] EM Sussman. Roles for macrophage polarity and WNT signaling in improved foreign body reactions. University of Washington PhD Thesis. 2012.
[103] Kyriakides, et al. The CC chemokine ligand, CCL2/MCP1, participates in macrophage fusion and foreign body giant cell formation. Amer J Path 2004;165:2157-66.
[104] Meng, et al. Blockade of tumor necrosis factor alpha signaling in tumor-associated macrophages as a radiosensitizing strategy. Cancer Res 2010;70:1534-43.
[105] Zeisberger, et al. Clodronate-liposome-mediated depletion of tumour-associated macrophages: a new and highly effective antiangiogenic therapy approach. Brit J Cancer 2006;95:272-81.
[106] Valentin, et al. Macrophage participation in the degradation and remodeling of extracellular matrix scaffolds. Tissue Eng Part A 2009;15:1687-94.
[107] Mooney, et al. Cellular plasticity of inflammatory myeloid cells in the peritoneal foreign body response. Am J Path 2010;176:369-380
[108] Begley, et al. CXCL5 Promotes Prostate Cancer Progression. Neoplasia 2008;10:244-254.
[109] Kuo, et al. CXCL5/ENA78 increased cell migration and epithelial-to-mesenchymal transition of hormone-independent prostate cancer by early growth response-1/snail signaling pathway. J Cell Physiol 2011;226:1224-31.
[110] Tse, et al. Preparation of hydrogel substrates with tunable mechanical properties. Current Protocols in Cell Biology 2010;10:10.16.1.
[111] Yeung, et al. Effects of substrate stiffness on cell morphology, cytoskeletal structure, and adhesion. Cell Motility and the Cytoskeleton 2005;60:24-34.
[112] Engler, et al. Matrix elasticity directs stem cell lineage specification. Cell 2006;126:677-89.
[113] Charest, et al. Fabrication of substrates with defined mechanical properties and topographical features for the study of cell migration. Macromolecular Bioscience 2012;12:12-20.

www.manaraa.com

[114] Pelham, et al. Cell locomotion and focal adhesions are regulated by substrate flexibility. Proc Natl Acad Sci USA 1997;94:13661-65.
[115] Khatiwala, et al. Intrinsic mechanical properties of the extracellular matrix affect the behavior of pre-osteoblastic MC3T3-E1 cells. Am J Physiol Cell Physiol 2006;290:1640-50.
[116] Wang, et al. Substrate flexibility regulates growth and apoptosis of normal but not transformed cells. American journal of physiology. Cell physiology 2000;279:1345-50.
[117] Brown, et al. Evaluation of polydimethylsiloxane scaffolds with physiologically-relevant elastic moduli: interplay of substrate mechanics and surface chemistry effects on vascular smooth muscle cell response. Biomaterials 2005;26:3123-9.
[118] Robinson, et al. Differential effects of substrate modulus on human vascular endothelial, smooth muscle, and fibroblastic cells. J Biomed Mat Res Part A 2012;100:1356-67.
[119] Klein, et al. Cell-cycle control by physiological matrix elasticity and in vivo tissue stiffening. Current Biology 2009;19:1511-18.
[120] Kraning-Rush, et al. Cellular traction stresses increase with increasing metastatic potential. PLoS ONE 2012;7:e32572.
[121] Bianchi-Frias, et al. The effects of aging on the molecular and cellular composition of the prostate microenvironment. PLoS ONE 2010;5:e12501.
[122] Bianchi-Frias, et al. Genetic background influences murine prostate gene expression: implications for cancer phenotypes. Genome Biology 2007;8:R117.
[123] van Rooijen, et al. Apoptosis of macrophages induced by liposome-mediated intracellular delivery of clodronate and propamidine. J Immunol Methods 1996;193:93-9.
[124] Chen, et al. Macrophage binding to receptor VCAM-1 transmits survival signals in breast cancer cells that invade the lungs. Cancer Cell 2011;20:538-49.
[125] Waters, et al. Data merging for integrated microarray and proteomic analysis. Briefings in Functional Genomics & Proteomics 2006;5:261-72.
[126] Soofi, et al. The elastic modulus of Matrigel as determined by atomic force microscopy. J Structural Biology 2009;167:216-19.
[127] Zhang, et al. The isolation and characterization of murine macrophages. Curr Protoc Immunol 2008;14.
[128] Lu, et al. Activation of MCP-1/CCR2 axis promotes prostate cancer growth in bone. Clinical & Experimental Metastasis 2009;26:161-9.
[129] Darash-Yahana, et al. The chemokine CXCL16 and its receptor, CXCR6, as markers and promoters of inflammation-associated cancers. PLoS ONE 2009;4:e6695.
[130] Ide, et al. Serum level of macrophage colony-stimulating factor is increased in prostate cancer patients with bone metastasis. Hum Cell 2008;21:1-6.

www.manaraa.com